Groningen Dynamic Model Update 2019

Quint de Zeeuw and Leendert Geurtsen

NAM

Datum October 2018

Editors Jan van Elk & Dirk Doornhof

General Introduction

The subsurface model of the Groningen field is used to model the first step in the causal chain from gas production to induced earthquake risk. It models the pressure response in the gas and water bearing reservoir formations to the gas extraction.

The reservoir model of the Groningen field was built in 2011 and 2012 and has a very detailed description of the faults in the field to support studies into induced earthquakes. The model was used to support Winningsplan 2013 (Ref. 1 to 3) and has since then been continuously improved (Ref. 4, 6 and 7). This report describes the continuous improvement of the subsurface model of the Groningen field and in particular the effort to update and improve the history match.

Pressure decline in the field is an important driver for compaction and therefore subsidence. Compaction in turn affects stress and strain and is therefore of importance for the mechanism inducing earthquakes. The model therefore has an important role in the optimization of the gas withdrawal from the reservoir to reduce seismicity.

For Winningsplan 2013 and Winningsplan 2016, the model was reviewed by the independent consultant SGS Horizon. An extensive assurance review (Ref. 5) with opinion letter has been prepared by SGS Horizon.

The reservoir model was updated to better forecast the development of pressure after gas production from the field has ceased, when initially intra-field pressure equilibration and later the response of lateral aquifers will dominate. The update therefore focused on:

- Gas-in-aquifer of the Slochteren formation
- Gas bearing Carboniferous
- Water bearing Carboniferous
- Depletion in the Lauwerszee aquifer resulting from the smaller fields Roden, Vries, Pasop and Faan.

References

1. Winningsplan Groningen 2013, Nederlandse Aardolie Maatschappij BV, 29th November 2013.
2. Technical Addendum to the Winningsplan Groningen 2013; Subsidence, Induced Earthquakes and Seismic Hazard Analysis in the Groningen Field, Nederlandse Aardolie Maatschappij BV (Jan van Elk and Dirk Doornhof, eds), November 2013.
3. Supplementary Information to the Technical Addendum of the Winningsplan 2013, Nederlandse Aardolie Maatschappij BV (Jan van Elk and Dirk Doornhof, eds), December 2013.
4. Groningen Field Review 2015 Subsurface Dynamic Modelling Report, Burkitov, Ulan, Van Oeveren, Henk, Valvatne, Per, May 2016.
5. Independent Review of Groningen Subsurface Modelling Update for Winningsplan 2016, SGS Horizon, July 2016.
6. Groningen Dynamic Model Update 2018, NAM, Henk van Oeveren, Per Valvatne and Leendert Geurtsen, September 2017
7. Groningen Dynamic Model Update 2019, Quint de Zeeuw and Leendert Geurtsen, NAM, October 2018

NAM

Title	**Groningen Dynamic Model Update 2018**	**Date**	October 2018
		Initiator	NAM
Autor(s)	Quint de Zeeuw and Leendert Geurtsen	**Editors**	Jan van Elk Dirk Doornhof
Organisation	NAM	**Organisation**	NAM
Place in the Study and Data Acquisition Plan	Study Theme: Prediction Reservoir Pressure based on gas withdrawal Comment: The subsurface model of the Groningen field is used to model the first step in the causal chain from gas production to induced earthquake risk. It models the pressure response in the gas and water bearing reservoir formations to the gas extraction. The reservoir model of the Groningen field was built in 2011 and 2012 and has a very detailed description of the faults in the field to support studies into induced earthquakes. The model was used to support Winningsplan 2013 and has since then been continuously improved. This report describes the continuous improvement of the subsurface model of the Groningen field and in particular the effort to update and improve the history match. Pressure decline in the field is an important driver for compaction and therefore subsidence. Compaction in turn affects stress and strain and is therefore of importance for the mechanism inducing earthquakes. The model therefore has an important role in the optimization of the gas withdrawal from the reservoir to reduce seismicity. For Winningsplan 2013 and Winningsplan 2016, the model was reviewed by the independent consultant SGS Horizon. An extensive assurance review with opinion letter has been prepared by SGS Horizon. The reservoir model was updated to better forecast the development of pressure after gas production from the field has ceased, when initially intra-field pressure equilibration and later the response of lateral aquifers will dominate. The update therefore focused on: • Gas-in-aquifer of the Slochteren formation • Gas bearing Carboniferous • Water bearing Carboniferous • Depletion in the Lauwerszee aquifer resulting from the smaller fields Roden, Vries, Pasop and Faan.		

Directly linked research	• Reservoir Compaction • Optimisation of the aerial distribution of production
Used data	Sub-surface data from the Groningen field; open-hole logs, core data, pressure data, production data etc.
Associated organisation	Independent consultant SGS Horizon
Assurance	For Winningsplan 2013 and Winningsplan 2016, the model was reviewed by an independent consultant SGS Horizon.

Nederlandse Aardolie Maatschappij B.V.

Shell UPO

Groningen Dynamic Model Update 2018 – V6

Date: October 2018

Issued by: Quint de Zeeuw, Leendert Geurtsen

EP number: EP201809202872

Name	Ref. Indicator	Role	Date	Signature
Hein de Groot	NAM-UPO/T/DL	Discipline Lead Reservoir Engineering		
Clemens Visser	NAM-UPO/T/GD	Discipline Lead Production Geology		
Emile Fokkema	NAM-UPO/T/DL	Discipline Lead Petrophysics		

1 Executive summary

As part of NAM's effort to increase the understanding of the production induced seismicity, a new dynamic model has been developed. It provides more focus on the anticipated dynamic effects associated with the 2030 field shut-in. With reducing production, the impact of the lateral aquifers and of the intra-field pressure equilibration will become relatively more important for the development of reservoir pressure over time. To this end, the V6 dynamic model update includes 4 major new items:

1) Gas-in-aquifer (Slochteren)
    - There is evidence of the presence of gas-in-the-aquifer. This will have a baffling effect on pressure depletion, and hence reduce compaction and subsidence which is needed to better predict subsidence in the north-west of the field. At the same time water encroachment in the north of the field is enhanced.
2) Gas bearing Carboniferous (Mores model was expanded to include the gas bearing part of the Carboniferous)
    - The depletion of the Carboniferous increases compaction and subsidence which is needed to better predict subsidence in the south of the field.
3) Water bearing Carboniferous
    - The water bearing Carboniferous is included in the model to obtain the possibility in long term subsidence forecasting to assess the impact of its depletion on subsidence.
4) Depletion in the Lauwerszee aquifer resulting from the land fields Roden, Vries, Pasop and Faan.
    - These fields lie outside of the model numerical grid, but their production history is likely to influence depletion within the model. Given the potential impact on the history and distribution of earthquakes in time and space, the depletion effect of these fields was included in the dynamic reservoir model.

The V6 model has been history matched up to 31 December 2017 with respect to the following data:

- Static down-hole pressure measurements (SP(T)G),
- Repeat formation test pressures (RFT),
- Closed-in tubing-head pressures converted to bottom-hole pressures (CITHP-to-CIBHP),
- Interpreted rise in gas-water contact (PNL),
- Stable subsidence data from 2 levelling surveys (time-lapse from 1972 to 2013)
- Strain data from the Zeerijp-3A DSS cable (from May 2016 to November 2017)
- Time-lapse gravity data (1996 and 2015)
- Expected pressure drop from earthquakes southwest of the field (2006 and 2017).

The reservoir GIIP (gas in Rotliegend sandstone above the FWL[1]) of the best-match dynamic model is 2859.50 N.Bcm. The GIIP in the Carboniferous and the gas-in-aquifer are 42.41 N.Bcm and 103.36 N.Bcm respectively. The overall match to the data available is:

- SPG RMS = 1.82 bar (V5 = 2.11 bar)
- CITHP-to-CIBHP RMS = 1.48 bar (V5 = 1.35 bar)
- RFT RMS = 12.72 bar (V5 = 11.88 bar)
- PNL RMS = 2.81 meter (V5 = 2.44 meter)[2]
- Subsidence RMS = 2.10 cm (V5 = 4.34 cm)

[1] Total GIIP in Rotliegend comprises both Slochteren Sandstone and Ten Boer Claystone

[2] The PNL data has data quality issues, the match should only be considered on wells which have an interpreted rise in GWC from the PNLs.

- Gravity RMS = 4.84 μGal (V5 = 5.44 μGal)
- ZRP strain DSS = 24.23 μstrain (V5 = n.a.)

The following recommendations can be considered to further improvement of the model:

- Basin Modelling provided new insights, which can be used in the model to initialise the gas-in-aquifer
- Further data acquisition may help to constrain the gas-in-aquifer modelling:
    1) The lateral extent of gas-in-aquifer towards the southwest of the field can be tested by PNX logging
    2) The presence of a paleocontact can be tested by PNX logging on a well deeper than 3158m TVDSS
    3) A dedicated production test (on a well completed only at the gas-in-aquifer zone) would provide an option to calibrate relative permeability model.
- The static model can be further improved by:
    1) updating the Ten Boer layer thickness modelling
    2) including the ZRP-3A data in the property modelling
    3) correcting the Ameland layer thickness spike near Bierum
    4) including the Vries, Roden, Pasop and Faan land fields
- Reassessment of the existing PNL logs can be done to QC the interpreted absence of GWC rise
- Locally the V6 history match can be further improved, specifically:
    1) the BDM-5 SPG match
    2) the BRW SPG match
    3) the EKL-13 PNL match
    4) the DZL PNL match

Contents

2 Introduction

2.1 Background

This V6 update of the dynamic reservoir simulation model of the Groningen field was done in support of the seismicity modelling, Long Term subsidence prediction, and production (capacity) forecasting. The causal chain that is modelled to predict the hazard and risk due to production-induced seismicity starts with production and the resulting pressure depletion. Due to the production-induced seismicity, on 29/3/2018 the Minister of Economic Affairs announced the ramp-down of production from the Groningen field, and ultimate cessation of production by 2030. For earlier dynamic reservoir models, the expectation was that future reservoir pressure development would be dominated by the continued offtake rates at the production clusters. However, with the onset of a gradual shut-in of the Groningen field, the reservoir pressure will increasingly be dominated by different mechanisms. At low offtake rates, the intra-reservoir equilibration of the current north to south pressure gradient will start to dominate the reservoir pressure behaviour. Furthermore, the relative importance of the lateral aquifers will grow in the total material balance. The long-term depletion of these lateral aquifers will become more significant for the predictions of reservoir compaction, earthquakes, ground motion, and house strengthening scope (a.o. underneath the city of Groningen, lateral to the Groningen field).

2.2 Model objective

This model sets out to meet the following objectives:

- Generate reservoir pressure predictions for Hazard and Risk Assessments. The mid case should provide a best estimate of what will happen after close-in of the field.
- Provide a framework with full functionality to accommodate any future history match requirements.
    - Include gas-in-aquifer
    - Include the Carboniferous in the numerical grid
- Close out recommendations from previous modelling studies. From Reference [1]:
    - Review presence and potential impact of gas-in-the-aquifer to improve subsidence match in the North-West (V5 model overpredicts subsidence) and GWC rise in the North of the field (V5 model underestimates water rise).
    - Explore the dynamic effect of a gas bearing Carboniferous formation in the south of the field, to improve the subsidence match (V5 model underpredicts subsidence in the south of the field).
    - Review impact of gas-in-aquifer on porosity modelling through seismic inversion. The connectivity issues between the northern observation wells and the northern production clusters as described in V4 still exist in the V5 model after the second iteration of the seismic inversion. From model based analysis of the gravity measurements it was demonstrated that the water influx as observed from PNL logs in wells in the north of the field is a regional phenomenon, rather than local coning around individual wells [3].
    - Investigate incorporation of semblance and delta-thickness maps in the History Matching workflow, to represent lateral spread of uncertainty in the static model. It is recommended to investigate how these maps can be used to steer areal adjustments to the static model, ideally as an integral part of the assisted history matching workflow.

2.3 New model elements

The V6 update of the MoReS model includes 4 major new items (Figure 2-1):

1) Gas-in-aquifer (Slochteren)
    - The baffling effect of gas-in-aquifer on pressure decreases compaction and subsidence which is needed to better predict subsidence in the north-west of the field.
2) Gas bearing Carboniferous (Mores model was expanded to include the gas bearing part of the Carboniferous)
    - The depletion of the Carboniferous increases compaction and subsidence which is needed to better predict subsidence in the south of the field.
3) Water bearing Carboniferous
4) Depletion in the Lauwerszee aquifer resulting from gas production from the land fields Roden, Vries, Pasop and Faan.

Items 1) and 2) were included to address the subsidence mismatches in the north and south of the field as indicated in Reference [2]. Item 3) was introduced to improve integration with the geomechanical modelling of earthquakes, allowing to feed Carboniferous pressure scenarios into geomechanical rupture modelling. Item 4) was introduced given the increasing relative importance of the lateral aquifers with time, as total field production is set to reduce towards zero by 2030. Earthquake research infers that earthquakes start to be induced beyond 90 bar depletion. Earthquakes were registered in the Lauwerszee aquifer at Paddepoel (2006) and Eelderwolde (2013). In order to establish such levels of aquifer depletion in the dynamic model, production of the nearby gas fields on the opposite site of the aquifer had to be incorporated.

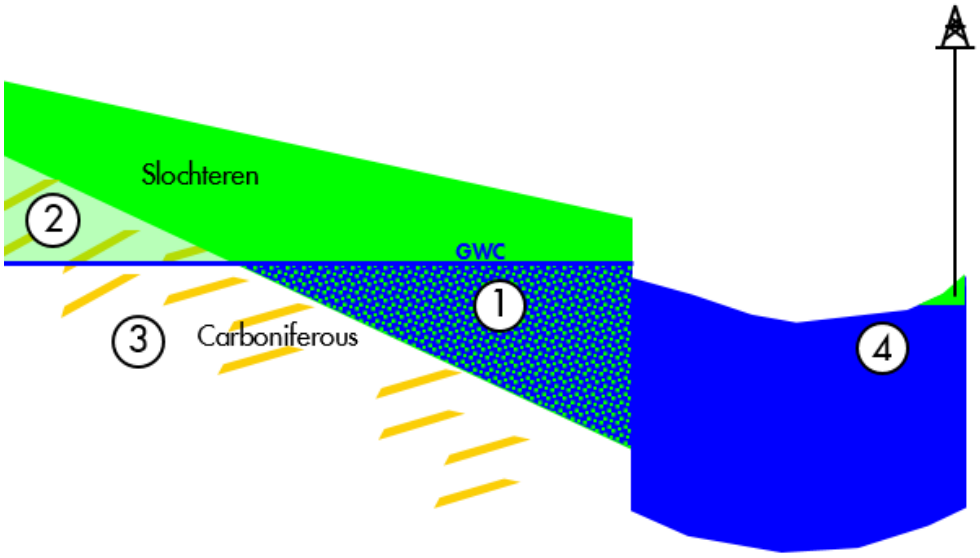

Figure 2-1: Schematic representation of new model elements

2.4 Report structure

The new model elements are described in chapters 3 to 5; respectively gas-in-aquifer, Carboniferous and Lauwerszee aquifer depletion. The history match is covered in chapters 6 to 8, describing the methodology, global match and regional matches. Chapter 9 captures the recommendations for further work.

3 Gas-in-aquifer

3.1 Introduction

In Reference [3] various indicators for gas-in-aquifer (below the GWC) were identified:

1) Petrophysical interpretations of Open Hole log data suggested gas saturations below the Groningen free water levels (albeit that these data have a high uncertainty below the gas water contact).
2) No Direct Hydrocarbon Indicator is observed from seismic. The static reservoir model is fairly well calibrated from 300-odd well penetrations in a layer-cake type reservoir. The static model was used to generate synthetic seismic. Only by introducing a gas saturation below the free water level was it possible to remove the DHI from the synthetic seismic and match the recorded seismic, Reference [4].
3) From RFT logging of infill wells the pore pressure depletion below the free water level has been observed to consistently lag with respect to the overlying gas column, Reference [2].
4) Subsidence data suggests very limited depletion of the lateral aquifer to the north-west of the field, which was difficult to history match.
5) The observed rise of the gas-water-contact in the north of the field (PNL data, gravity data) has been difficult to match, and was typically underpredicted in previous dynamic models, References [2] and [3].

Especially the combination of elements 4) and 5) proved incompatible. In its previous configuration the dynamic model cannot choke off the lateral aquifer from depletion and yet have sufficient bottom water drive to match the water encroachment.

Theoretically, introducing gas below the free water level could provide a physical explanation for the observed dynamic behaviour, as indicated in Figure 3-1. Introducing a second (gas) phase in the aquifer will significantly reduce the aquifer permeability due to the relperm effect. This may explain a lag in the depletion of the aquifer with respect to the overlying gas column. Simultaneously, gas-in-aquifer will dramatically increase the compressibility of the aquifer, both arresting the depletion of the aquifer and increasing the aquifer encroachment (boosting GWC movement).

Appendix D provides an analytical evaluation of the effect of the inclusion of gas-in-aquifer on the water rise in the field.

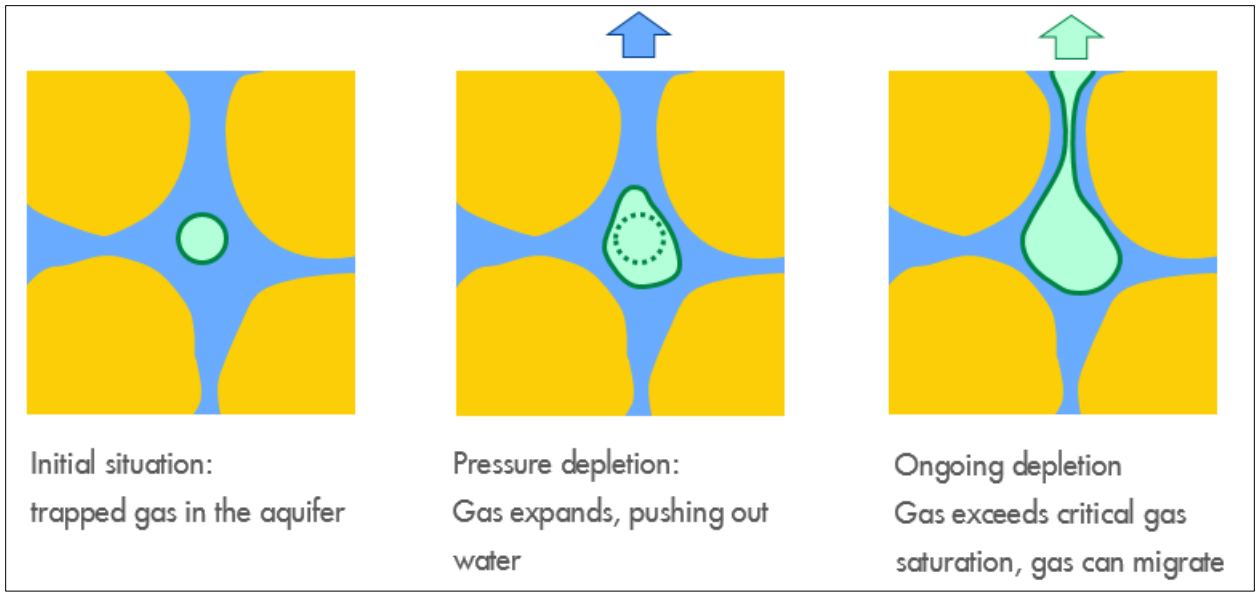

Figure 3-1: Schematic overview of the dynamic impact of gas-in-aquifer.

Additional surveillance was done to establish conclusive evidence:

- The presence of gas below the free water level was confirmed by PNX measurements in 2017. There was a conclusive measurement of gas below the contact from a Cased Hole PNX log at Uithuizen-1 in April 2017, Reference [5]. Two more PNX measurements at Uithuizermeeden-1A and Zeerijp-3A in the same year also showed gas below the free water level, Reference [6].

Section 3.2 summarizes the petrophysical analysis of the Cased Hole PNX data, and the review of the available Open Hole data with a focus on the water leg. The spatial extent of the gas-in-aquifer presence was investigated using seismic, section 3.3.

3.2 Petrophysical analysis

The bulk of the available open-hole log data was acquired between 1960 and 1980. As part of the 2012 Groningen Field Review, Reference [7], a detailed review was done of the 2002 petrophysical work, Reference [8]. Both studies focussed on the gas leg, and the parameters for the water leg were only approximated. The interpreted gas saturations below the GWC were in the range of 0-30su.

To support the implementation of gas-in-aquifer in the full field model a new petrophysical study was done, References [5] and [6].

The 2012 interpretation of gas saturations above the contact was left unchanged.

3.2.1 Saturations from Open Hole Logging data

The existing Open Hole Waxman-Smits model was scrutinized and established to remain valid in the water leg. Well ZRP-3A provides the best dataset in the field. The dataset includes both an open hole Induction log and a cased hole PNX log. These logs were acquired within a limited time window (2015 and 2017, respectively) without production from the well, thus minimizing the odds of production induced differences. The well was drilled with Oil-Based-Mud. Good consistency was found in the interpreted saturations between two independent methods. Hence it was concluded that the existing Open Hole Waxman-Smits model can be applied to the water leg, thus raising confidence in the PNX measurements.

Due to the very saline formation water (some 260 kppm) the gas-in-aquifer saturations are very sensitive to water-based mud invasion. It was established on wells PPS-Z1 and RYSM-Z1C that a small deviation in resistivity values can lead to a significant increase in the interpreted gas-in-aquifer saturations, see Reference [6].

The historical open hole resistivity logs are typically laterolog type measurements. Those have a limited depth of investigation and may not see beyond the invaded zone (which can be relatively high for a good quality rock). In case of water-based drilling mud, the relatively low (< 200 kppm) salinity of the mud-filtrate increases the measured resistivity (the laterolog tool measures a resistive invasion effect). It is impossible to discriminate the increased resistivity readings between the presence of gas or to the measurement of mud-filtrate for old laterolog measurements. More recent Induction tools have a larger depth of investigation and in addition to raw data provide inverted resistivities to compensate for the invasion effect.

Figure 3-2 gives a spatial overview of available Open Hole logs with an aquifer leg penetration, and the respective assessed presence of gas-in-aquifer.

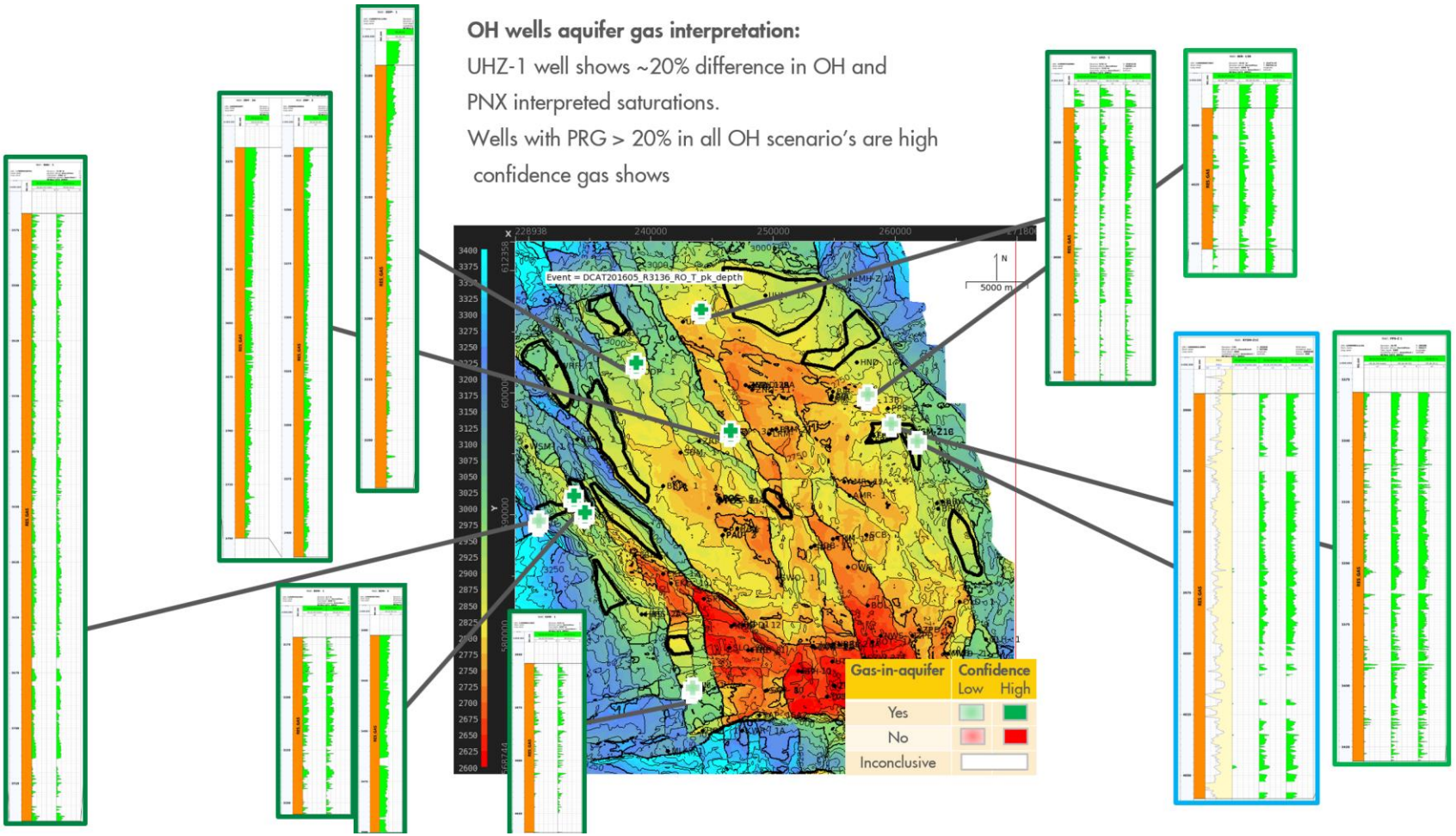

Figure 3-2: Spatial overview of observed gas-in-aquifer from Open Hole log data

3.2.2 Saturations from Cased Hole logging

In 2017 it was decided to acquire additional data to confirm the gas-in-aquifer presence and constrain its model implementation. None of the existing Groningen wells have a bare-foot completion (i.e. open hole). All wells have cased hole, or have been completed with uncemented liners.

Sigma

The assessment of hydrocarbon saturation in a cased hole environment is difficult as compared to an open hole environment. In an open hole the resistivity can be measured, which is distinctly different for gas and water, allowing for quantification of their respective saturations. In a cased hole, resistivity cannot be measured and typically pulsed neutron logs (PNL) are used. However, such measurements are more suited to establish a qualitative change in saturation with respect to a known baseline, and cannot provide an accurate actual saturation value. The most common methodology to calculate hydrocarbon saturation in cased hole is based on the usage of a single measurement, such as Sigma. Sigma, the capture cross section, represents the ability of a given formation to capture thermal neutrons and therefore is a measure of the number of hydrogen atoms present.. The Sigma time-lapse technique (i.e. comparing various Sigma measurements in the same well over time) is designed for reservoir monitoring purposes.

To monitor GWC movement over the production life of the field, PNL logs have been acquired and also those show the presence of residual gas, not only in the 'swept zone' but also below the initial (i.e. at start of production) GWC. The PNL logs were evaluated with a NAM in-house script which allows to determine gas saturation. This curve can be used for a qualitative assessment.

PNX Logging

Schlumberger's PNX tool is a very recent expansion of the logging tool suite for cased hole (first introduced in literature/brought to the market as a commercial product 'Pulsar' in 2017). It acquires an extended set of independent measurements. In addition to Sigma also neutron porosity, fast-neutron cross section, and elemental concentrations are measured. These measurements can be combined in multi-parameter petrophysical models to obtain a quantitative assessment of saturation values, rather than only a qualitative change with respect to a baseline.

Well selection for additional data acquisition

Only a limited number of wells in the Groningen field have significant penetration into the aquifer. The wells for PNX data acquisition were selected because they all have a full penetration of the Rotliegend and are located relatively down-dip in the reservoir (Figure 3-3). Consequently, they have a long penetration of the water leg, some 175m for ZRP-3A and UHM-1A, and 100m for UHZ-1. Wells UHM-1A and UHZ-1 were drilled as appraisal/observation wells in 1965 and 1978 respectively. Zeerijp-3A was drilled in 2015 as part of the seismicity research project as governed under the Study & Data Acquisition Plan and cored a significant part of the Rotliegend section.

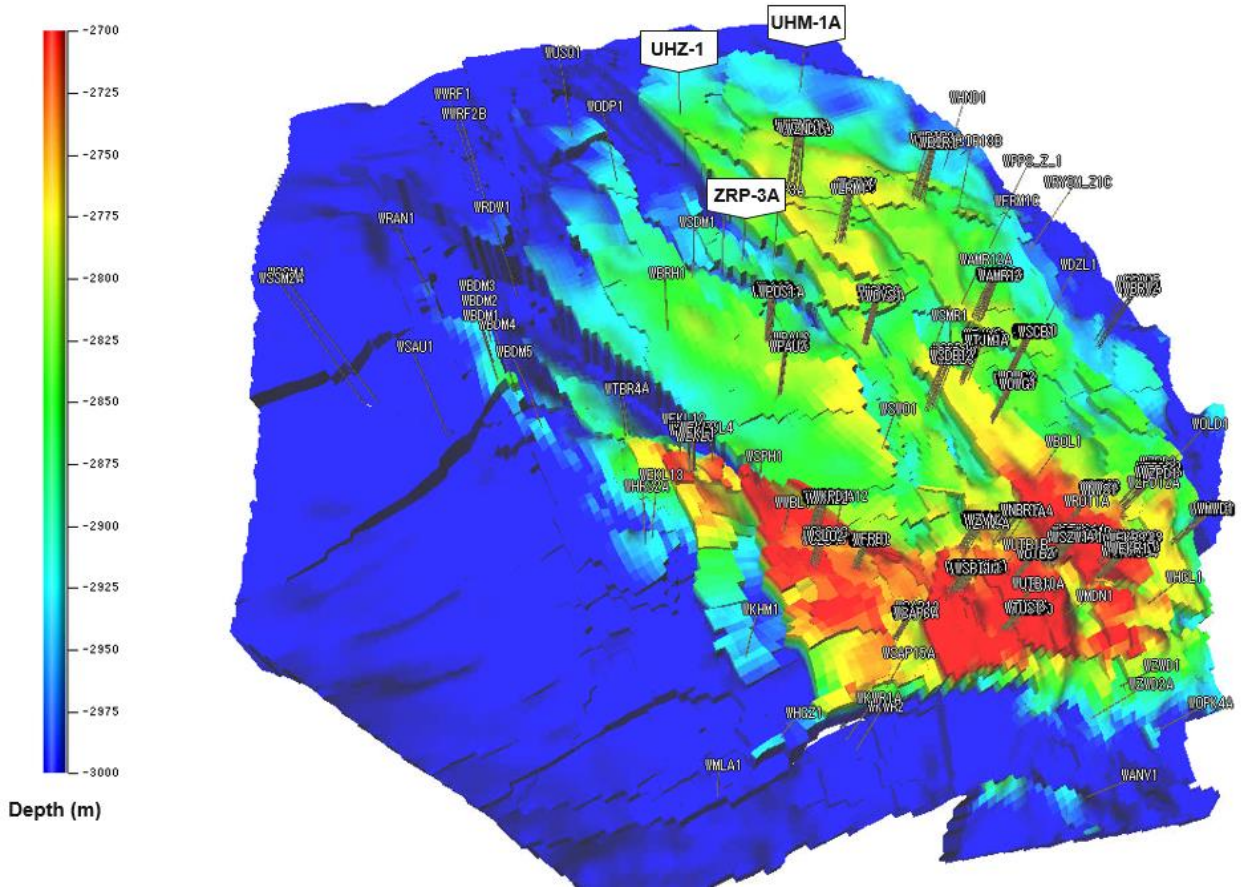

Figure 3-3: Depth map from the simulation grid, indicating the location of the PNX logging at wells UHZ-1, UHM-1A and ZRP-3A

The occurrence of gas saturations below the Gas-Water-Contact was conclusively proven by a Cased Hole PNX log at Uithuizen-1 in April 2017, Reference [4]. Subsequently, two more PNX measurements at Uithuizermeeden-1A and Zeerijp-3A were acquired in the same year, which also showed gas below the free water level, Reference [6].

PNX interpretation

PNX logging is still a novel, exploratory tool. The interpretation involves complex, multi-parameter petrophysical models. From the available PNX logs (ZRP-3A, UHZ-1 and UHM-1A), the data quality is best in ZRP-3A. In this well the conditions under which the logs were acquired were the best. It is recommended to use the ZRP-3A data as the basis for the residual gas saturation used in the dynamic model: in the order of 20-30%.

An independent assessment of the PNX logs was done by Schlumberger for all 3 wells. They also concluded that the best and most reliable data was acquired in ZRP-3A. The Schlumberger assessment of UHZ-1 is somewhat different from NAM's in-house evaluation. The Schlumberger evaluation of this well is more in line with the other 2 wells.

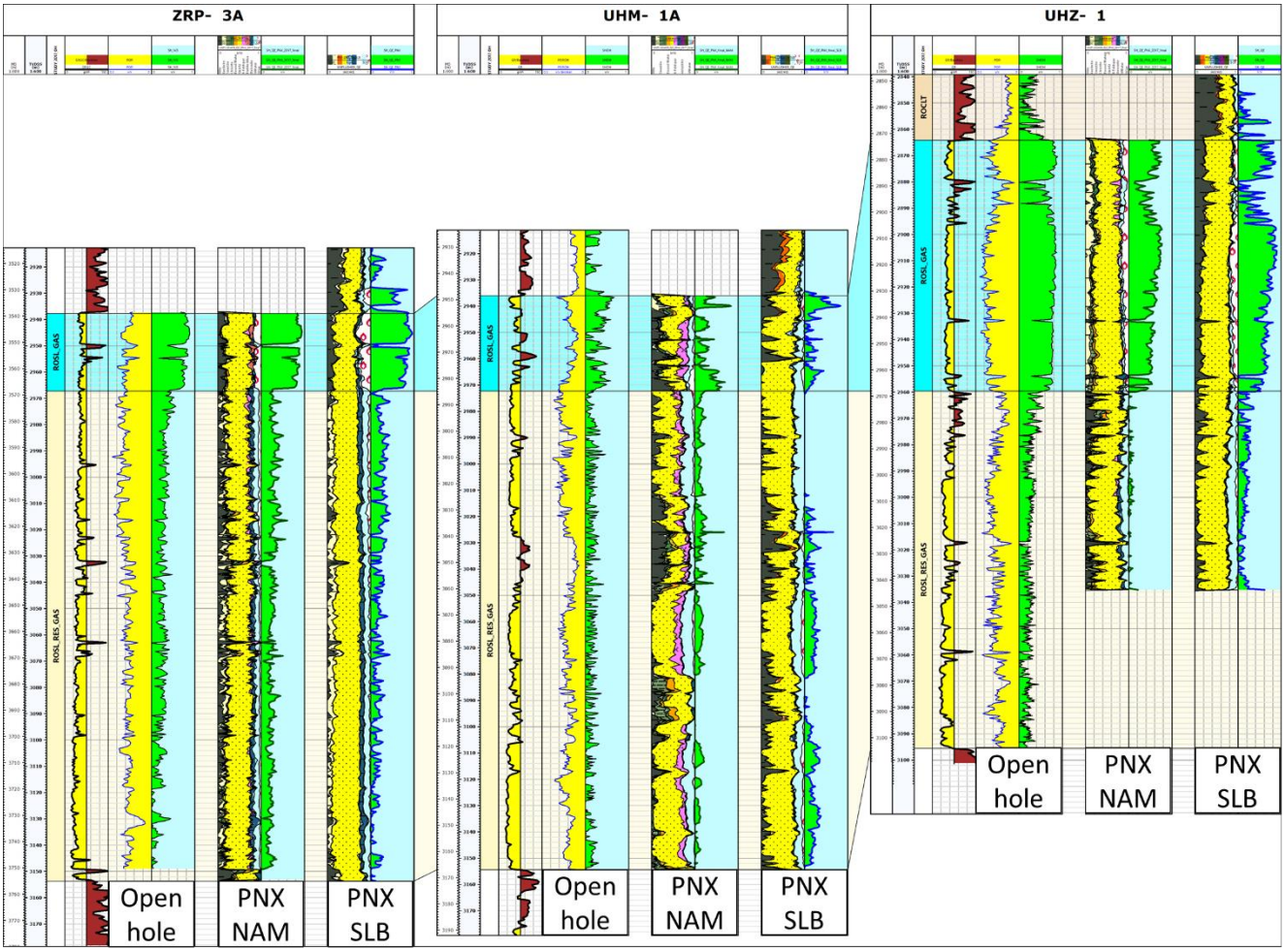

Figure 3-4: Assessment of gas-in-aquifer using different methodologies is shown in green. The columns show GR, open hole derived porosity and gas saturation, the NAM PNX interpreted mineral model and gas saturation and the Schlumberger PNX interpreted mineral model and gas saturation for each well.

NAM saturation interpretation

Figure 3-4 shows NAM in-house interpretations of the open hole and PNX data for UHZ-1, UHM-1A and ZRP-3A, labelled 'Open hole' and 'PNX NAM' respectively. Reference [9] describes in detail the setup of the Multi-Mineral Petrophysical Analysis. The interpretations distinctly show gas below the GWC for all three wells. Saturation values range between 0 to 30su, and are consistently measured all the way down to Base Rotliegend.

Schlumberger saturation interpretation

Given the novel (exploratory) character of the PNX logging, Schlumberger was requested to carry out an (independent) analysis of the logging data. The results are summarized below:

- At ZRP-3A, saturations are interpreted around 20su down to base Rotliegend at 3750mAH, which is consistent with NAM's in-house interpretation.

- In UHM-1A, no gas saturations were interpreted in the top 50m of the water leg. Below, fairly constant saturations around 20su are reported down to Base Rotliegend at 3170mAH. No such distinct absence of saturations had featured in NAM's interpretation.
- UHZ-1 shows fairly consistent saturations around 20 su. This is significantly higher than Shell's in-house interpretation, which estimates some 0-5 su.

All the gas saturation curve determined by Schlumberger have been included in Figure 3-4, labelled 'PNX SLB'.

Table 3-1: Average gas saturation determined

Well	**Dataset**	**Average gas saturation below contact**
ZRP- 3A	Open hole	26%
	PNX NAM	26%
	PNX SLB	18%
UHM- 1A	Open hole	7%
	PNX NAM	10%
	PNX SLB	12%
UHZ- 1	Open hole	24%
	PNX NAM (logged interval only)	2%
	PNX SLB (logged interval only)	15%

Discussion of the various interpretations

For each well three calculated hydrocarbon saturations are depicted in Figure 3-4. Both NAM and Schlumberger interpretations of PNX data, as well as the open-hole data, show gas presence in the aquifer. There is a difference in the amount of gas that is interpreted. This difference can be explained by the high uncertainty when assessing these low saturation levels.

More specifically, the open-hole interpretation is based on data acquired at the time of drilling. The other two saturations are based on the same PNX data through casing but were independently assessed in-house by NAM as well as by Schlumberger. Differences between the open-hole hydrocarbon saturation and the PNX saturation are a result of uncertainties in the various parameters used to calculate saturation from the measured data, a measurement uncertainty and possibly near wellbore reservoir fluid changes over time. The latter obviously does not apply to the two independent interpretations of the same PNX dataset. However, given the fact that the PNX data interpretation relies on complex, multi-parameter petrophysical models to assess the saturation, the parameter uncertainty plays a significant role.

Comparing the differences in saturation from the various methods gives a qualitative sense of the uncertainty in the assessment of the saturation of gas in the aquifer in this environment. In a ZRP-3A situation, where the data quality is high and all the data is taken in a short-timeframe[3] the uncertainty is less compared to the

[3] Open hole induction log and a cased hole PNX log were acquired in 2015 and 2017 respectively, thus minimizing the odds of production induced differences. The well was drilled with Oil Based Mud.

others[4] as can be clearly seen from the consistency in interpretations. Generally, across all the three wells all interpretations point to levels of gas saturation ranging from about 2 to 26 s.u. on average.

Spatial overview of interpretations

Figure 3-5 gives a spatial overview of the interpreted gas-in-aquifer from Cased Hole logging and the respective confidence levels.

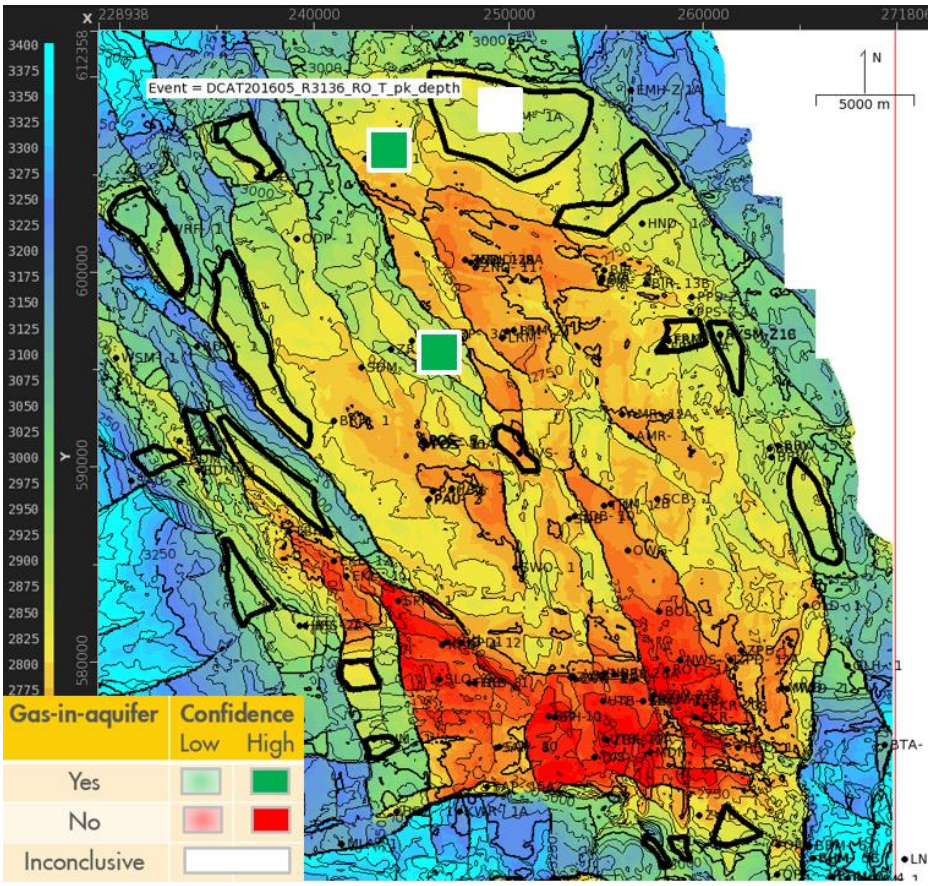

Figure 3-5: Spatial overview of observed gas-in-aquifer from Cased Hole log data

3.2.3 Petrophysical conclusions gas-in-aquifer

The 2012 petrophysical interpretation of the gas leg (gas saturations above the GWC) was left unchanged. The ZRP-3A open hole and cased hole data sets both independently indicate the presence of gas in the aquifer. This confirms that the open-hole Waxman-Smits model and PNX data can both be used to assess the gas saturation in the water leg.

[4] The gas-in-aquifer saturations for wells UHM-1A and UHZ-1 in 2017 (PNX logging) are likely to be different from the saturations in 1965 respectively 1978 (open hole logging) due to the intermediate years of reservoir depletion.

All interpretations indicate presence of gas-in-aquifer. However, significant differences were found between independent PNX gas-in-aquifer saturation interpretations. The difference in the independent interpretations of the PNX logs by NAM and Schlumberger show local differences up to 20su in the top zone of gas below the contact in UHM-1A and overall differences of 15su in the UHZ-1 well.

At the time of completing the dynamic model there was insufficient data/understanding to relate the observations to any meaningful vertical/areal trends to initialise the simulator with a 3D gas-in-aquifer grid. Single-value initialisations were used.

A complicating factor to the model initialisation is explained in Figure 3-1, showing increasing gas-in-aquifer saturations as a function of the reservoir depletion in time. As such, the recent PNX measurements (after more than 50 years of depletion) can only indirectly constrain the model initialisation. They provide an upper limit to the gas saturation, but do not necessarily constrain the initial saturations.

Reviewing existing open hole log data interpretations below the gas water contact in other wells in the Groningen field, show gas saturations in the order of 20su. This is similar to the saturation that is expected for a paleo contact scenario, as described in section 3.6.1 of this document. This insight post-dated the finalisation of the V6 dynamic model.

3.2.4 Petrophysical recommendations

1) Investigate scope for resolving spatial trends in gas-in-aquifer

   It has become clear that the options for resolving the 3-dimensional distribution of gas-in-aquifer based on saturation logs are limited. An alternative approach could be to establish a relationship between saturation and another property that is better constrained (e.g. Vshale, porosity). Such a relationship would allow to introduce vertical/lateral trends of gas-in-aquifer based on trends in that property.

   This would require further investigation of the complete log suites of ZRP-3A, UHM-1A and UHZ-1. It may also be worthwhile to investigate potential differences between the water leg and the gas leg.

   It is also recommended to run the PNX log in one of the Southern locations as the current wells do not provide a full spread over the field. Also, from a basin modelling point of view, the Southern part of the Groningen field is an important calibration point

2) There is an opportunity to correlate PNX spectroscopy data to core measurement at ZRP-3A.

   A study is ongoing (DiAMICT) to acquire near-continuous X-ray fluorescence spectra from the ZRP-3A core and process these to obtain mineral composition at very high vertical resolution. Comparing the results to the PNX data may provide insights in the relation between mineral composition and saturation.

3) Impact of mineralogical model on saturation parameter determination on UHZ-1.

   The Multi-Mineral Petrophysical Analysis can be sensitive to its input parameters. The mineralogical model used for the UHZ well -1 is an average of the mineral composition obtained for the ZRP-3A and ODP-1 wells. An overview of different saturation interpretations for UHZ-1 based on only the ODP-1 and only the ZRP-3A mineralogical model could provide more clarity on the impact of the mineralogical model.

3.3 Indications from seismic

Absence of Direct Hydrocarbon Indicator

In a scenario where no gas would be present in the aquifer, theoretically a Direct Hydrocarbon Indicator should be visible on seismic. However, for the majority of the field such a DHI is absent. This absence can be evaluated with synthetic seismic when introducing gas below the free-water-level. Already at very small gas saturations below the free-water-level (around 3%) the DHI can no longer be reproduced from the synthetic seismic.

CTD stack analysis

Despite the impossibility to assess the values for gas below the free-water-level on seismic, a qualitative study has been done to assess the lateral presence of gas below the free-water-level under the Groningen field, Reference [4]. The DHI effects on a synthetic seismic signal are compared to the CTD stacks of measured seismic in areas of interest[5]. Results are summarized in Figure 3-6. The areas of interest were selected where the Slochteren Sandstone is partly gas- and partly water-bearing, i.e. with a GWC within the formation. Only areas with associated larger fault structures were selected.

[5] The Groningen seismic data is of poor quality. CTD stacking is applied to increase the signal to noise ratio.

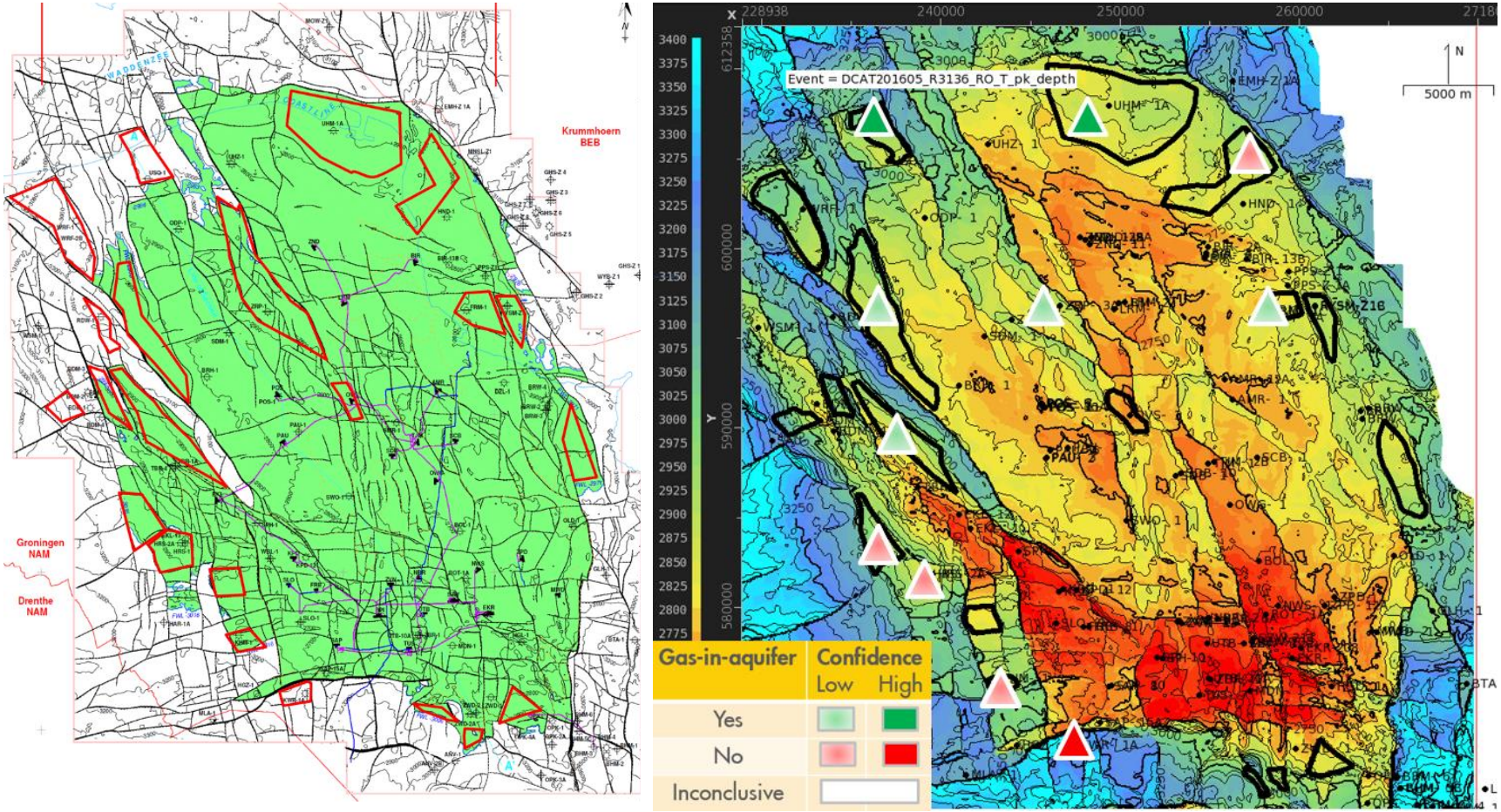

Figure 3-6 Areas investigated on presence of DHI on seismic (left figure) and remaining (low) confidence interpreted areas. Green fill represents presence of gas-in-aquifer, red fill represents no presence of gas-in-aquifer. The confidence in the assessment is indicated by the intensity of the colour: semi-transparent fills represent a low confidence interpretation, solid fill represents a medium confidence interpretation.

3.4 Other indications of gas-in-aquifer

3.4.1 Inference from seismicity

In section 5.1 it is explained how seismicity in the Lauwerszee aquifer is indicative for (partial) depletion. Note that the presence of gas within the Lauwerszee aquifer would have a suppressing effect on depletion.

3.4.2 Inference from subsidence

As discussed in Reference [10], a proxy was implemented in the dynamic reservoir model to calculate surface subsidence as a function of depletion/compaction of the reservoir. Using this proxy, the earlier V5 model distinctly overestimated the depletion/compaction in the north-west. Introducing gas-in-aquifer reduces the depletion in this area and thus improves the subsidence match (Figure 3-7).

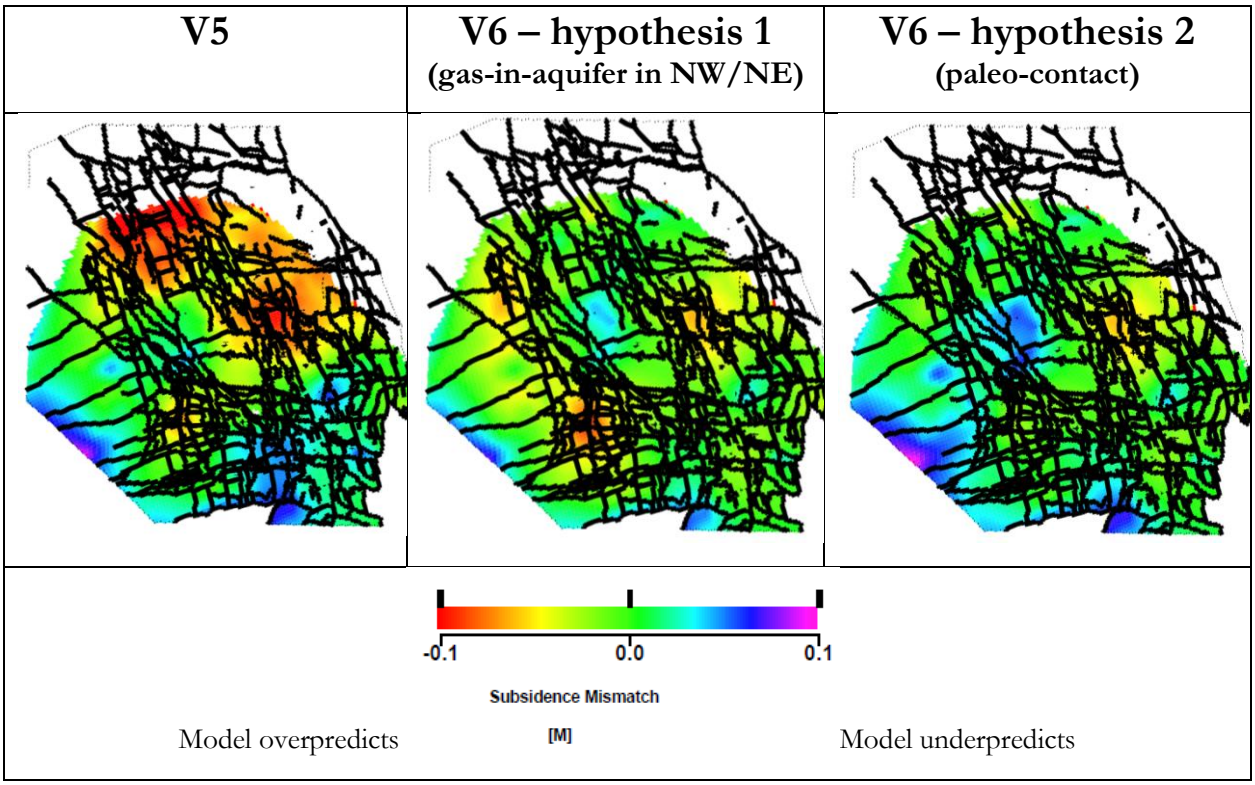

Figure 3-7: Subsidence match (using proxy calculation) for three different full field model realisations, see section 3.6.

3.4.3 Inference from RFT data

Without gas-in-aquifer, the model does typically not show any lag in depletion between the gas leg and the aquifer leg (Appendix D). When introducing gas-in-aquifer, the model starts to show pressure lags in the aquifer. Especially across the Ameland shale, which is laterally continuous in the North of the field, pressure breaks are calculated. The many faults in the area cause local juxtaposition between Upper and Lower Slochteren, thus breaking up the vertical sealing capacity of the Ameland shale. Only a combination of sealing Ameland shale and gas-in-aquifer yields pressure lags in the model. By itself, neither of these two mechanisms can recreate material pressure lags in the model.

From this sensitivity evaluation, the following assumptions were derived:

- If a pressure lag is observed from RFT, then gas-in-aquifer is likely to be present.
- If no vertical baffle (shale) is present, then residual gas would not yield a pressure lag, hence the absence of a pressure lag in the RFT data does not provide a definitive answer as to whether or not gas-in-aquifer is present.

Based on these assumptions, the presence of gas-in-aquifer as inferred from the available RFT data is summarised in Figure 3-8.

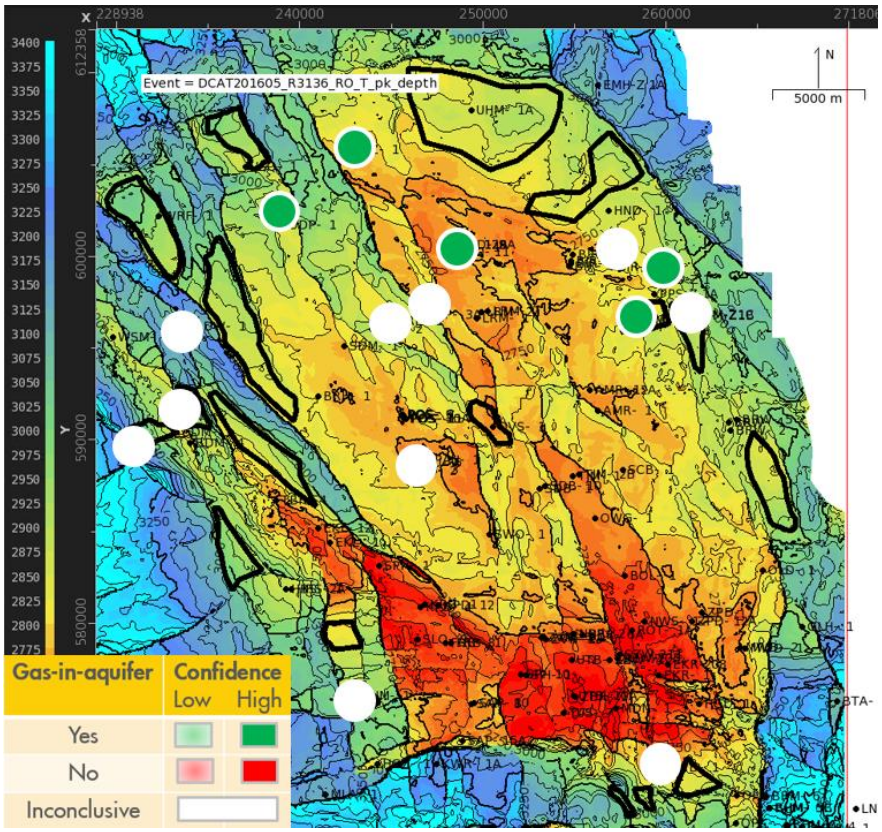

Figure 3-8: Spatial overview of inferred gas-in-aquifer from RFT data

3.4.4 Inference from PNL data

The full field dynamic modelling effort to date did not manage to provide a very good match of the rise in gas-water-contact as observed from PNL measurement interpretations. However, in this V6 model update, when introducing gas-in-aquifer, the aquifer becomes a lot more responsive.

From sensitivity modelling work, the following was inferred:

- Gas-in-aquifer is inferred to be present if it is impossible to obtain a GWC rise in the model without gas-in-aquifer.
- If the measured GWC rise is much lower than the response of the V6 model with gas-in-aquifer (in areas where the other data is well matched), it is inferred that there is no gas-in-aquifer.

If introducing gas-in-aquifer in the model does not impact the GWC, or if the PNL interpretation is questioned, the data is marked as inconclusive.

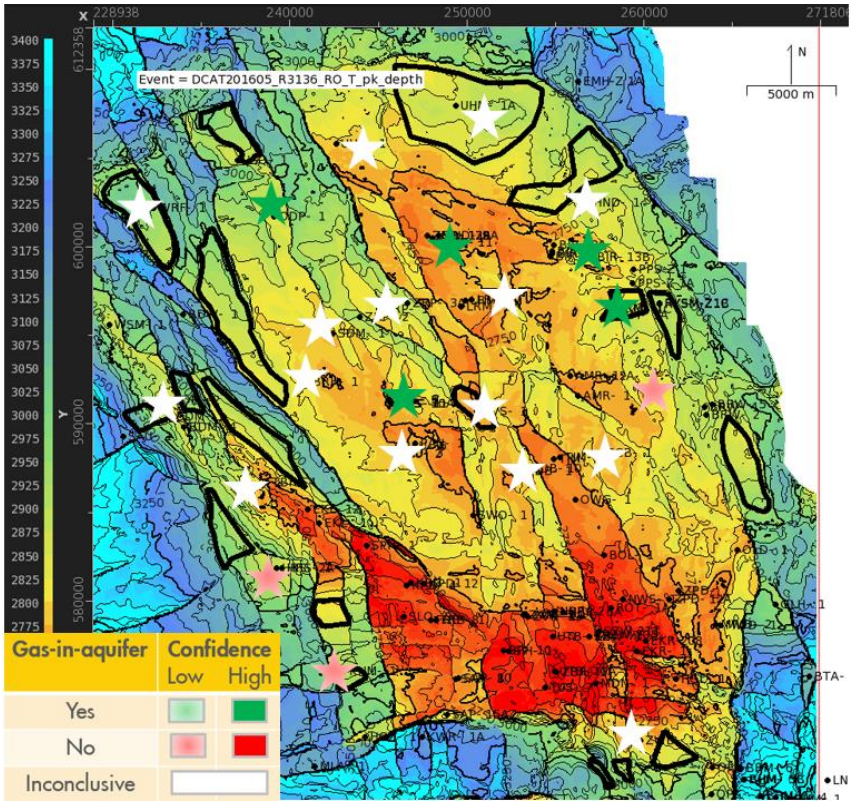

Figure 3-9: Spatial overview of inferred gas-in-aquifer presence based on PNL data

3.5 Integration of available data

The available indications of gas-in-aquifer presence are summarized in a map view in Figure 3-10. By itself, these were found to be insufficient to resolve lateral trends in the actual saturation values. However, interpretations can be conceived by relating observations on the lateral presence/absence of gas-in-aquifer to geological features (Figure 3-10 right-hand side).

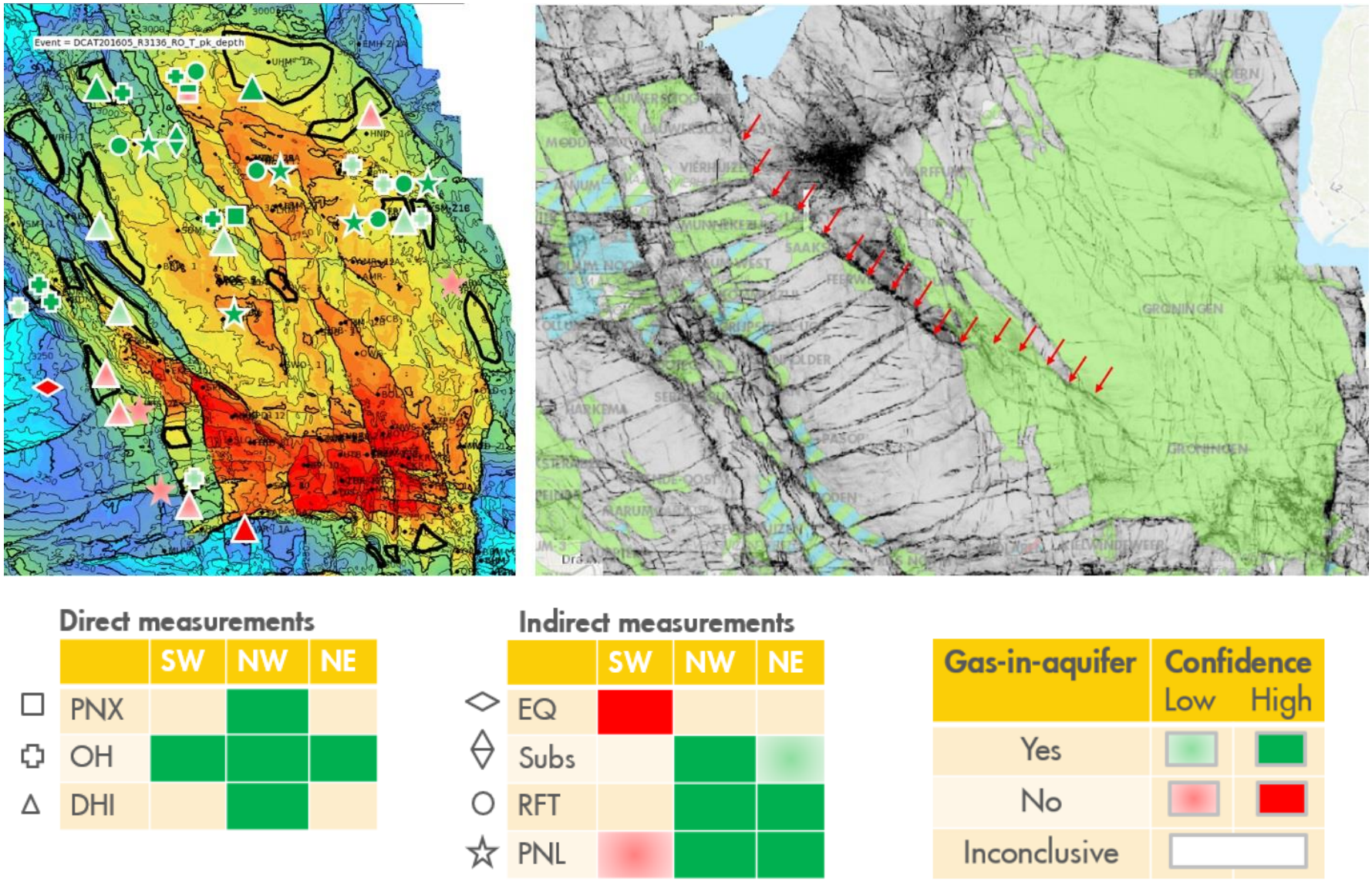

Figure 3-10: Inferred lateral extent of gas-in-aquifer (North of geological feature highlighted by red arrows)

3.6 Model implementation

3.6.1 Spatial extent of gas-in-aquifer

To implement the (spatial) observations of gas-in-aquifer across the entire full field model, a physical explanation of its occurrence was sought. Two hypotheses were developed.

Hypothesis 1 – Bottom charge

The bottom charge hypothesis assumes that the occurrence of gas-in-aquifer is a remnant from the charge history. In this hypothesis, gas from the underlying Carboniferous source rock would have percolated up through the Slochteren aquifer in a relatively homogeneous way, Figure 3-11. Consequently, gas can be present throughout the entire Slochteren, all the way down to top Carboniferous (Figure 3-14 left-hand graph).

Figure 3-12 gives an associated schematic on a pore scale. Gas-in-aquifer saturations would increase up to the critical gas saturation, after which (over geological time) gas starts to migrate along to the overlying trap, without changing the saturations. Consequently, the gas/water relative permeabilities should be modelled by a drainage process.

In the full field model implementation, the gas-in-aquifer saturation should be initialised in alignment with the available critical gas saturation data (from ZRP-3A SCAL drainage experiment), which is around 5%. These initial saturations could be reduced somewhat due to preferential charge paths and to reflect diffusion effects after the charge phase.

At the time this hypothesis was developed, it was fully supported by the available data. The initial PNX interpretation of well UHZ-1 indicated gas-in-aquifer saturations around 5% across the entire water leg.

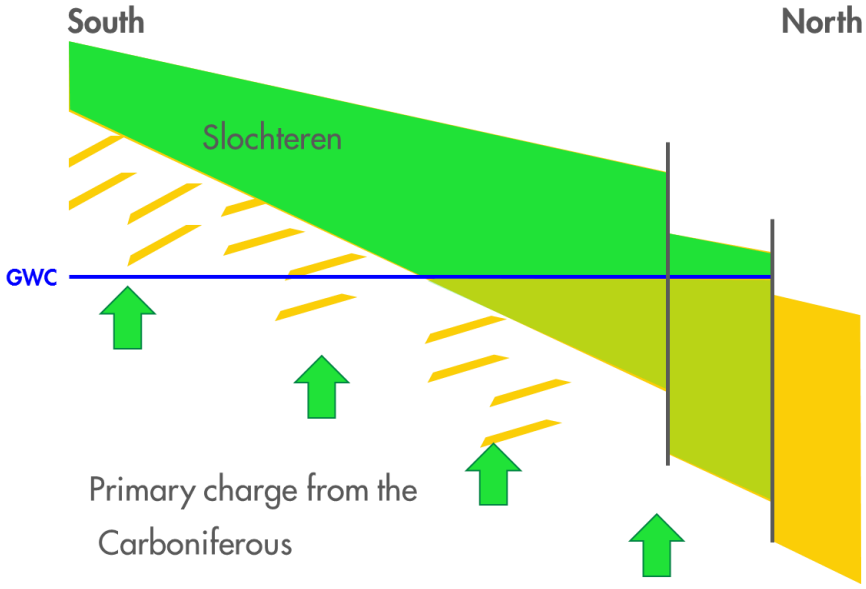

Figure 3-11: Schematic describing the occurrence of gas-in-aquifer as a result of bottom charge on a reservoir scale

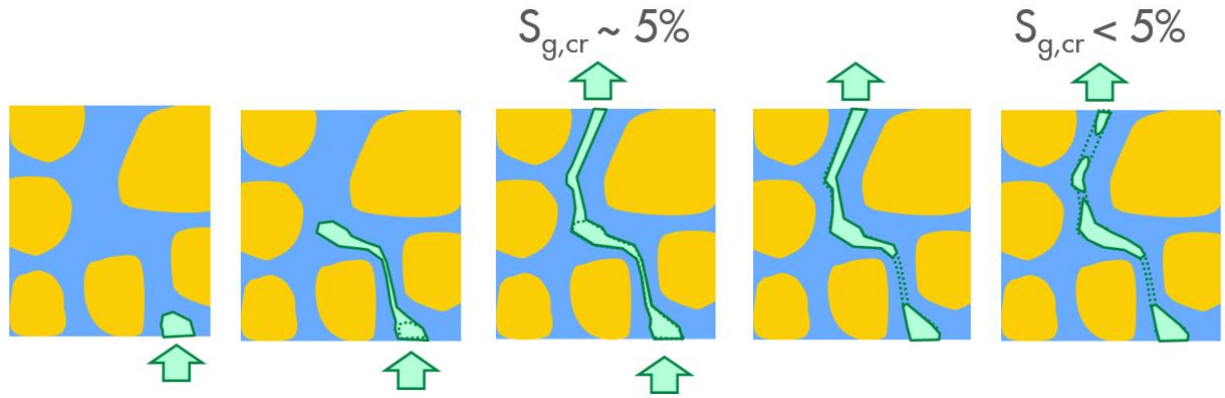

Figure 3-12: Schematic describing the occurrence of gas-in-aquifer as a result of bottom charge on a pore scale

Hypothesis 2 – Paleo-contact

A second hypothesis was derived in conjunction with basin modelling work, Reference [11]. This hypothesis assumes a paleo-contact, which is plausible given the burial and charge history of the Groningen field. Residual gas is present below the (present-day) Gas Water Contact, down to a palaeo-contact constrained by the spill-point for the Groningen closure at 3158mTVDSS (Figure 3-14 right-hand graph). Areal differences could be possible, given late secondary charge phase and differential uplift.

The gas-in-aquifer is residual gas, with water being the mobile phase. The relative permeabilities are the same as in the gas reservoir (imbibition), where the remaining gas saturation is around 22%.

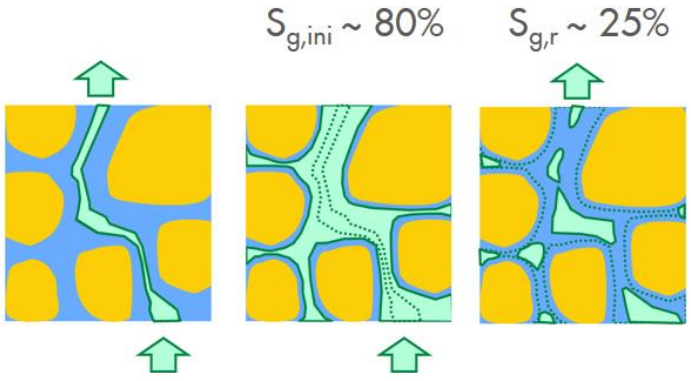

Figure 3-13: Schematic describing the occurrence of gas-in-aquifer due to a paleo-contact on a pore scale

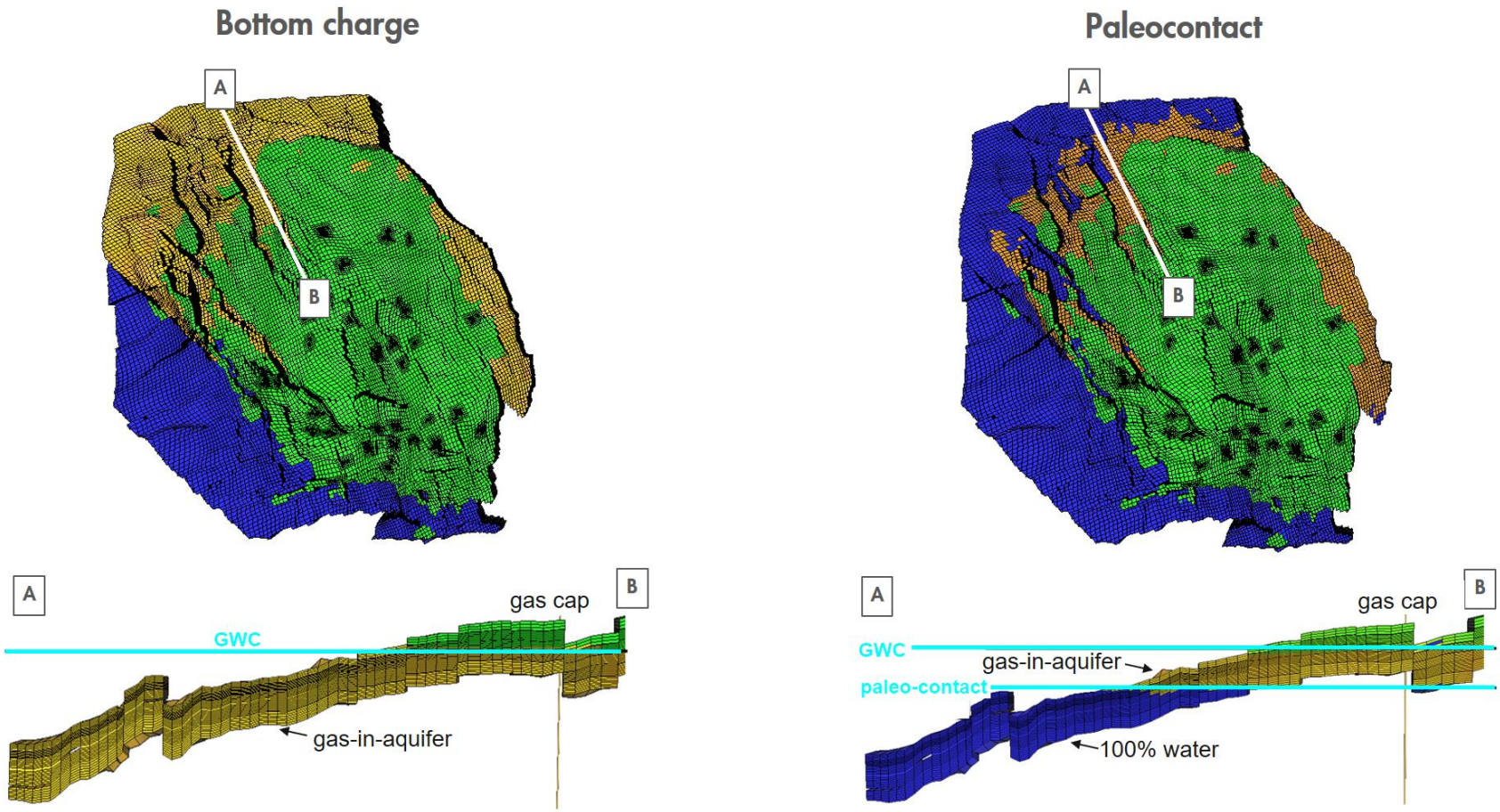

Figure 3-14: Hypotheses for initialisation of the full field model

3.6.2 Model initialisation

When including gas-in-aquifer, the initialisation of the dynamic model is a two-stage process. First, the model is initialised hydrostatically in a conventional way, without gas-in-aquifer. Next, mass accumulations are derived for all grid blocks within the gas-in-aquifer zone, based on the (residual) gas saturations. These mass accumulations overwrite the hydrostatically initialised grid blocks which do not contain any gas.[6]

3.6.3 Gas-in-aquifer relative permeabilities

Given the available data at the time of modelling, hypothesis 1 was implemented in the dynamic model: the water leg has observed only partial imbibition, whereas the gas leg has seen the full imbibition curve[7]. Hence the gas-in-aquifer relative permeabilities are implemented different from those in the gas reservoir. There is no SCAL data to support the expected differences, but it is likely that over geological time, the wettability of the paleo gas has developed differently from the gas leg.

The relative permeabilities are described using Corey models. Dedicated sets of Corey parameters were defined for the gas reservoir and for the gas-in-aquifer. The different Corey exponent for the gas might provide a faster/slower migration of the gas below the free-water-level, Figure 3-15.

[6] An alternative option is to initialise the model hydrostatically, then insert the residual gas saturations which are initialised by a P_SAT initialisation. This automatically calculates the correct mass accumulations.

[7] Given the recent petrophysical, basin modelling and ZRP-3A core study work the paleo contact scenario (hypothesis 2) seems probable and is worth testing in the dynamic model.

	Relative permeability curves (linear scales)	Relative permeability curves (semi-log scales)	Fractional flow curves
Gas reservoir	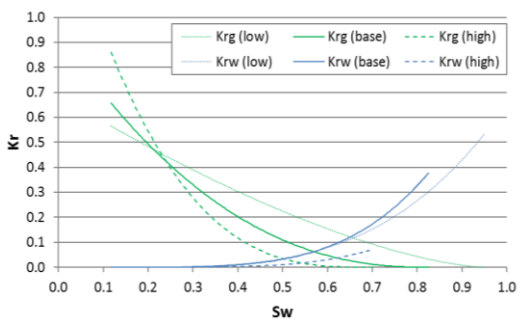	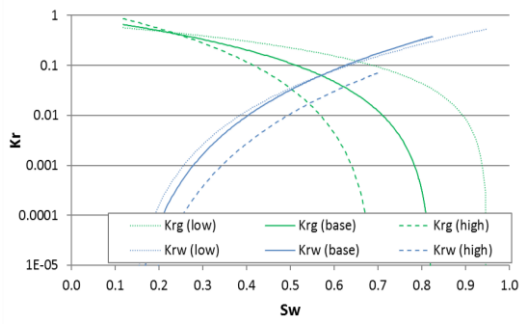	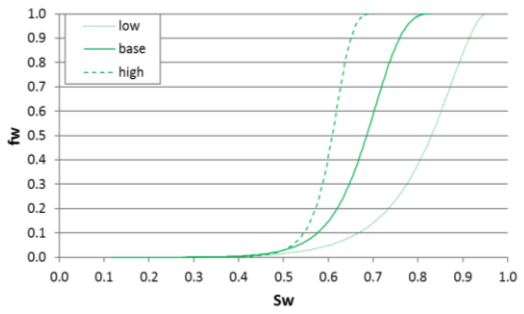
Gas-in-aquifer	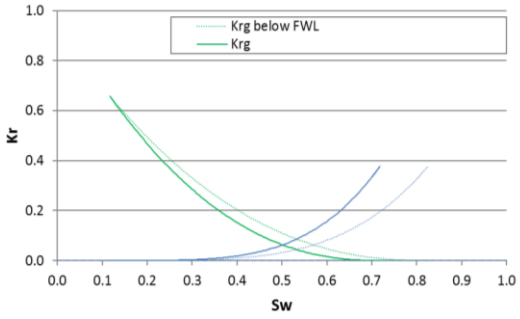	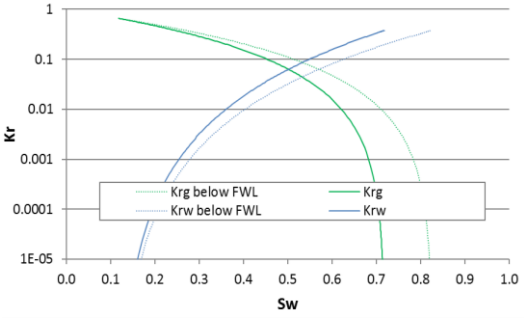	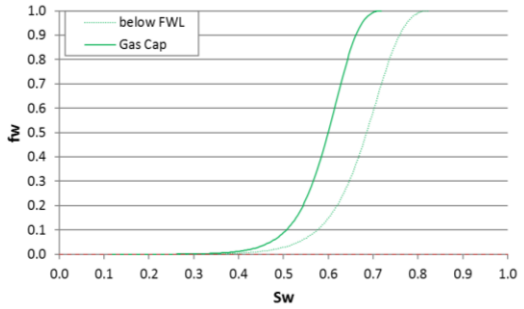

Figure 3-15: Relative permeability models for gas reservoir and for gas-in-aquifer

3.6.4 History matching variables

Four history matching variables were used to capture the dynamic effect of gas-in-aquifer (section 7.1):

- Areal presence of gas-in-aquifer
- Initial saturation of gas-in-aquifer
- Critical gas saturation of gas-in-aquifer, $S_{g,cr}$
- Corey exponent of gas-in-aquifer, n_g

4 Carboniferous

4.1 Modelling objective

Depletion of the Carboniferous will have an impact on the long-term subsidence modelling and seismological modelling. The Carboniferous reservoir is included in the V6 model such that different depletion scenarios of the Carboniferous can be further progressed in the long-term subsidence and seismological modelling workflows.

The V6 model develops a best matched Carboniferous depletion scenario, from which parameters can be changed to generate alternative depletion scenarios in later work.

4.2 Static modelling

4.2.1 Data availability

The first Groningen well that penetrated the Carboniferous was Delfzijl-1 in 1960. In the early 1980s, the Carboniferous sands underneath the Groningen Field were appraised by deepening 16 wells from the Rotliegend and by drilling 3 new wells. No dedicated Carboniferous drilling was done thereafter, except for Uithuizermeeden-2 in 2001 which targeted deep Carboniferous formations well below the Groningen contact.

Earlier work on the Carboniferous was done to investigate the feasibility of a commercial reservoir development, References [12] and [13] . The work inventorized the available data, which comprises:

- Well penetrations: 219 wells [14]
- Well logs: 39 wells [15]
- Spot cores: 25 wells [13]
- Core intervals: 5 wells [15]
- Capillary pressure data: 2 wells [13]

4.2.2 Geological overview

The Carboniferous formations are part of the Limburg Group, Figure 4-1, which was deposited in a period of thermal sag during the Silesian (Middle-Late Carboniferous). Subsidence rates were very high and due to the erosion of the rising Variscan mountain belt in the south a vast amount of clastic sediment was transported into this foreland basin. The Westphalian deposits in the Groningen area have been deposited in a sedimentary environment characterised by poorly drained floodplains, delta-plains and pro-delta lacustrine conditions.

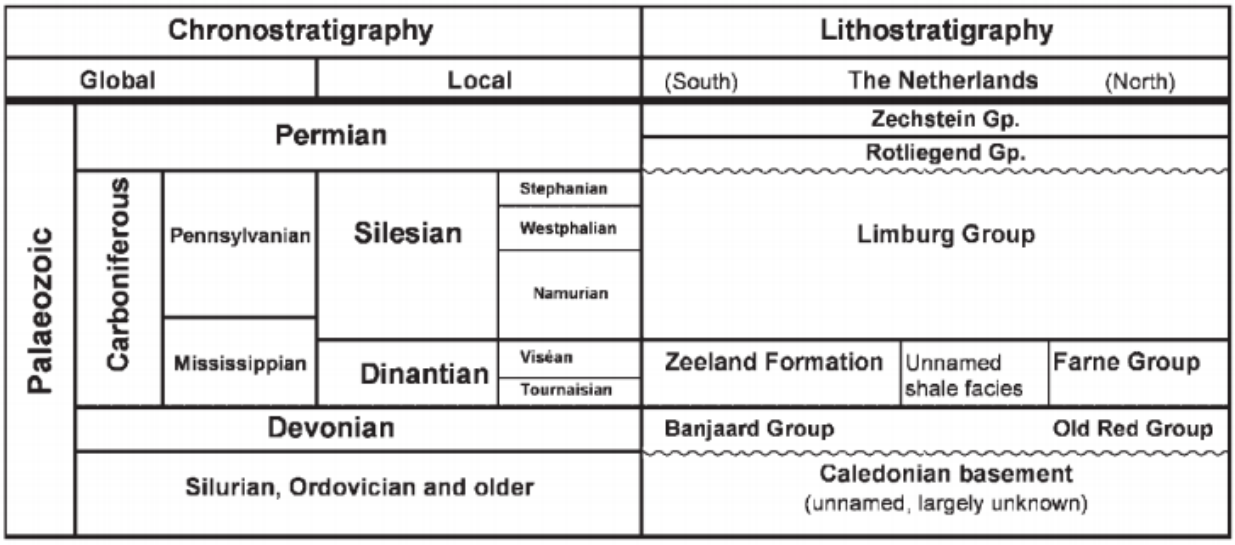

Figure 4-1: Lithostratigraphic and chronostratigraphic chart with detail on the Carboniferous, source: Van Hulten and Poty, 2008.

A regional cross-section of the Carboniferous stratigraphy is given in Figure 4-2. A Base_Rotliegend subcrop map of the Groningen area is given in Figure 4-3. Figure 4-4 shows the outline of the gas-bearing Carboniferous section. The penetrated stratigraphic interval of all wells in the area is depicted in Figure 4-5. In the upper 300m of the Carboniferous the fluvial lacustrine Ruurlo Formation is dominant (95% shale/siltstone, 5% sand). The Ruurlo formation consists of floodplain and fluvial deposits. The underlying Baarlo Formation has more deltaic intervals.

The Rotliegend fault pattern commonly extends into the Upper Carboniferous and occasionally deeper. However, the Carboniferous has a more structurally complex history than the overlying Rotliegend due to N-S Asturian compression which was followed by thermal uplift, peneplainisation and subsequent removal of locally more than 1500 meters of vertical Carboniferous succession of sediments prior to Permian deposition. As such, the compartmentalisation of the Carboniferous sequence is much stronger.

The Carboniferous encountered at the well penetrations was in most cases dominated by clay-rich sediments, with only poorly developed channel deposits and no sand development trends could be defined. Gas-bearing Carboniferous sandstones were found to be present mainly in the area below the southern part of the Groningen Gas Field down to at least the Rotliegend spill point. Production tests showed poor deliverability and/or very small connected volumes.

A comprehensive petrophysical review of the Carboniferous section of the Groningen Field was performed in 1994, Reference [15]. During this review, methodologies for determining Net Sand, porosity and saturation from the available logs suites were developed and applied in 30 wells from across the field. Subsequently, in 2004-2006, the Carboniferous log evaluations from 21 Groningen wells were QC-ed and in some cases revised to enable preliminary assessment of GIIP and recovery factors, Reference [13]. As part of this work, first pass porosity-permeability relationships and saturation height functions were also

developed. It should be noted that given the paucity of reference core data from the Carboniferous interval in the Groningen area, these relationships were established on the basis of data from analogue Carboniferous fields in other parts of the Netherlands.

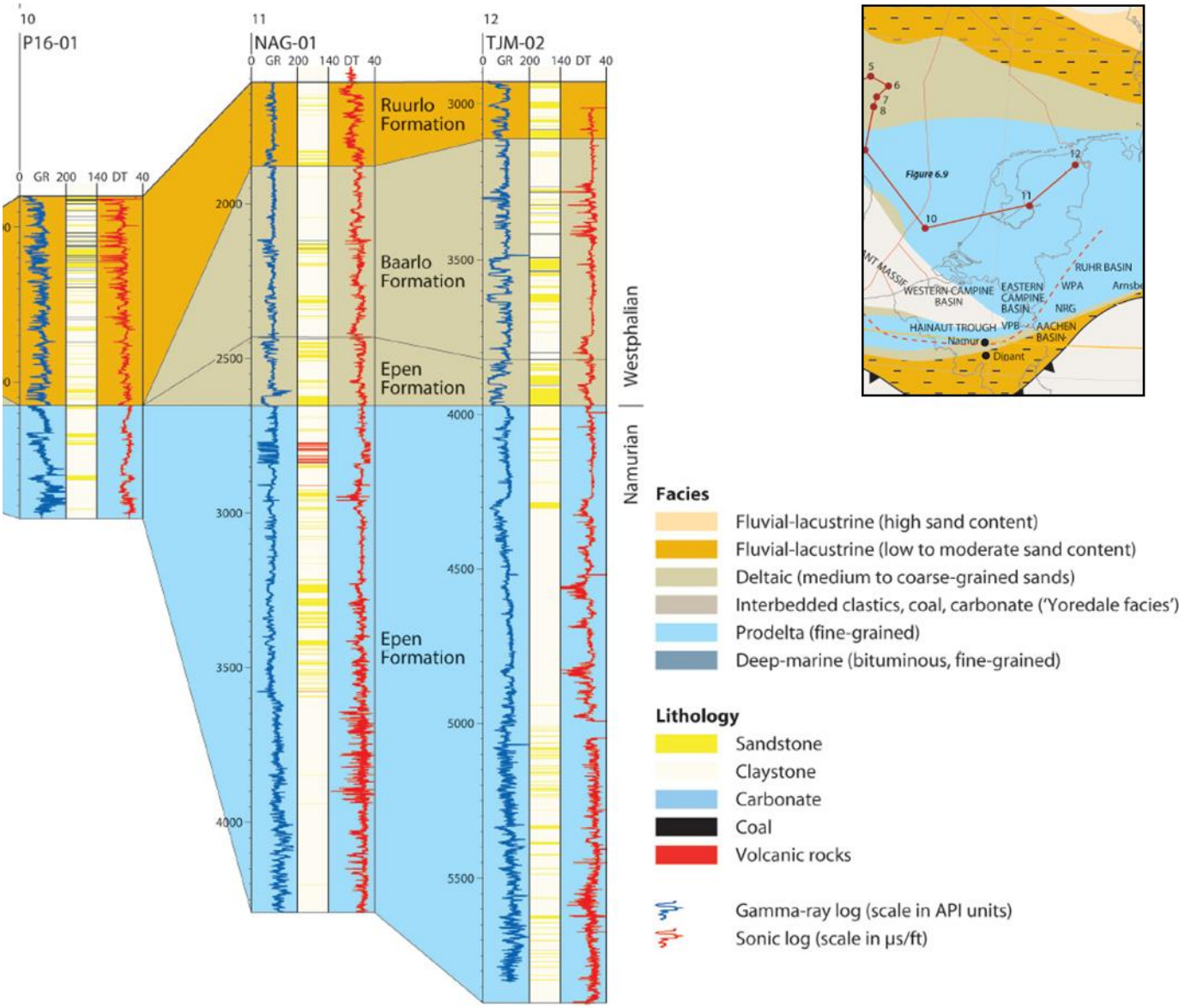

Figure 4-2: Regional Carboniferous stratigraphy, source: Southern Permian Basin Atlas, TNO, 2010

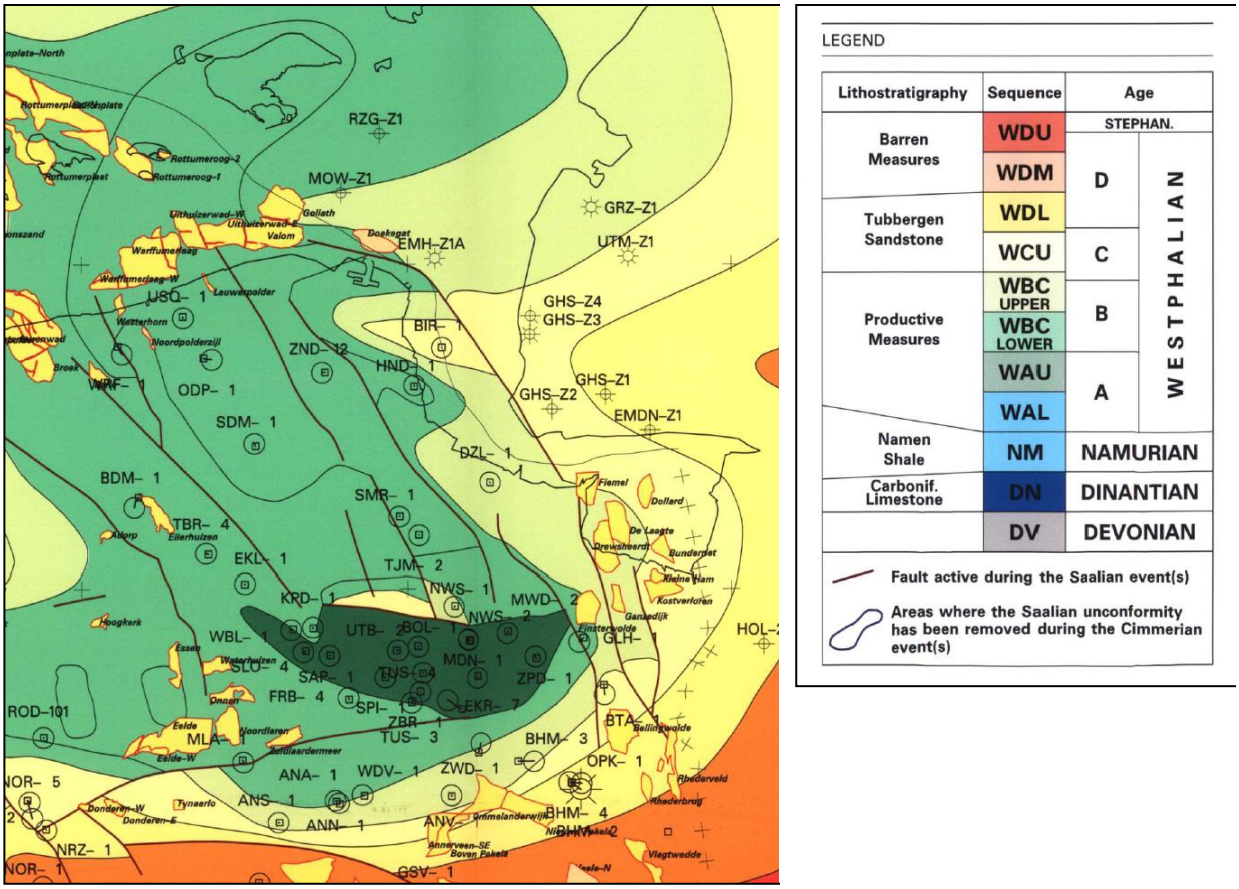

Figure 4-3: Carboniferous subcrop map of the Groningen area, Den Hartog Jager et al., 1993

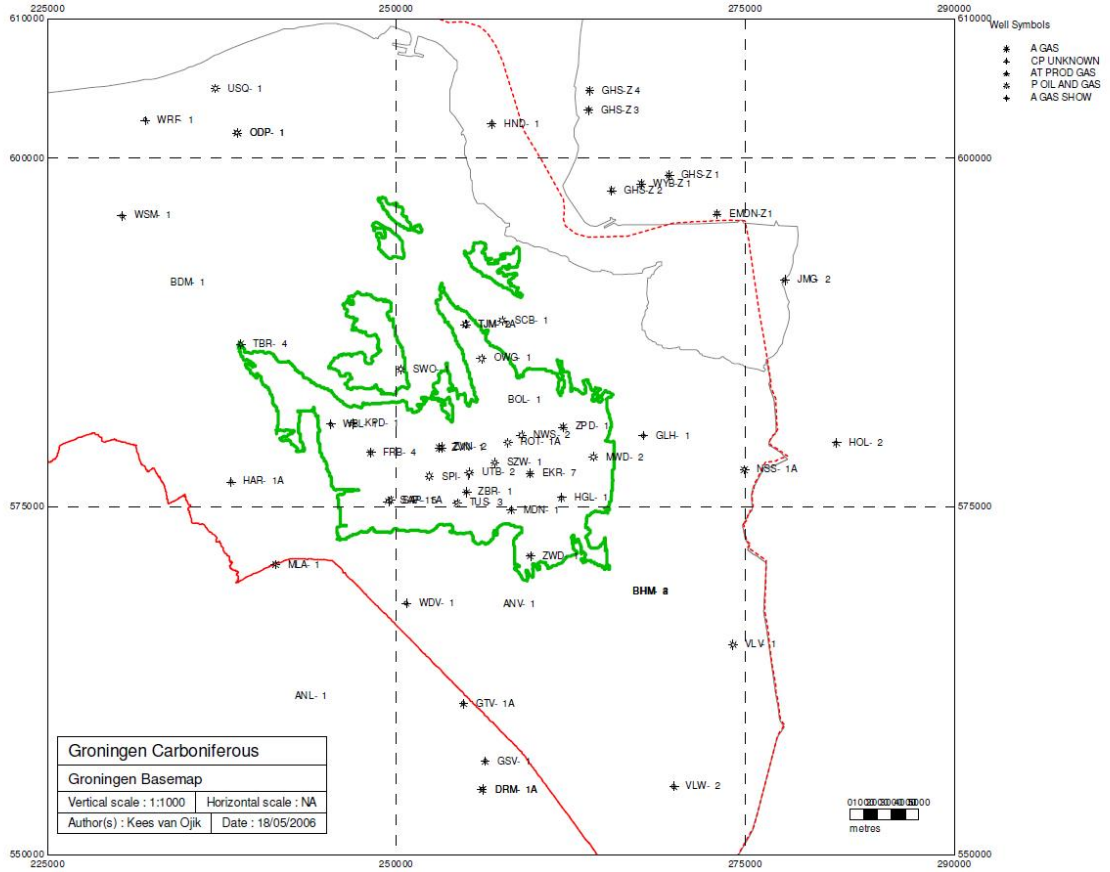

Figure 4-4: Outline of the gas-bearing section of the Carboniferous in the Groningen area, Van Ojik, 2008

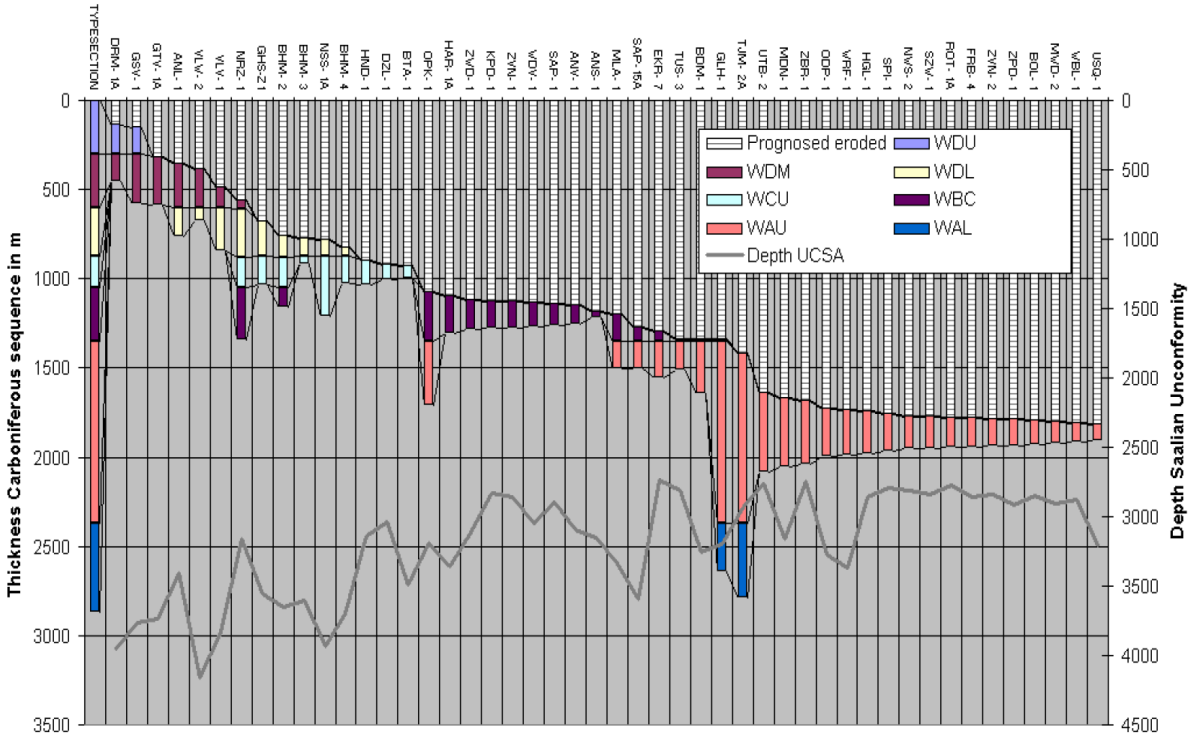

Figure 4-5: Carboniferous stratigraphy of Groningen well penetrations, Van Ojik, 2008

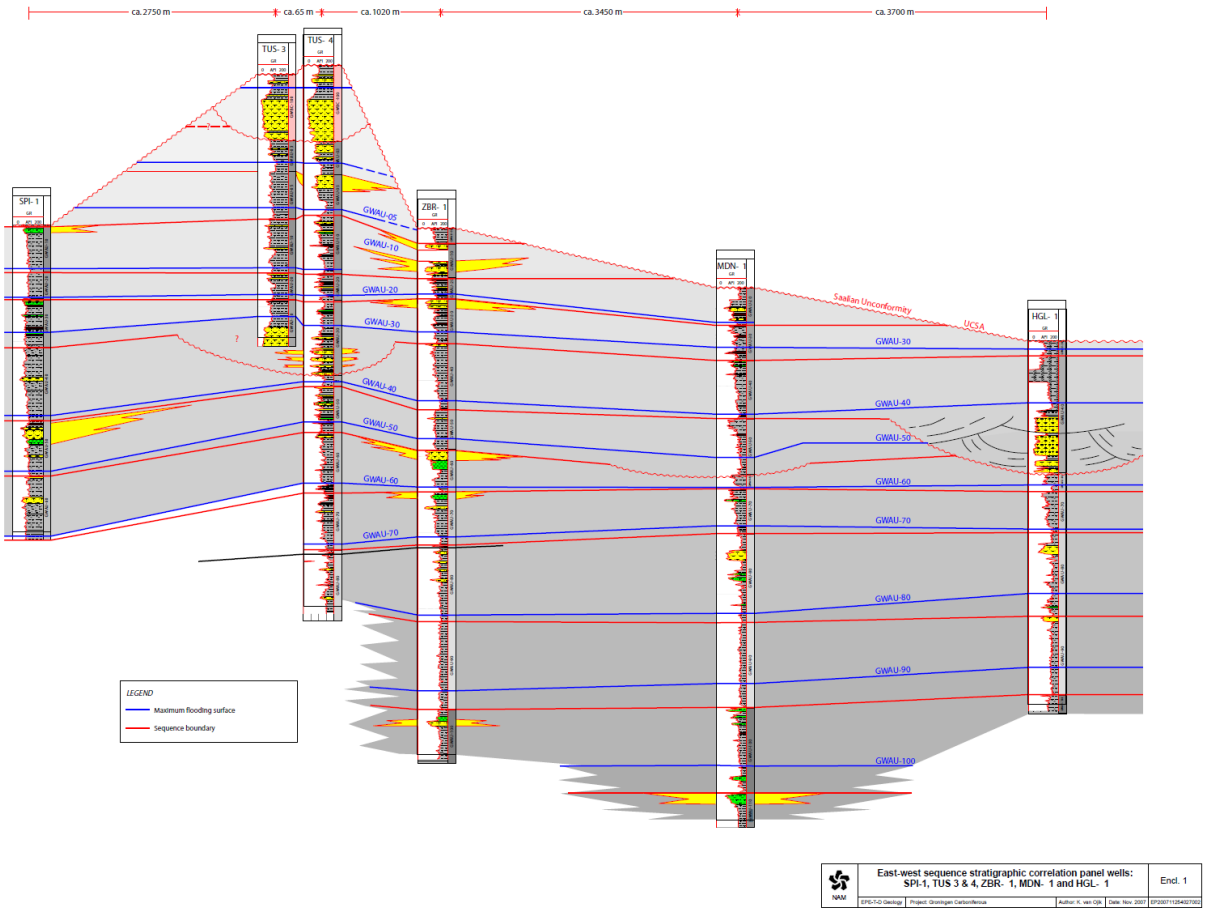

Figure 4-6: Groningen area sequence stratigraphic correlation, Van Ojik, 2008

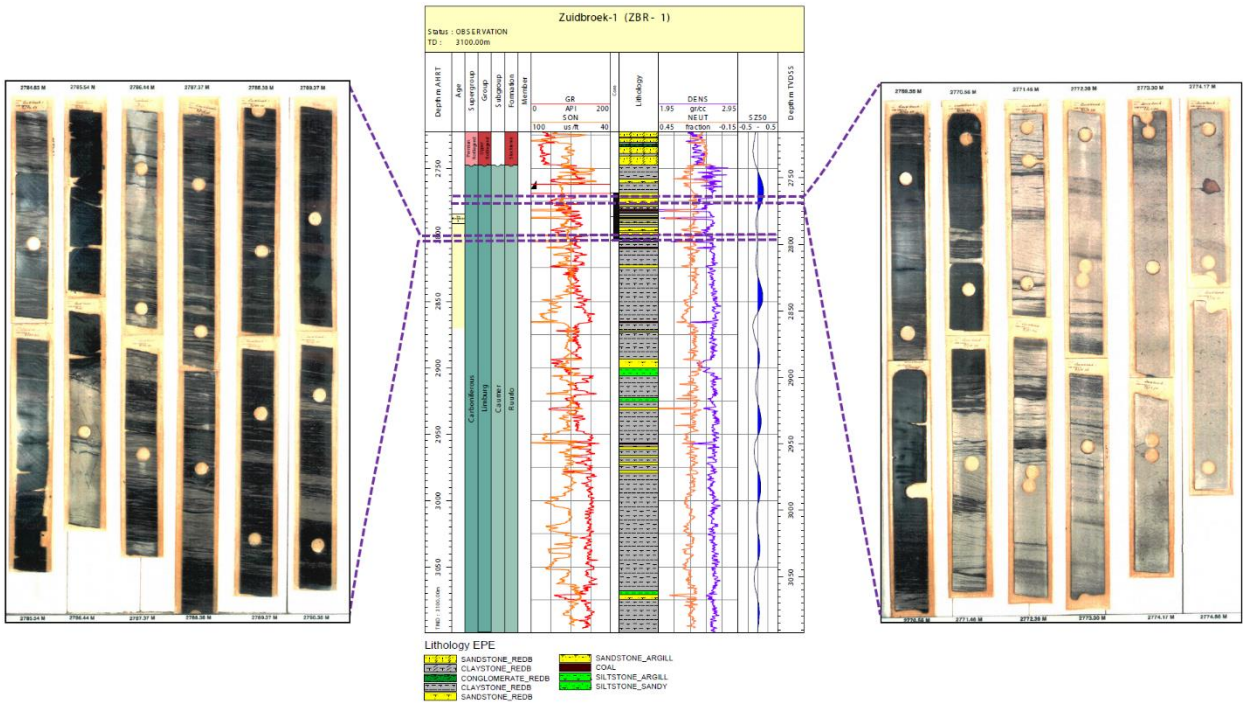

Figure 4-7: Cored sections from Zuidbroek-1

4.2.3 Modelling strategy

To meet the modelling objective, some level of vertical and lateral granularity is needed. However, the limited available data in combination with a high degree of vertical and lateral heterogeneity does not justify building detailed static labyrinth-type models. Therefore, a simple and pragmatic approach was taken:

1) The Carboniferous was built into the full field model by downward isopaching of the Base_Rotliegend surface (Figure 4-8). This simplified approach was taken because the available data provides insufficient geological control to properly reflect the architecture of the angular unconformity formed by the interface between the Carboniferous and the Rotliegend (the Saalian unconformity). Moreover, a correct representation of the angular unconformity would lead to too high complexity of the static (and dynamic) model grid.

2) There is a lack of information on the lateral spread of properties in the Carboniferous to capture the actual heterogeneity. Constant static reservoir properties were assumed to populate the entire Carboniferous, and were varied in scenario analyses. The reference model was populated with property values based on averages from the available log and core data:

   Porosity = 6.3 %

   Permeability = 11.8 μD

   NtG = 0.2

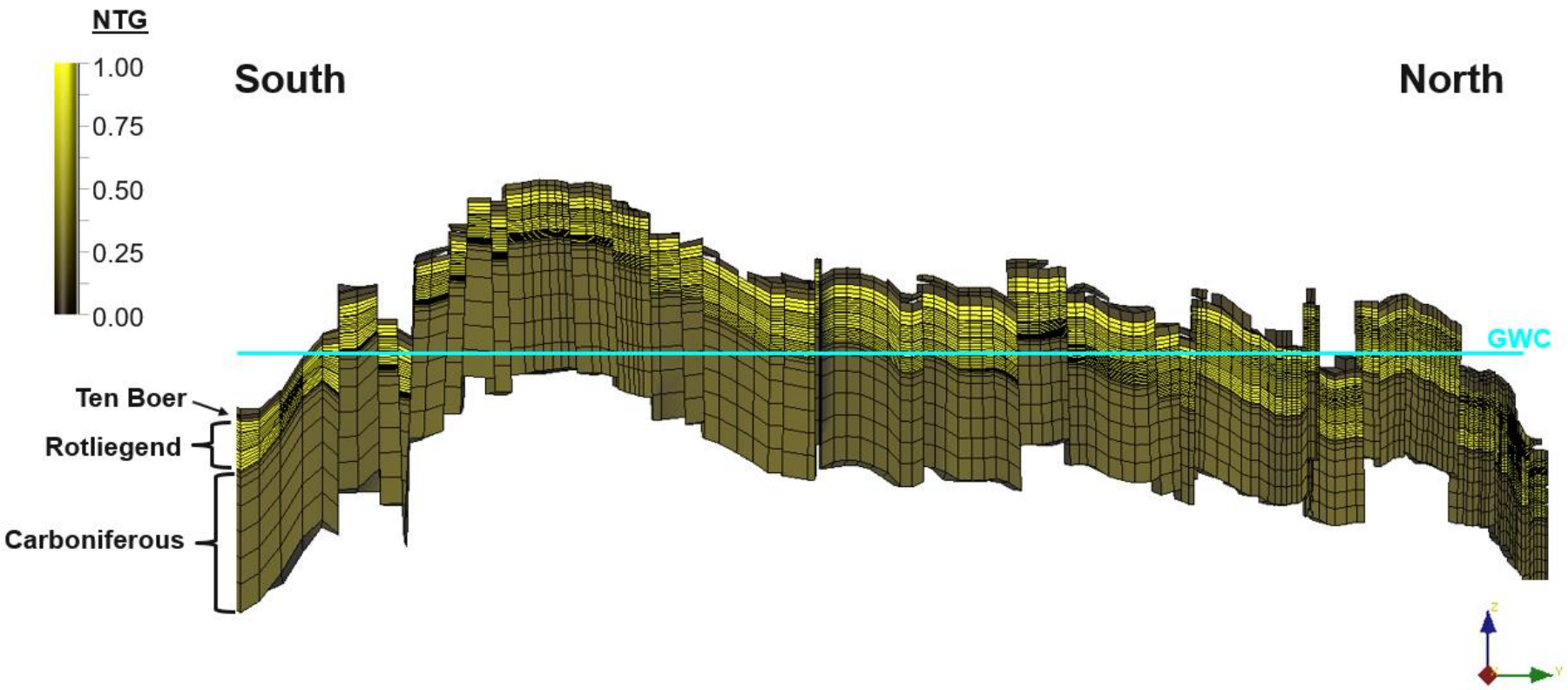

Figure 4-8 North-South cross-section through the simulation grid.

4.3 Indication of depletion

Indications of depletion of the Carboniferous were derived/inferred from a variety of sources.

4.3.1 Pressures

Pressure measurements of the Carboniferous have been obtained from RFTs, FITs and FBUs on multiple wells, Reference [16], as well as from SPG measurements on MDN-1 and HGL-1. A schematic of the available pressure measurements is given in Figure 4-9. Overall, the data shows that some of the Carboniferous sands are depleting, but others are not. Furthermore, depletion can be very local (e.g. wells ZBR-1 and ZPD-1 have observed depletion in a shallow sand layer, but no depletion in a deeper sand layer).

In addition, the quality of the pressure measurements is often impaired due to a variety of reasons:

- Unfinished build-ups from RFT measurements, e.g. ZPD-1.
- Uncertainty on the source of the observed depletion in the sands:
    - KPD-1 is potentially being drained by an earlier well test of KPD-4 in the same Carboniferous sand.
    - The cement bond log on well HGL-1 suggests that there could potentially be a leak path from the Carboniferous to the Rotliegend
- The vertical variability in depletion (e.g. shallower sands are encountered at virgin pressure and deeper sands are found depleted in ZBR-1)
- Reservoir impairment due to unfavourable drilling practices

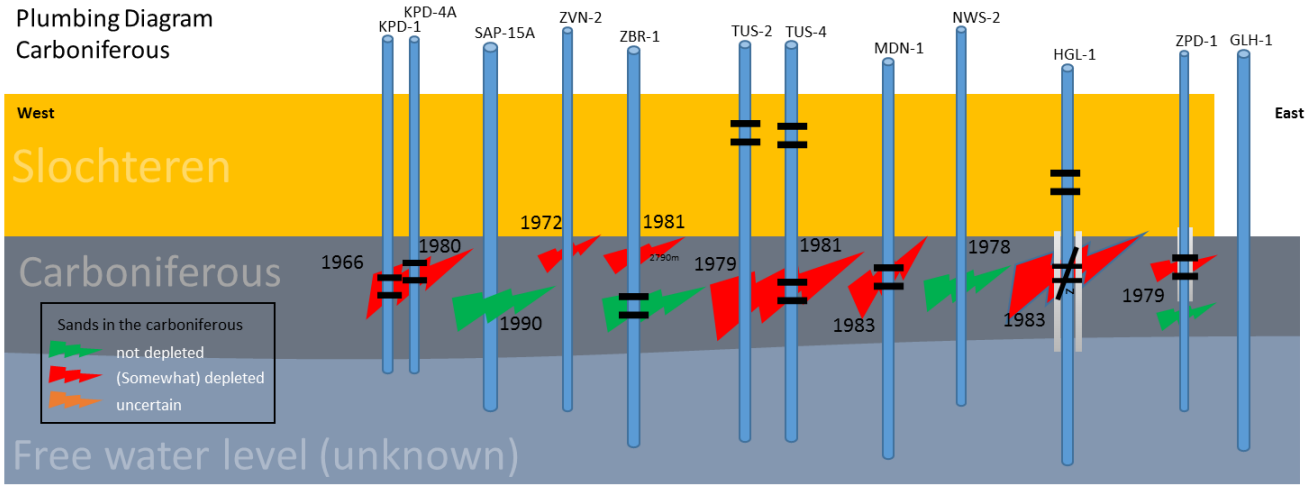

Figure 4-9: Schematic overview of observed reservoir depletion in the Carboniferous as from Reference [17]. The red sections indicate depleted sands, the green sections indicate virgin sands.

4.3.2 Strain

Carboniferous strain measurements are available from the distributed strain sensing cable (DSS) in Zeerijp-3A. The DSS cable in Zeerijp-3A has measured non-zero strain values along the entire Carboniferous interval over the measurement period from May 2016 until November 2017, thereby indicating depletion. The strain measured is in the water bearing Carboniferous in the north of the field as indicated in Figure 4-11.

Note that also CMI measurements have been carried out in the Carboniferous in some wells. The CMI measurements will be reviewed and interpreted by Baker Hughes. This is work in progress and therefore not included in the V6 modelling work.

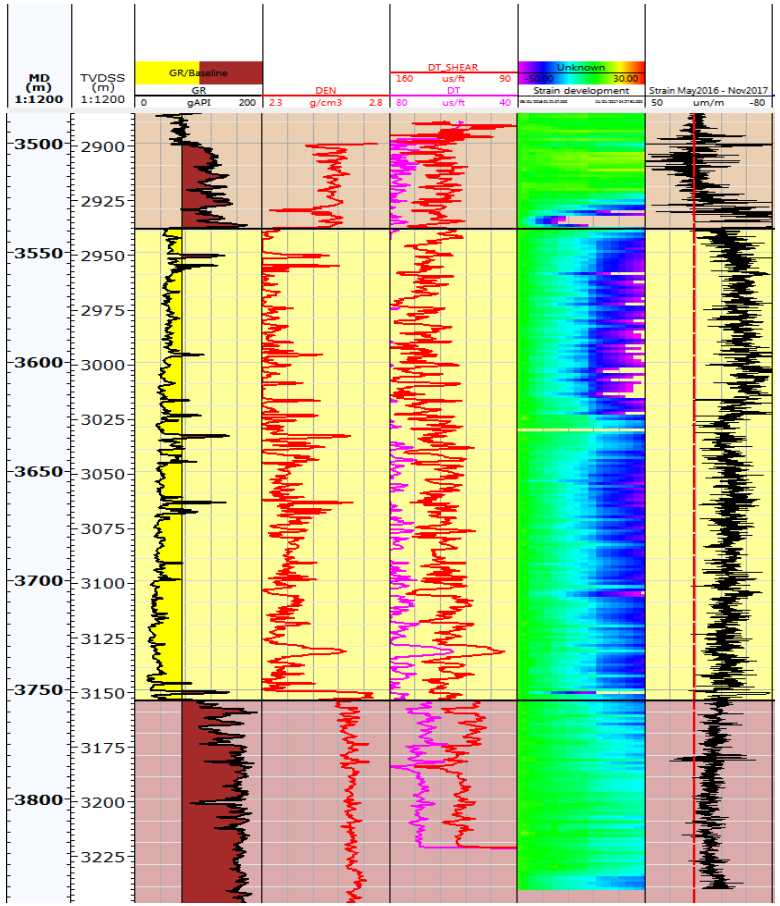

Figure 4-10 Zeerijp-3A GR, density and sonic logs. The second last overview shows strain development over time, the most right overview shows the total strain measured from May 2016 to November 2017.

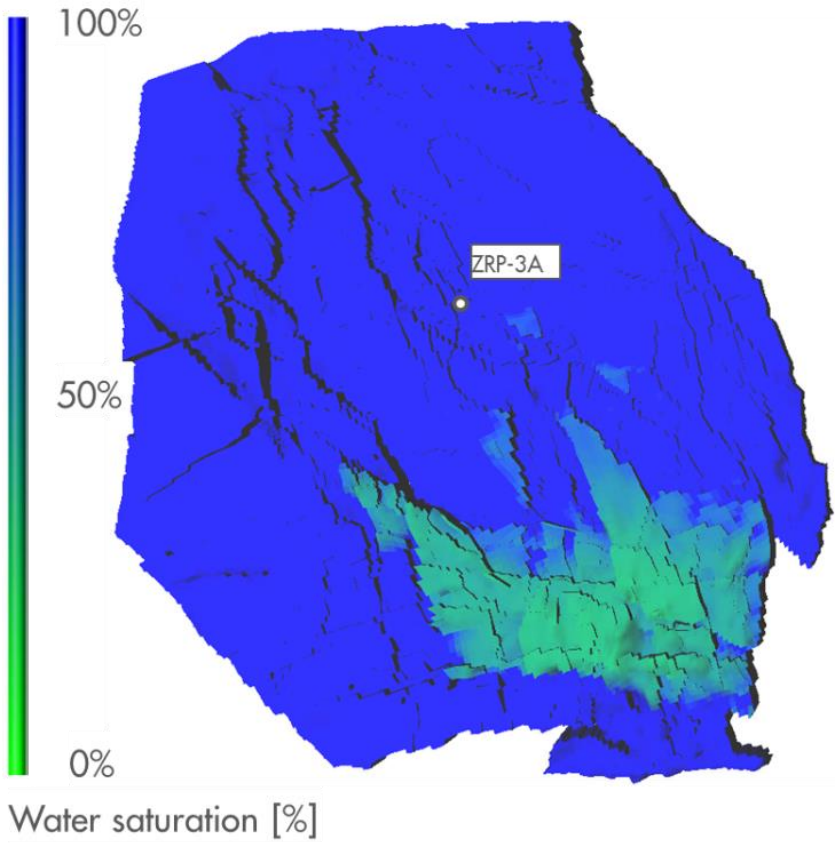

Figure 4-11 Initial gas saturation in the top Carboniferous layer in the V6 model. The location of the ZRP-3A well providing strain measurements from the DSS cable is highlighted.

4.3.3 Subsidence

In previous models, the subsidence in some areas in the south of the field was underestimated. The left-hand picture in Figure 4-12 shows the subsidence match as obtained from the V5 model, highlighting the outline of the gas bearing Carboniferous. The right-hand picture shows the height above the FWL of the Carboniferous. Several areas show an underestimate of subsidence in the model (coloured blue), which seem to coincide with the thicker gas bearing Carboniferous areas and could be indications of depletion.

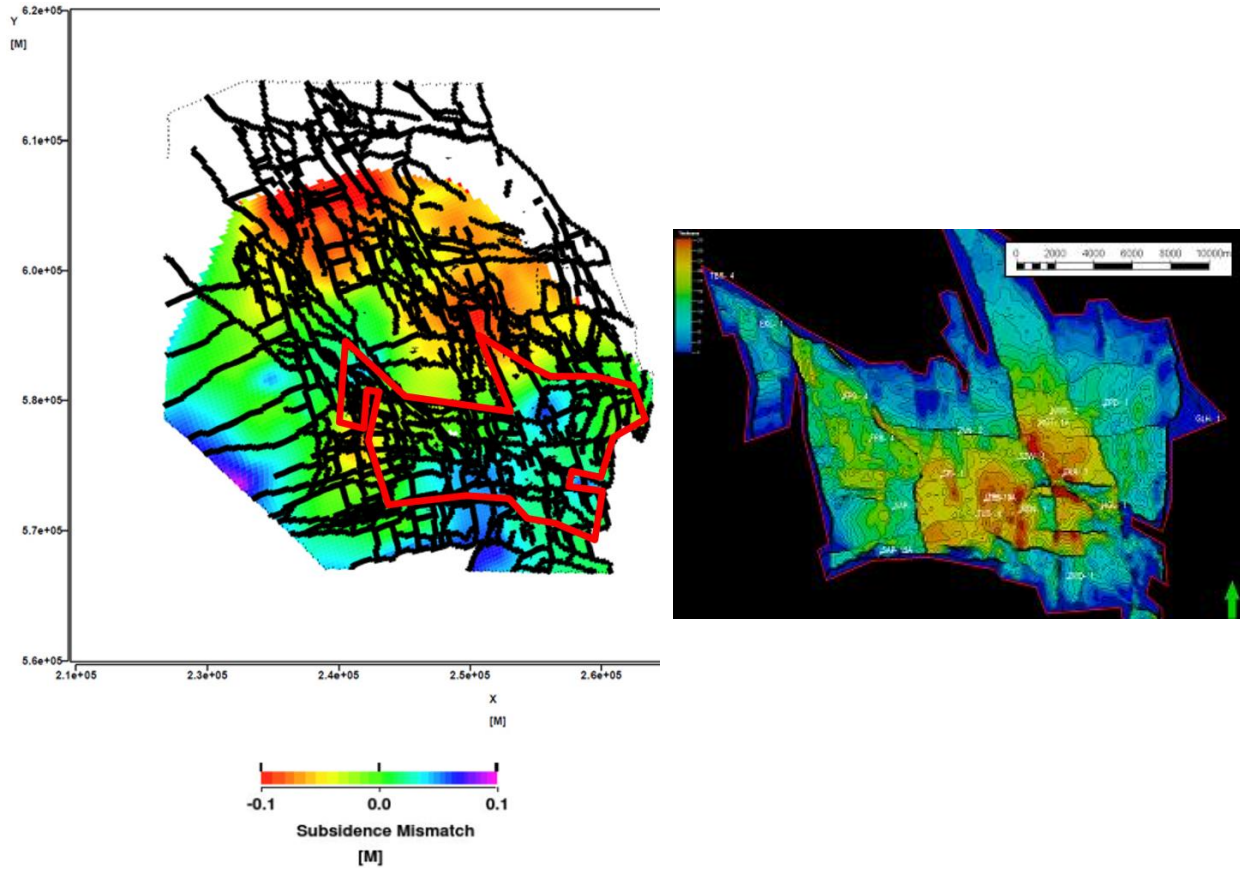

Figure 4-12 Left: V5 subsidence match using the initial compressibility estimate where compressibility is a polynomial function of porosity [2]. The figure shows the difference of the model output and the measurement. Warm colours indicate too much subsidence, cold colours indicate too little subsidence and a good match is green. Right: Carboniferous height above FWL as from [12].

4.3.4 Gravity

When calculating synthetic gravity data for previous models, it was observed that insufficient gravity reduction was modelled in the south of the field, see Figure 4-13. This lack of gravity change can be related to a lack of mass reduction.

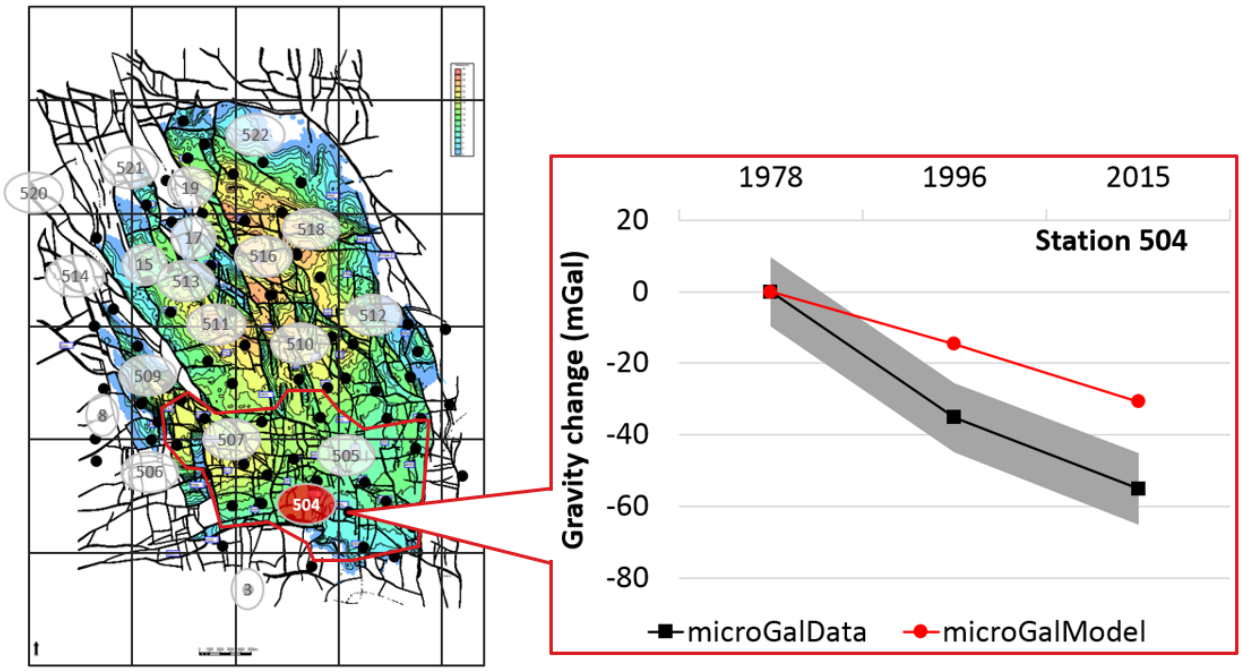

Figure 4-13 Measured (black) versus modelled (red) gravity change for Station 504, including uncertainty band (shaded).

A sensitivity analysis was done to investigate the impact of a depleting Carboniferous on the gravity field, Reference [18]. The potential depletion of the Carboniferous was tested with synthetic scenarios. A 3D model was built to investigate the impact of a potential mass reduction in the Carboniferous. The Matlab grid which is used to evaluate the mass changes as obtained from the dynamic reservoir simulation model was locally expanded in the South to include the depleting Carboniferous formation. In light of the combined uncertainty in net sand and depletion, it was assumed that the entire Carboniferous closure can be represented as a homogeneous tank, e.g. using single parameters to reflect average static and dynamic properties. Two scenarios were tested:

- Scenario 1: includes a Carboniferous with a GIIP of 100 N.Bcm of gas and an 80 bar pressure drop.
- Scenario 2: includes a Carboniferous with a GIIP of 150 N.Bcm of gas and a 100 bar pressure drop.

It was found that the inclusion of a depleting Carboniferous below the Groningen field can improve the gravity match, Figure 8-11.

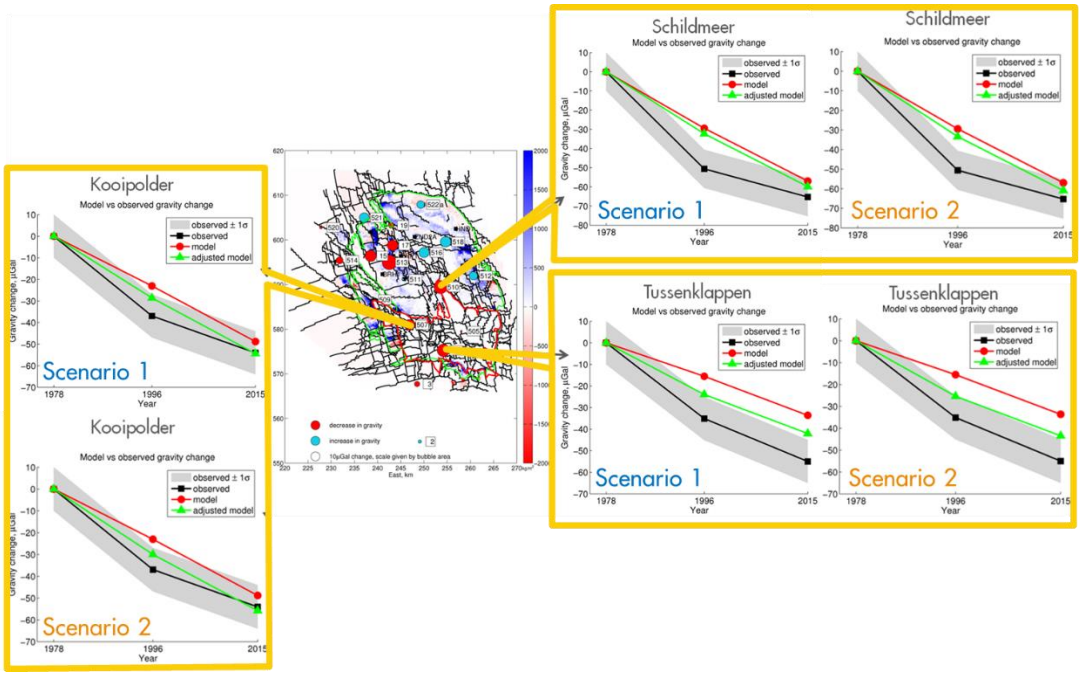

Figure 4-14 Sensitivity analysis of different Carboniferous scenario's to the Groningen gravity match.

4.4 Dynamic model implementation

4.4.1 Vertical upscaling

To meet the modelling objectives, a certain minimum vertical grid resolution is required to capture the vertical pressure gradient in the Carboniferous.

The extended static model includes 60 voxel layers within the Carboniferous. Various upscaling schemes were tested, Figure 4-15. The impact of the upscaling schemes on the total calculated compaction for the Carboniferous is given in Figure 4-16: no significant changes in compaction (and thus depletion) was found beyond upscaling to 8 zones. The effects of upscaling on runtimes, GIIP and ultimate recovery for the Carboniferous are shown in Figure 4-17. Upscaling below 4 layers results in instabilities in GIIP and recovery. Runtimes are not significantly affected by introducing more layers to the Carboniferous.

The final upscaling scheme applies an increasing thickness with depth, thus avoiding big thickness variations across the Carbonifeous/Rotliegend interface to minimize numerical dispersion whilst limiting the grid size and run times (highlighted in Figure 4-15).

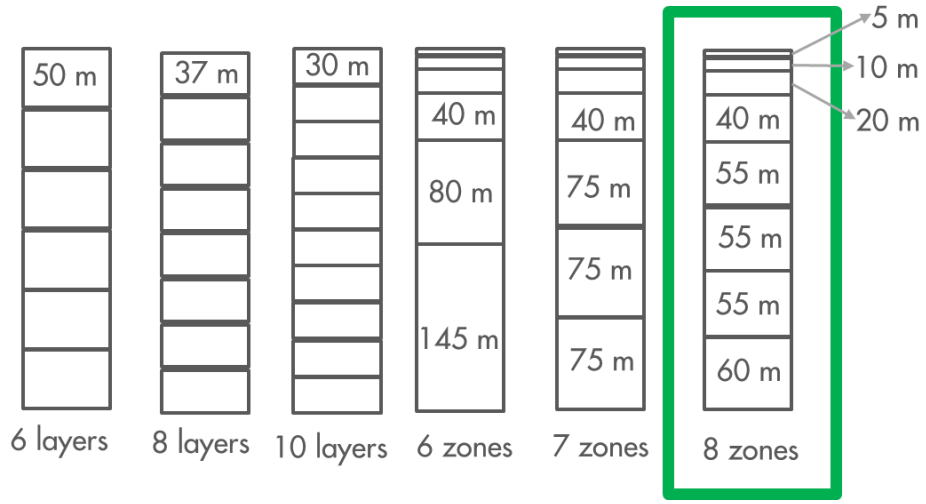

Figure 4-15 Schematic drawings of different tested upscaled Carboniferous grids with grid block thickness indicated.

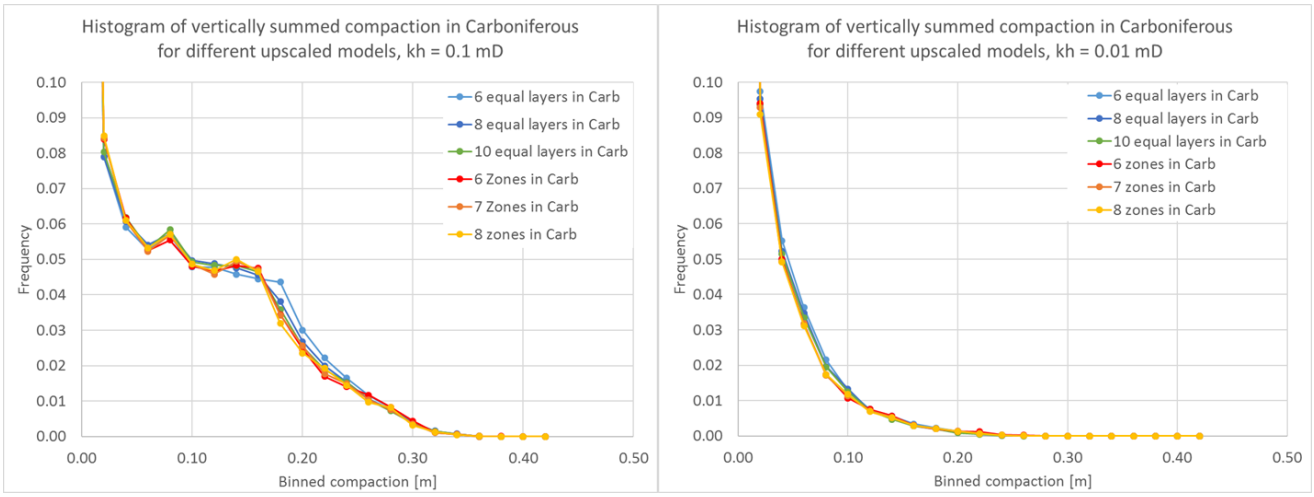

Figure 4-16 Histograms of summed compaction from Carboniferous for different upscaled grids. Left: histogram for a well-connected Carboniferous. Right: histogram for a not well-connected Carboniferous

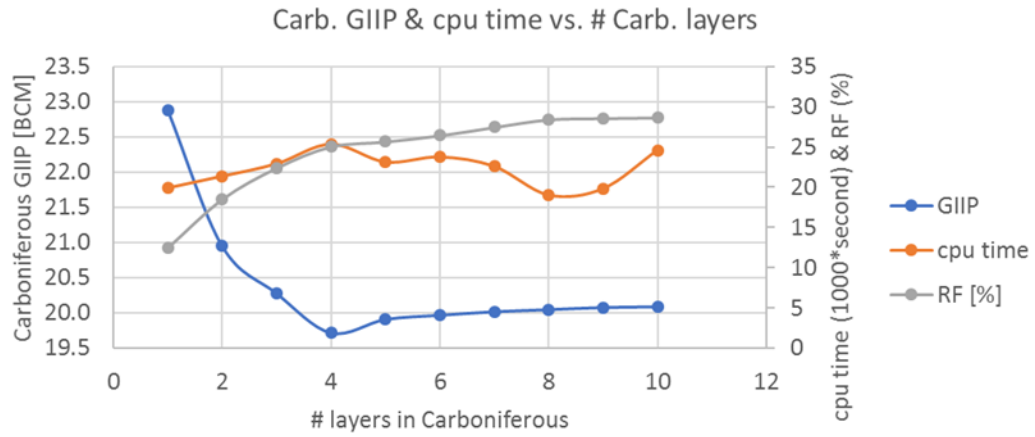

Figure 4-17 GIIP, RF and computer time for full field simulations with an increasing number of Carboniferous layers.

4.4.2 Capillary pressures

Capillary pressure curves were fitted to the available Carboniferous saturation height data, Reference [13]. The Carboniferous capillary pressure curves show a distinctly poorer rock quality as compared to the Rotliegend, Figure 4-18.

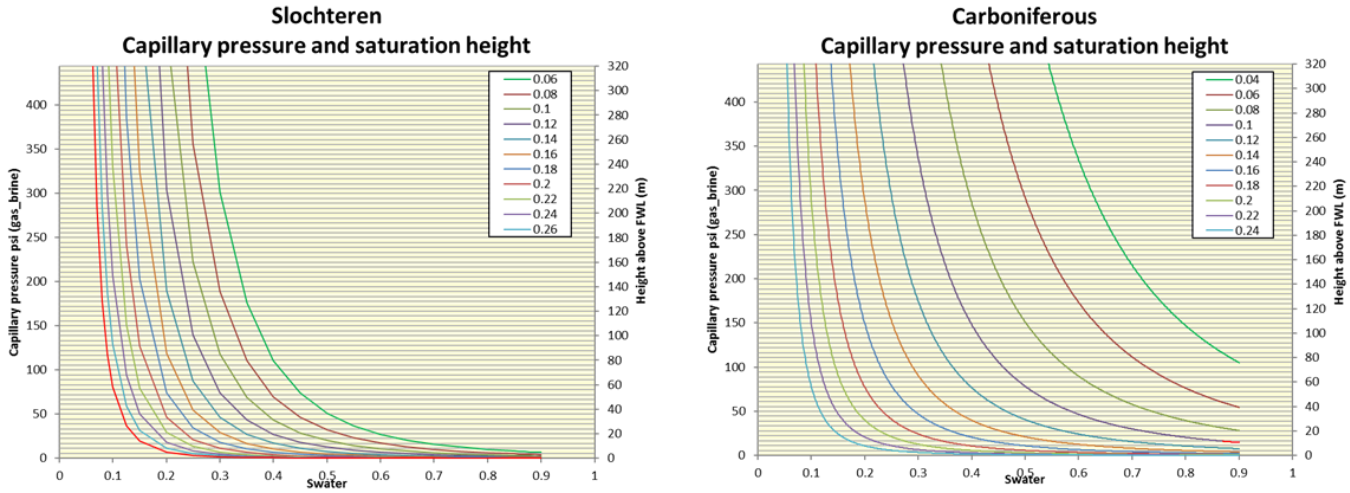

Figure 4-18 Capillary pressures and corresponding height above the FWL for different porosities classes in the Slochteren/Rotliegend (left) and in the Carboniferous (right).

4.4.3 Residual water saturation

Residual water saturations in the Groningen full field model are determined from a cut-off on the capillary pressure gradient. The residual water saturations are correspondingly updated for the Carboniferous based on the capillary curves, see Figure 4-19.

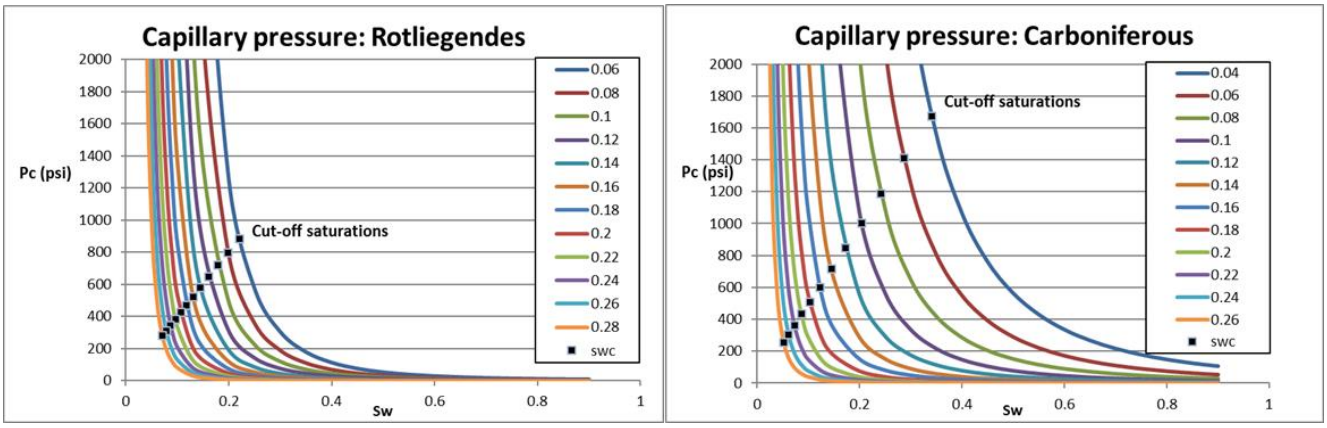

Figure 4-19 Cut-off saturations plotted on the capillary pressure curves for the Slochteren formation (left) and the Carboniferous formation (right).

4.4.4 Relative permeabilities

The Carboniferous relative permeabilities are modelled applying the same Corey curves as used for the Rotliegend, only updated for the residual water saturations. Figure 4-20 shows a comparison between the relative permeabilities from the Rotliegend and the Carboniferous for 8% porosity.

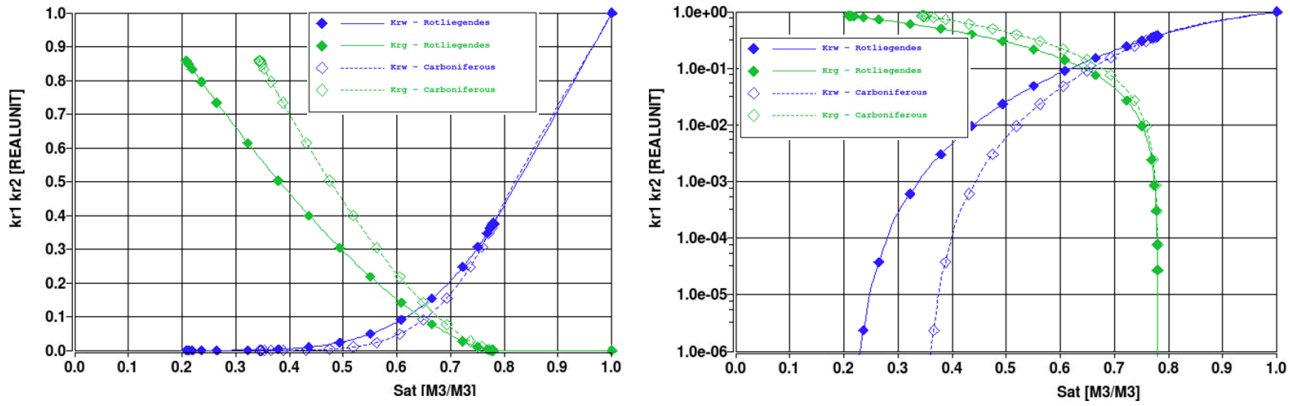

Figure 4-20 Relative permeability curves for Rotliegend (solid lines) and Carboniferous (dotted lines), at 8% porosity.

4.4.5 Rock compressibility

Reference [19] describes how the uniaxial rock compressibility used in the V6 model is back-calculated from sonic logs over gross Carboniferous intervals from fields in the north-eastern Netherlands[8]. The work includes a high-level assessment of the ZRP-3A DSS data to confirm the validity of the range:

$$c_m = 1 - 10 \text{ µstrain/bar}$$

In MoReS, the pore volume compressibility is used for subsidence calculations. The pore volume compressibility can be calculated from the uniaxial compressibility as [20]:

$$CR = \frac{c_m}{\phi}$$

where:

CR	pore compressibility (MoReS input)
c_m	uniaxial compressibility in 10^{-5} /bar

MoReS uses the compressibility only on the net reservoir. Therefore the compressibility is scaled up by dividing it by the Net-to-Gross.

[8] No core derived compressibility data exists for the Carboniferous in the Groningen area. Analysis of the Carboniferous section of the ZRP-3A core is currently ongoing, but no results were yet available to constrain the V6 dynamic model update.

4.5 History matching variables

4.5.1 Porosity

The range in which the 6.3% average porosity is allowed to vary within the history matching process is driven by the resulting GIIP range. The Carboniferous GIIP should fall within the expected range of 20 to 70 N.Bcm GIIP based on references [14] and [21], see Figure 4-21. The GIIPs resulting from a range of porosities was analysed to derive at the following porosity multiplier range (see Figure 4-22):

- 1 < Porosity multiplier < 1.65

This corresponds to a porosity between 6.3 and 10.5 %.

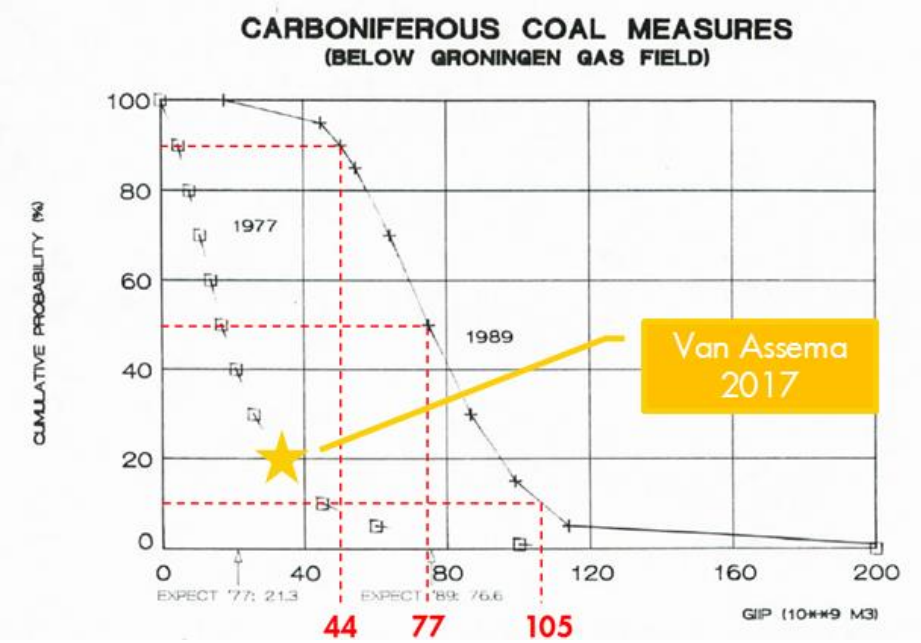

Figure 4-21 Historical Carboniferous GIIP estimates from [21] and [14].

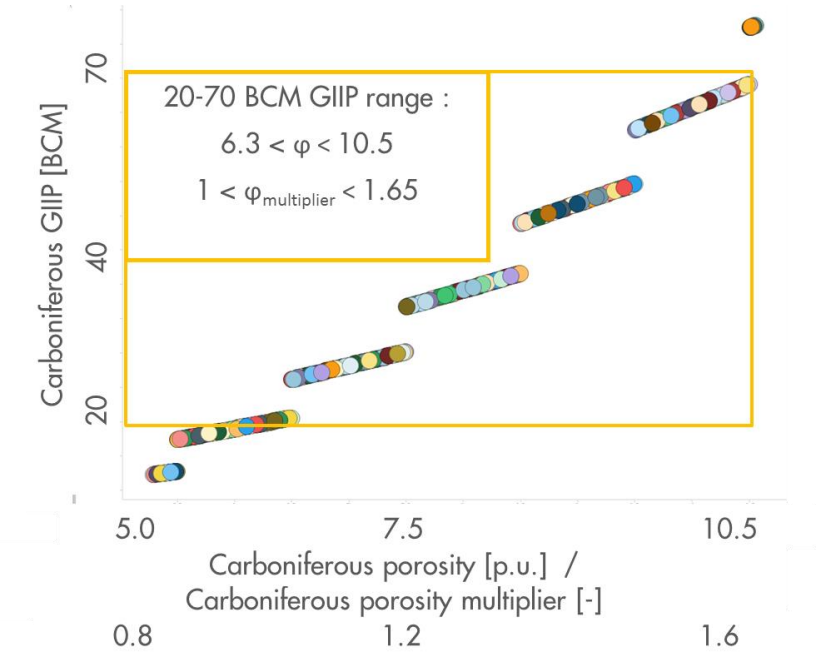

Figure 4-22 Carboniferous GIIP resulting from different porosity values

4.5.2 Horizontal permeability

Figure 4-23 shows the in-situ porosity-permeability relation from core-data for Carboniferous sandstones in Groningen and the Eastern Netherlands. Based on the core data, a range in permeability values within the Carboniferous porosity range deemed acceptable is:

- 0.01 mD < k_h < 1 mD

The high case value was selected relatively aggressively to include a scenario that will drain the full Carboniferous.

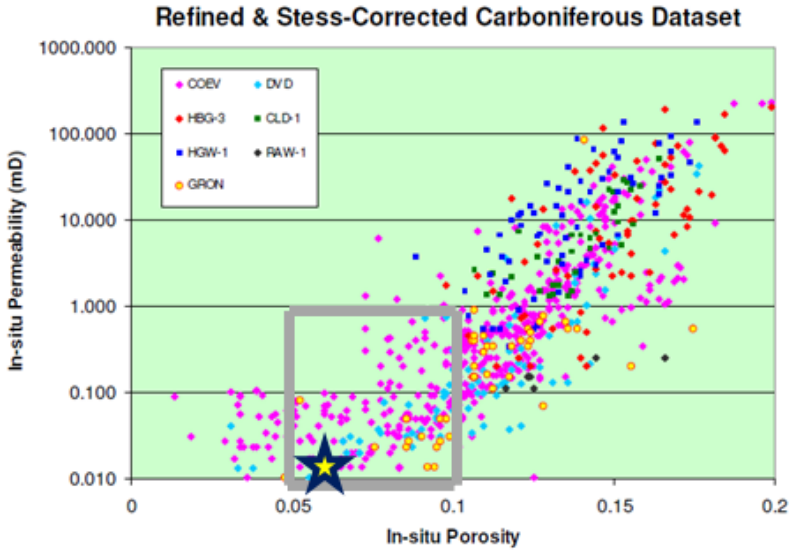

Figure 4-23 In situ poro-perm relation for Carboniferous sandstones in the Northern and Eastern Netherlands [13]. The grey box marks the uncertainty range for the permeability and porosity in the V6 model. The star-shaped point indicates the porosity and permeability values from the reference model.

4.5.3 Vertical permeability

The vertical permeability in the Carboniferous is implemented using a k_v/k_h multiplier, ranging from:

- $0.01 < k_v/k_h$ multiplier < 1

No extremely low values are used since the Carboniferous grid is concordant with the Slochteren grid, whereas in reality the angular unconformity could locally give some more vertical connectivity.

4.5.4 Connectivity across Carboniferous – Rotliegend unconformity

The Saalian unconformity separates the Carboniferous and the Rotliegend. This time hiatus represents a significant period of weathering and non-deposition affecting Carboniferous reservoir properties along the surface and consequently reducing the vertical connectivity. This effect was incorporated in the V6 model as a seal factor applied to the surface between the Carboniferous and the Rotliegend grid blocks, ranging from:

- $0.0001 <$ seal factor < 1

4.5.5 Rock compressibility

The rock compressibility range is described in section 4.4.5:

- $1 < c_m < 10$ μstrain/bar

4.6 History matching observables

4.6.1 Direct data

Pressure

Apart from the qualitative indications of depletion described in chapter 4.3, the Carboniferous pressure data was found to be unsuitable as an observable for the V6 modelling. Pressure variation between individual sand lenses in the Carboniferous is not captured by the homogenous reservoir model implementation. Any model realisation between a fully depleted and undepleted Carboniferous falls within the data range, Figure 4-24.

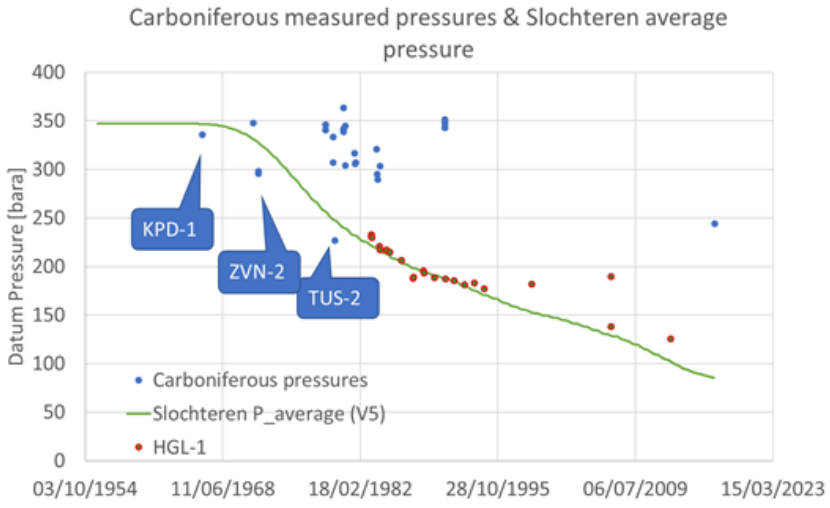

Figure 4-24 Carboniferous pressures converted to Groningen datum level compared to the average simulated Slochteren pressures from the V5 dynamic model.

Strain

The strain measurements from the Zeerijp-3A DSS cable (2 cm interval resolution) were upscaled to grid block size, Reference [22]. The upscaling is reproduced in Figure 4-25, which includes an error band from the data.

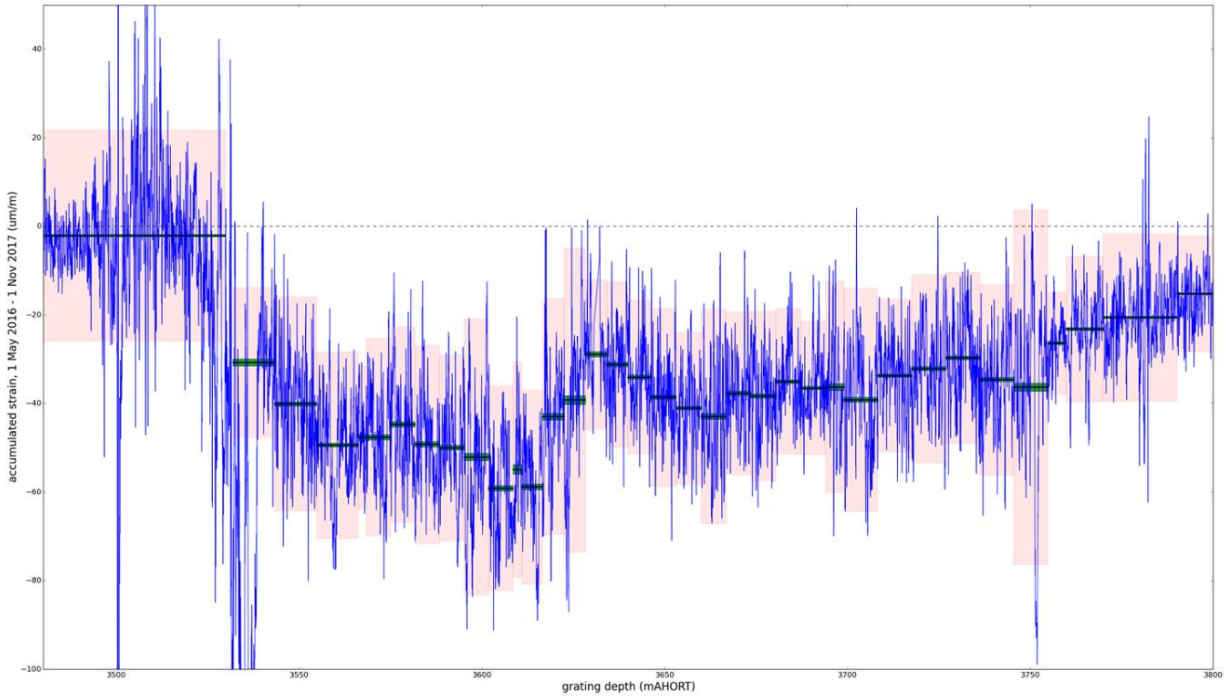

Figure 4-25 Measured strain (blue) with the grid block interval strains (black, horizontal lines). The green shaded area around the mean marks the uncertainty of the interval strain. The red shaded areas mark the zone of two standard deviations around the mean, which can be used as a minimum and maximum strain case. The figure is obtained from reference [22].

4.6.2 Indirect data

Rotliegend pressures

Pressures measured from wells in the Rotliegend are affected by energy support from the (gas-bearing) Carboniferous. The pressures are not used as direct measurements, but the Carboniferous modelling should be such that these pressures are matched as well.

Subsidence

The subsidence from the Groningen field is a combination of compaction in the Rotliegend as well as in the Carboniferous and can therefore not be used as a direct observable. However, the previous models have already indicated that the Carboniferous is expected to impact the subsidence mismatch, mainly in the south of the field where the Carboniferous is gas-bearing.

Gravity

Gravity changes in the Groningen field are a combination of mass changes (depletion) in the Rotliegend and in the Carboniferous and can therefore not be used as a direct observable. The previous models have already

indicated that the Carboniferous is expected to impact the gravity mismatch, mainly in the south of the field where the Carboniferous is gas-bearing.

4.6.3 Sensitivity

From a sensitivity analysis on the indirect observables it was found that the horizontal permeability, porosity and compressibility have the largest impact, Figure 4-26.

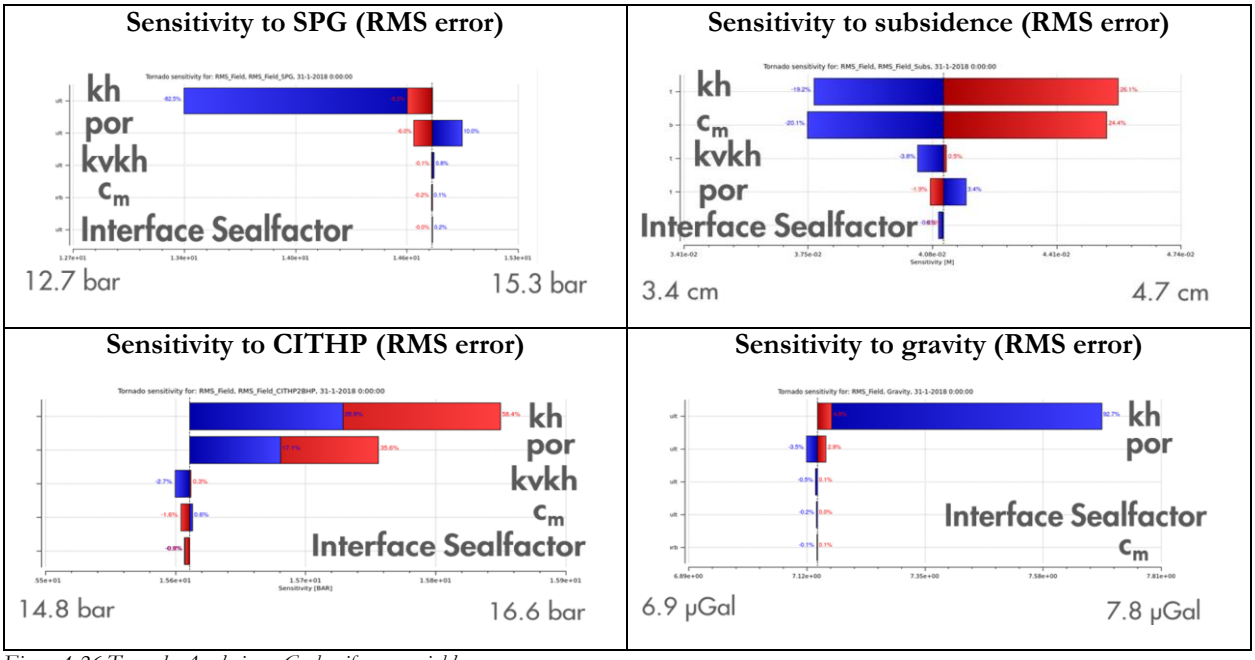

Figure 4-26 Tornado Analysis on Carboniferous variables

5 Lauwerszee aquifer

5.1 Inferred depletion based on seismicity

In previous model vintages, the depletion in the Lauwerszee aquifers[9] to the southwest of the Groningen field was solely constrained by subsidence. However, the occurrence of the earthquakes at Eelderwolde (2006) and Paddepoel (2017) may provide additional information to constrain the modelled depletion in this area, Figure 5-1. It was established in Reference [23] that production-induced earthquakes at gas fields in the Netherlands only occur beyond a minimum of 90 bar depletion. Therefore, a minimum depletion of 90 bar depletion was used as a (soft) history matching parameter.

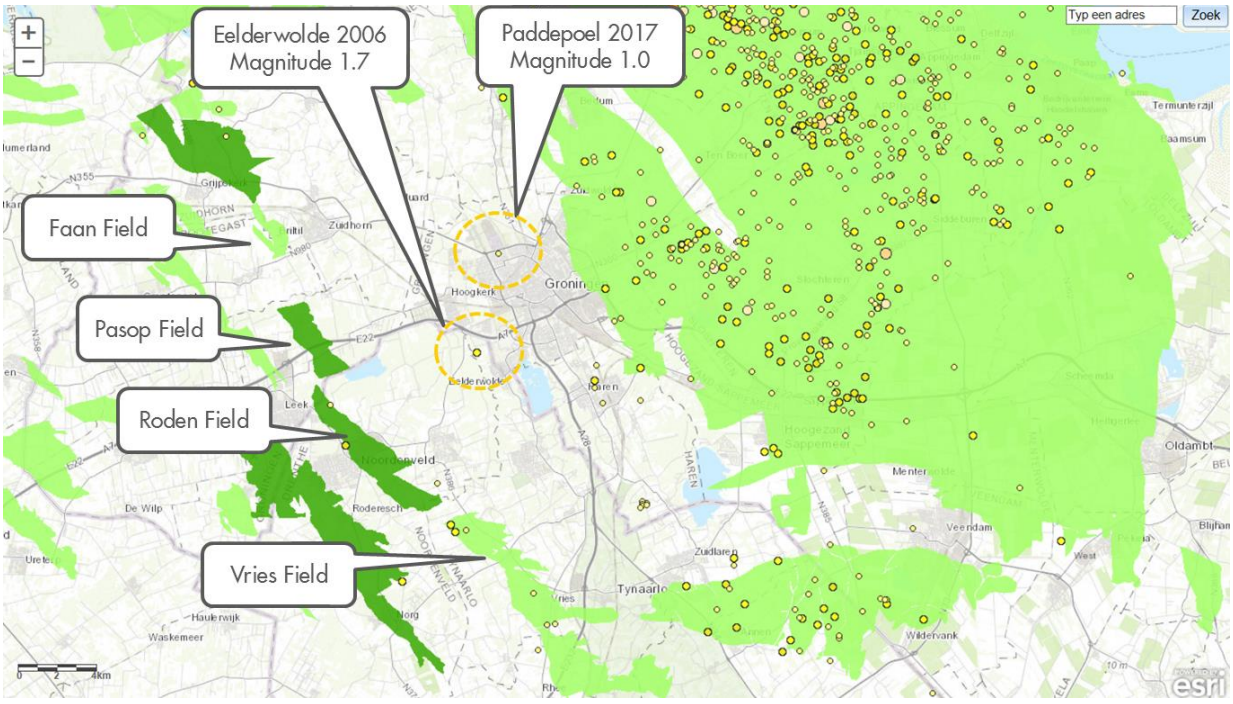

Figure 5-1: Gas fields towards the southwest of Groningen, historical earthquakes and city planning as from https://nam-feitenencijfers.data-app.nl/geotool/nam.html . Eelderwolde and Paddepoel earthquakes and Faan, Pasop, Roden and Vries gas fields highlighted.

5.2 Depletion by peripheral fields Roden, Pasop, Vries and Faan

In its initial setup, it proved to be impossible in the V6 model to achieve ≥90 bar of depletion in the Lauwerszee aquifer by 2006. Even a scenario with a high permeability in the Lauwerszee aquifer did not provide enough depletion at the time of the Eelderwolde earthquake, see left-hand panel of Figure 5-2. At the same time, such a high permeability scenario was dismissed based on the observed pressure built-up from the pressure data at EKL-13 (right-hand panel).

It was concluded that pressure interference with the peripheral gas fields at the western edge of the Lauwerszee aquifer could not be neglected. The location of the Eelderwolde earthquake is centred between the Groningen field and the Roden and Pasop fields, Figure 5-1 and Figure 5-3. The fault map in Figure 5-3

[9] A map of all aquifers connected to the Groningen field can be found in Figure C-3

shows that a good connectivity is expected from West to East and there has been significant production from the Roden and Pasop fields (as well as for Vries and Faan), see Figure 5-3. The inclusion of the production of these land fields west of the Groningen field provides the additional depletion needed in the Lauwerszee aquifer, without applying an unrealistic permeability multiplier, see Figure 5-2.

The extent of the numerical grid of the V6 MoReS model did not include these fields. A proxy was applied to reflect the dynamic effect of the depletion of these fields in the Groningen model. Pseudo wells were introduced in the aquifer at the edge of the numerical grid. The historic gas production (G_p) as extracted from the small fields was converted to a water equivalent production (W_p) based on the gas expansion factor (E_g), and applied as a production constraint. An additional scaling factor (α) was applied to these water production volumes, to reflect the fact that the numerical grid is smaller than the fault blocks.

$$W_p = G_p / E_g \times \alpha$$

Due to the high permeability within these actual gas fields, the reservoir pressures will be roughly uniform within the gas bearing part of each fault block. However, when mimicking pressure depletion with a pseudo-well that produces water, strong radial pressure gradients are created. Therefore, along the edge of the reservoir grid, permeability towards the pseudo-well was increased by a factor 20.

	High perm multiplier Lauwerszee aquifer	Low perm multiplier Lauwerszee aquifer + Roden and Pasop fields
Harkstede SPTG	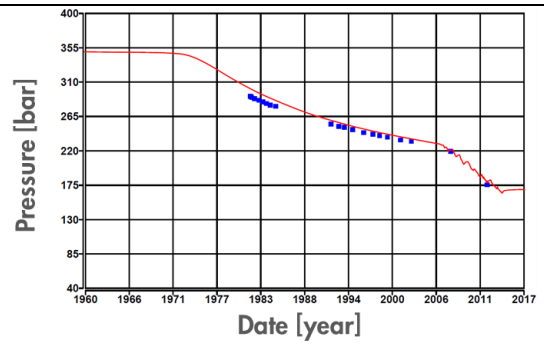	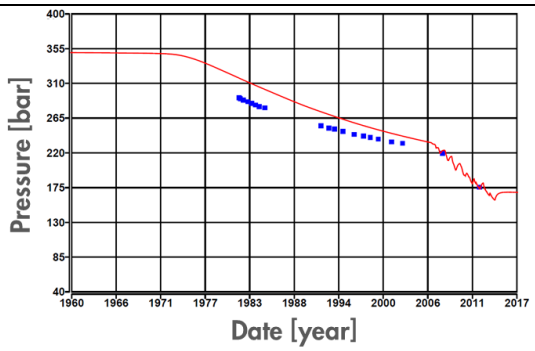
Eemskanaal-13 CITHP	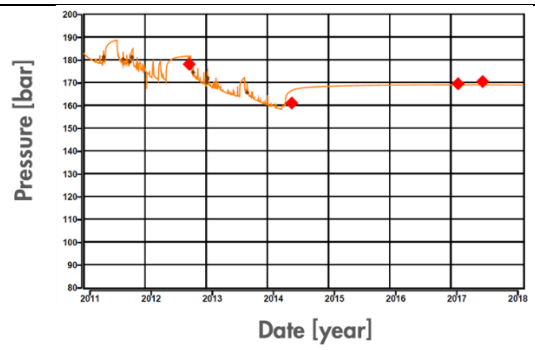	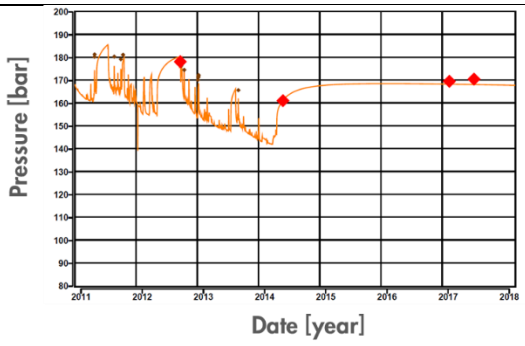
Pressure drop Eelderwolde/ Paddepoel	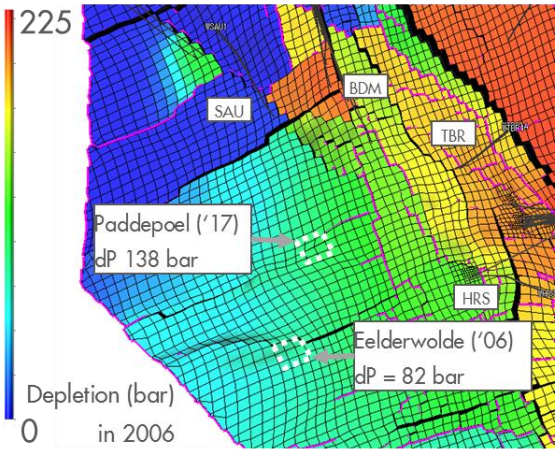	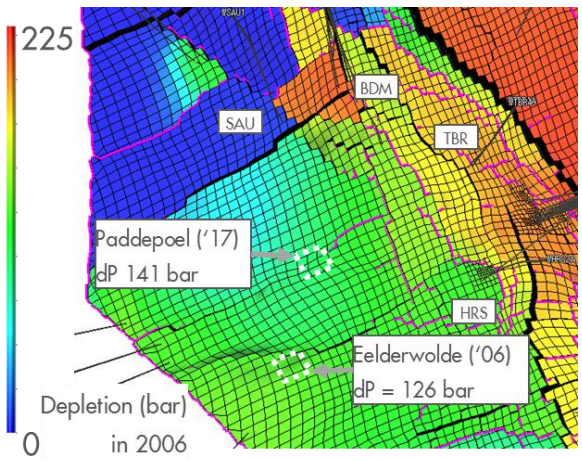

Figure 5-2 Comparison of main output for scenario's to obtain 90+ bar depletion at Eelderwolde and Paddepoel earthquake locations. The left figures show a scenario where the permeability in the Lauwerszee aquifer is strongly increased. The right figures show a scenario where the permeability in the Lauwerszee aquifer is in line with the Eemskanaal area permeability, but the depletion effects of the Roden and Pasop fields have been included.

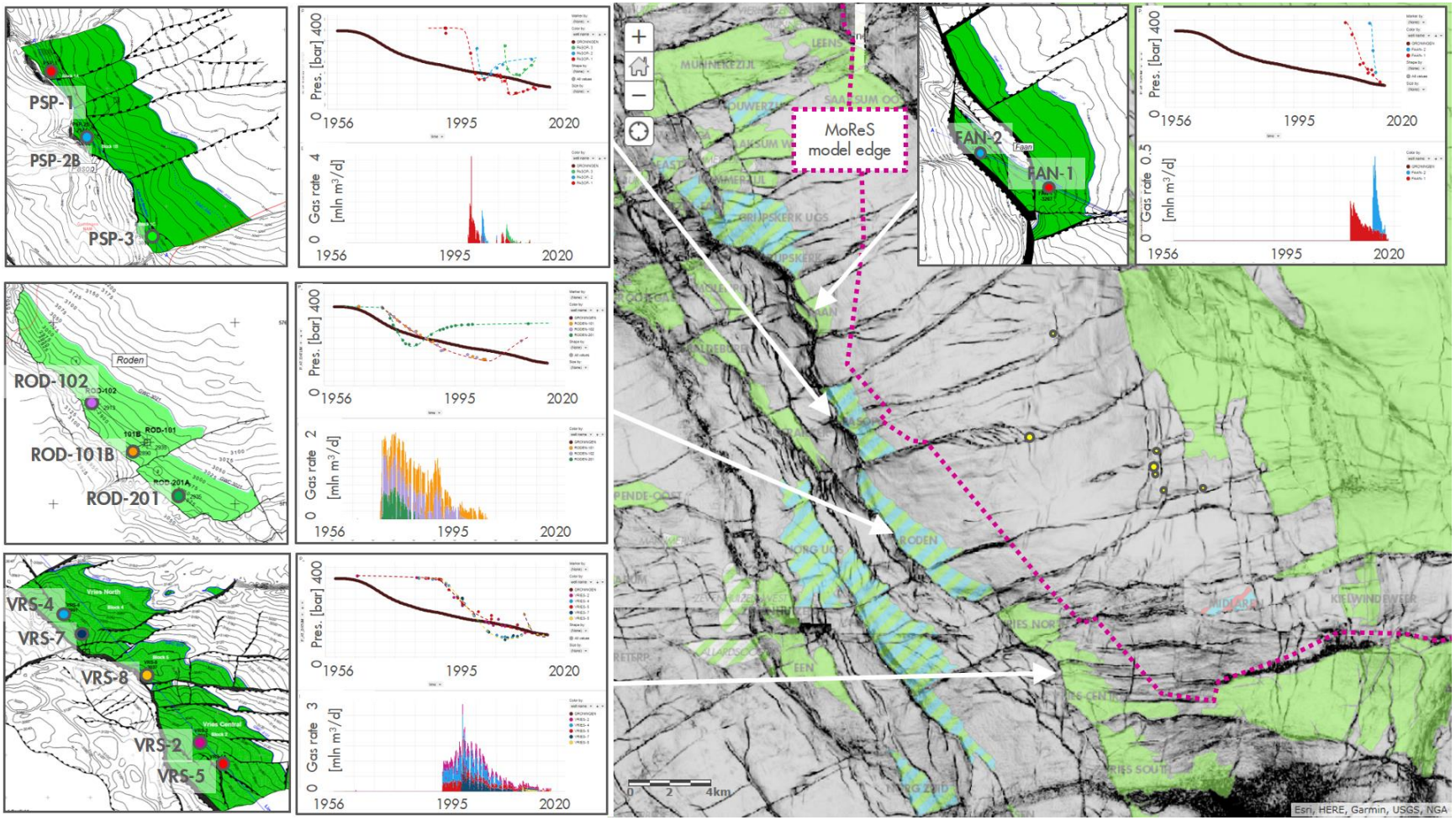

Figure 5-3 Semblance map of the bottom Zechstein indicating the peripheral gas fields and highlighting the edge of the dynamic model grid. The pressure and production history and field top maps of the Rotliegend are outlined for the Pasop, Roden and Vries fields. The average Groningen pressure is shown as a black curve through all pressure plots.

6 History Match – Methodology

6.1 Workflow

For the V6 model update, a similar history matching workflow was applied as for the V2.5/V4/V5 model updates. This workflow was described in detail in the GFR2015 report, Reference [10]. The extension of the history matching method with the Adjoint was described in the report on the V4 model update, Reference [2].

6.2 Permeability modelling

It was evident from previous history matching efforts (V4 and V5) that the North-Eastern area of the field could not be history-matched with the property model as obtained from seismic inversion, References [2] and [3]. The modelled permeabilities in the area were too low. However, the earlier V2.5 model vintage (pre-dating the seismic inversion) did yield a good match in the area, Reference [10].

In these previous history matching set-ups, permeability uncertainty was addressed by a single multiplication factor. That effectively constitutes a vertical translation on a semi-log porosity-permeability plot, and does not acknowledge the porosity dependency in permeability uncertainty.

Further investigation of the uncertainty in permeability modelling revealed that there is much more permeability variation for lower porosity classes than for higher porosities. Care was taken in the static modelling to preserve the spread in k/ϕ as observed from the core data in the static model. The upscaling in the dynamic model preserves the flow characteristics due to the lateral variability. Figure 6-1 investigates the porosity and permeabilities of the upscaled grid blocks on a box and whisker plot, indicating P90/P50/P10 permeability bands for each porosity bin. There is a clear trend in data spread: at 5% porosity the P10 to P90 permeability band stretches over 2 log cycles, whereas at 25% porosity it is less than half a log cycle.

The observed porosity dependence in the permeability uncertainty is included in this model update. The P10 and P90 permeability bands permeability bands from Figure 6-1 were normalized to the P50, see Figure 6-2. Thus, the permeability uncertainty was defined based on a single scalar, α:

$$\alpha \in [-1, 0] \quad k' = k \cdot 10^{(3.611 \cdot \phi - 1.0955) \cdot \alpha} \qquad \text{(permeability increase)}$$

$$\alpha \in [0, 1] \quad k' = k \cdot 10^{(-4.112 \cdot \phi - 1.1948) \cdot \alpha} \qquad \text{(permeability decrease)}$$

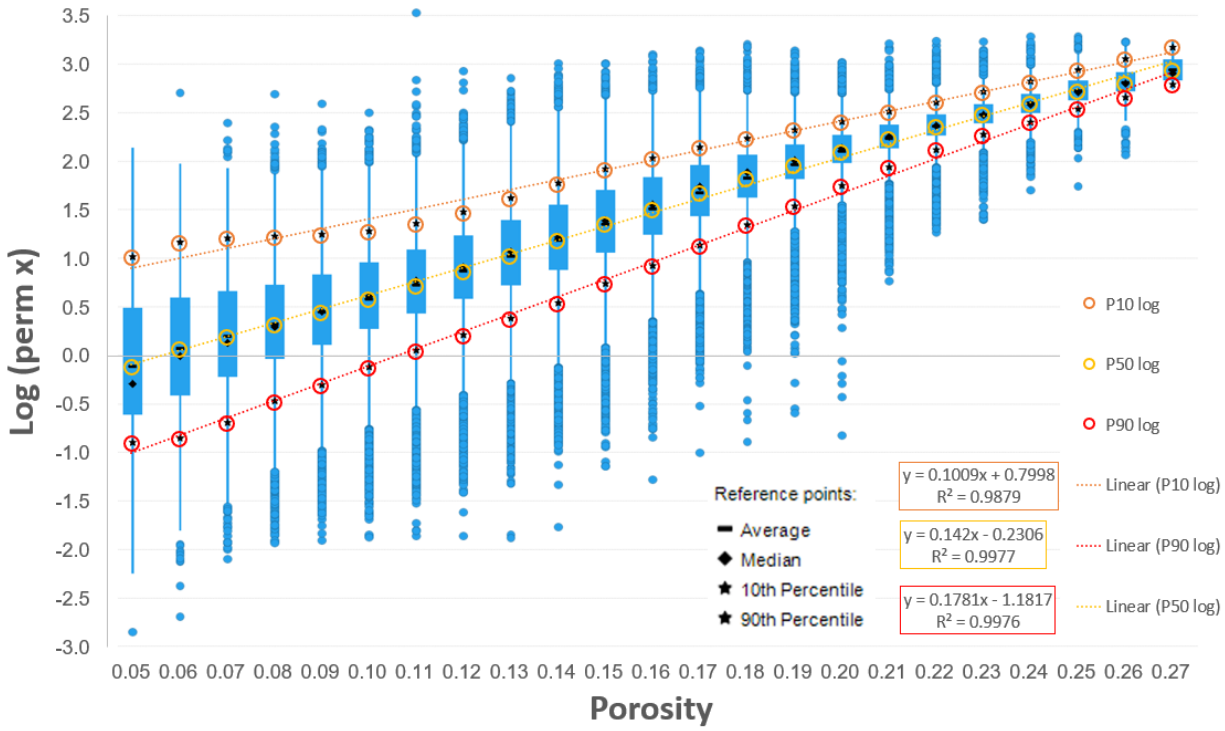

Figure 6-1: Box-and-whisker plot of gridblock permeability indicating P10/P50/P90 permeability values by porosity bin.

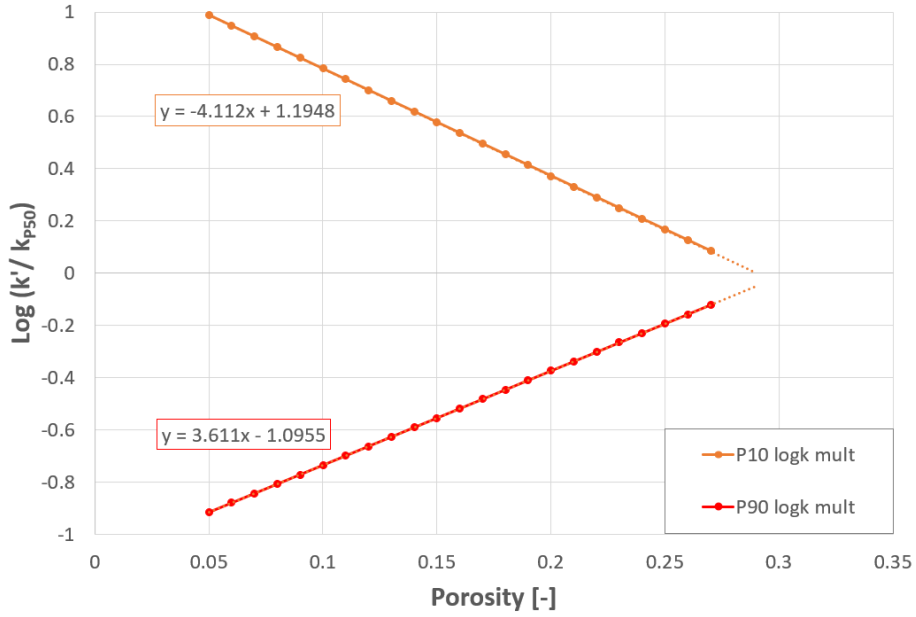

Figure 6-2 P10 and P90 permeability uncertainty bands as normalized to the P50.

6.3 Relative permeability model

The relative permeability model (for the Rotliegend gas reservoir) was maintained as per the V5 model, Reference [2]. Dedicated relative permeability models were derived for the gas-in-aquifer and for the Carboniferous, as described in chapters 3.6.2 and 0.

7 History Match – Global

7.1 Gas-in-aquifer

From a dynamic modelling point of view, the inclusion of residual gas below the Gas Water Contact has led to an improved match. The latest version of the dynamic model, however, still contains gas in the entire aquifer. It is recommended to update the model with residual gas not extending beyond to the paleo-contact. The residual gas saturation should be taken from the ZRP-3A PNX evaluation.

Note: in the current model too much energy is coming from the gas-in-aquifer, and the residual gas saturations therefore had to be adjusted down to very low levels (5-10%). By constraining the residual gas to the paleo GWC the energy level is expected to be more in line with the observed behaviour, and there should not be a need to adjust down the residual gas saturation.

SCAL data – imbibition capcurves and relative permeability curves – have been acquired and provide a further source of data. The remaining gas saturation resulting from a GWC rise during production, i.e. in the 'swept zone', is governed by the residual gas saturation (S_{gr}). This is already captured in the current dynamic model. The residual gas saturation is in line with the proposed remaining gas saturation, in the order of 20-30%. In principle, the same curves could be used to describe the gas-in-aquifer. That will however be quite a major effort and is more of a 'nice-to-have'. The use of a single remaining gas saturation below the initial GWC is considered fit-for-purpose and supported.

7.1.1 Areal presence of gas-in-aquifer

Hypothesis 1 as defined in section 3.4 was used to initialise the areal presence of gas-in-aquifer, Figure 7-1.

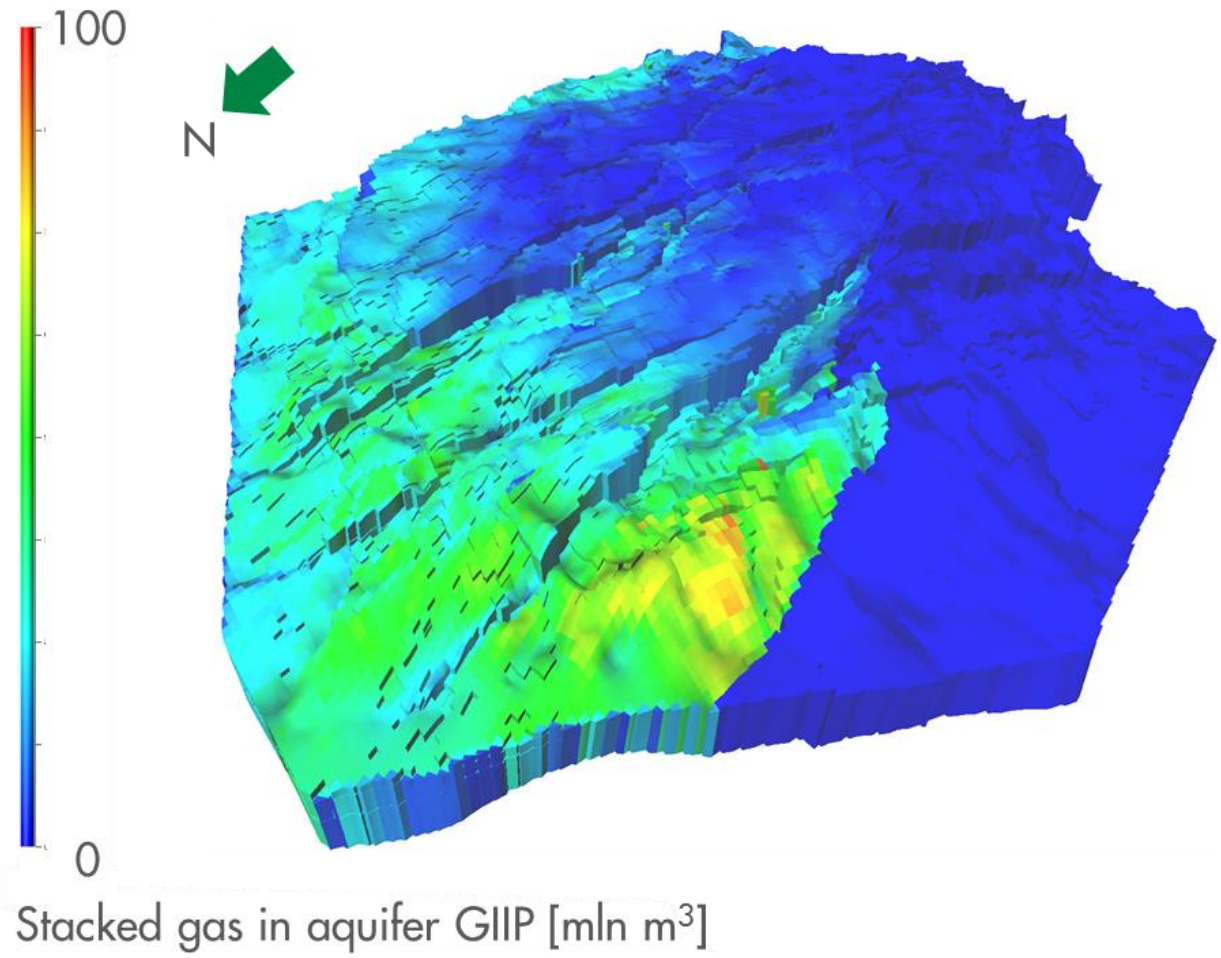

Figure 7-1 Overview of the lateral spread in GIIP from the gas-in-aquifer ($S_{g,aq}$ = 3%). Note the boundary at the geological feature near Bedum as indicated in Figure 3-10. Also note that the higher GIIP northwest of Bedum is due to a larger porosity in this area.

7.1.2 Initial saturation of gas-in-aquifer

The setting of the saturation of gas-in-aquifer is mainly determined by the pressure match for all SPGs and for the subsidence match of the field. Pressures in the field indicate low saturations of the gas-in-aquifer are needed to maintain reservoir pressures low enough, the saturation should be $S_{g,aqf} < 4\%$. There will be too much subsidence however if there is insufficient gas-in-aquifer present to block the propagation of the pressure drop through the aquifer: the saturation should be $S_{g,aqf} > 2\%$. Based on both indications, the saturation of gas-in-aquifer is set to $S_{g,aqf} = 3\%$.

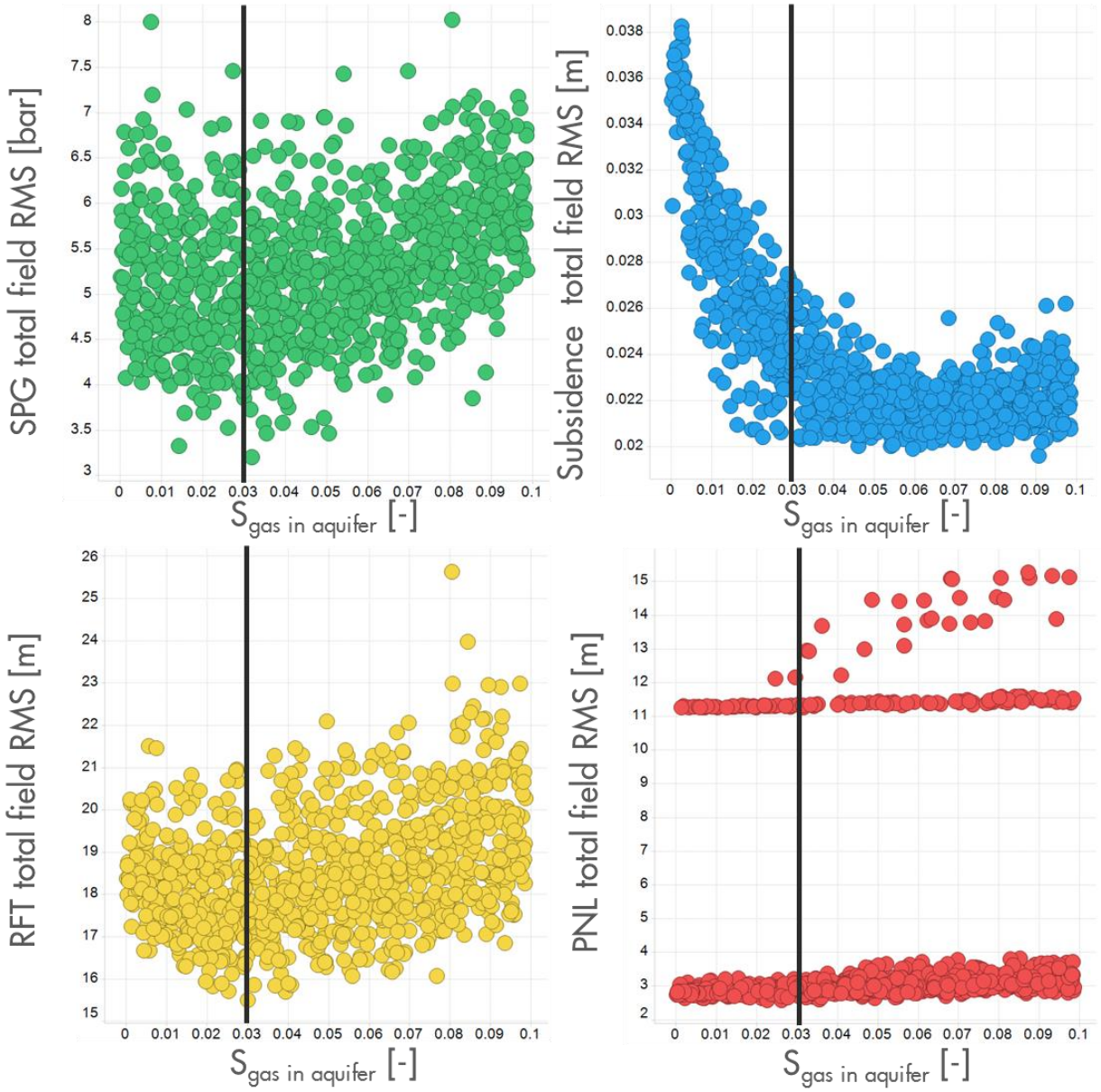

Figure 7-2 Field wide match for SPG, subsidence, RFTs and PNLs for varying saturations of gas-in-aquifer. The black vertical line indicates the best matched gas-in-aquifer saturation. Note that GBVs, permeability and gas mobility have also been varied simultaneously within their uncertainty bands to cater for enough other pressure support options.

7.1.3 Critical gas saturation of gas-in-aquifer

Setting the critical gas saturation (at which the gas-in-aquifer becomes mobile higher than the saturation the model is initialised with) does not improve any of the field wide matches. There is no further evidence of this higher critical gas saturation. Therefore, the critical gas saturation for the gas-in-aquifer is set equal to the initialised gas-in-aquifer saturation.

7.1.4 Corey exponent of gas-in-aquifer

There is no evidence for adjusting the Corey exponent for the gas-in-aquifer either. This is therefore kept at the base case for the Corey exponent. The resulting relative permeabilities and fractional flow curves for the gas-in-aquifer are shown in chapter 7.3.

7.2 Carboniferous

The decoupling between porosity and permeability ensures that the porosity in the Carboniferous only impacts the pressures in the southern area of field where the Carboniferous is gas-bearing. An acceptable match could be obtained using the base case porosity in the Carboniferous. Figure 7-4 shows the associated areal distribution of gas initially in place.

The main indication of Carboniferous connectivity is found to be the shape of the strain decrease in the Zeerijp-3A DSS cable. The depletion is governed by a balance between the horizontal and vertical connectivity. The former is determined by the horizontal permeability allowing depletion via faults near Zeerijp-3A which juxtapose the Carboniferous to the Slochteren. The latter is determined by the vertical permeability and the Saalian unconformity sealing capacity. Figure 7-3 shows the impact of increasing horizontal respectively vertical permeability: the steeply declining trend of strain with depth below the Saalian unconformity is no longer reproduced by the model.

The compressibility is set such that the balance between Slochteren and Carboniferous strain is in line with the strain observed in Zeerijp-3A DSS cable as well as the overall subsidence, see section 7.9.

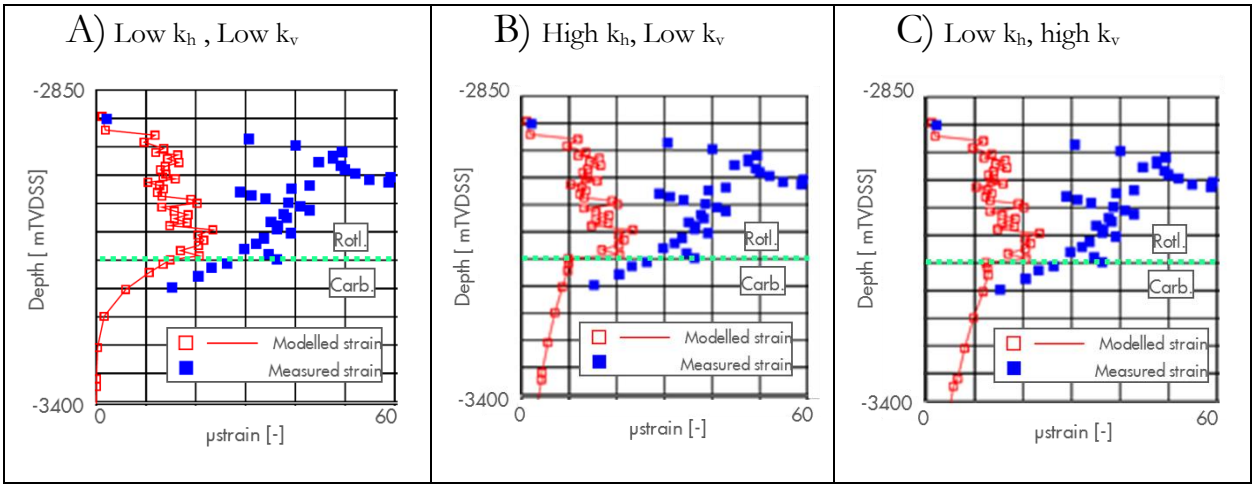

Figure 7-3 Strain behaviour under Carboniferous horizontal and vertical permeability variation. The effect of adjusting the Saalian unconformity transmissibility is comparable to adjusting the vertical permeability.

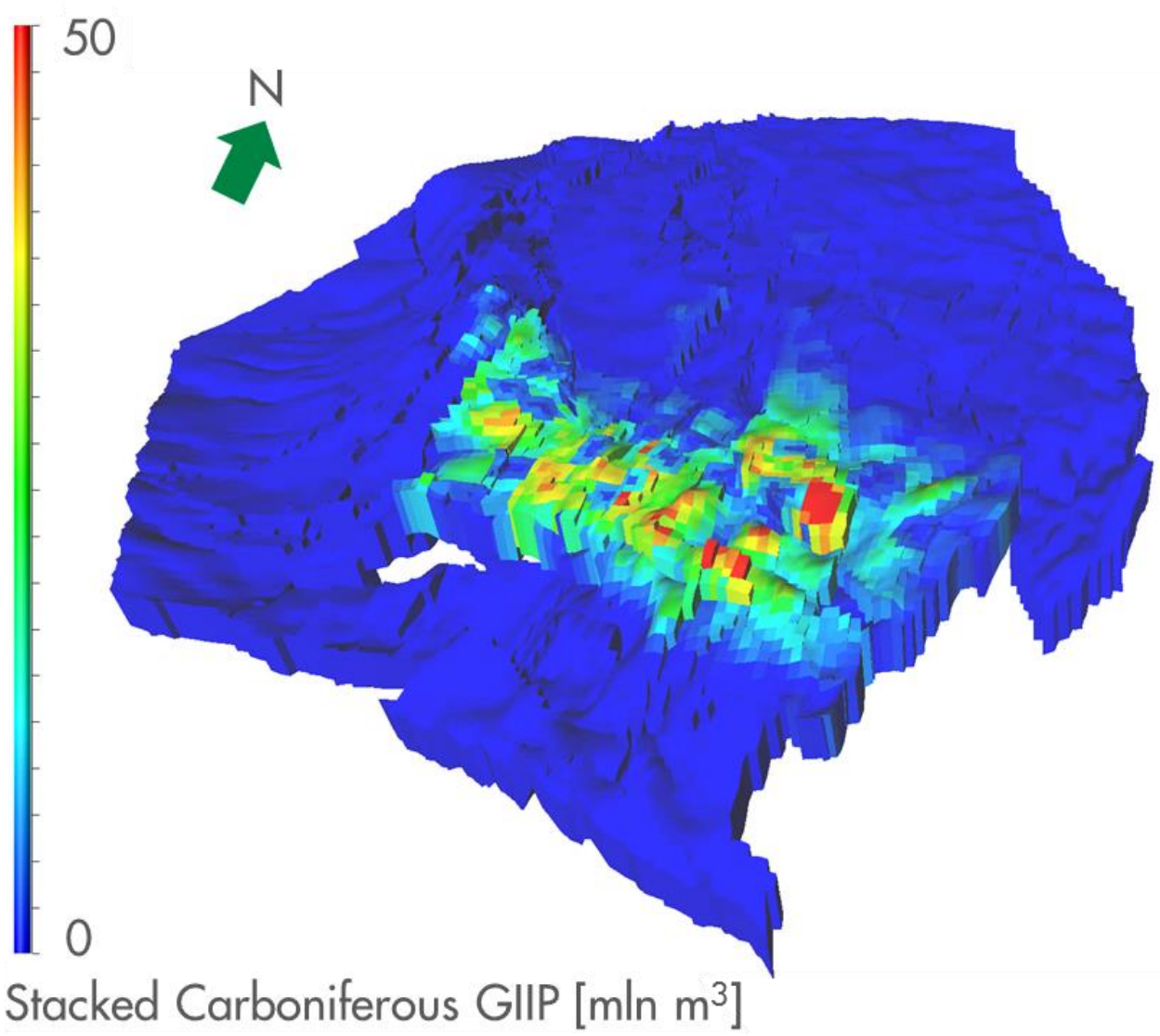

Figure 7-4 Areal distribution of gas initially in place in the Carboniferous.

7.3 Relative permeability

Similar to absolute permeability, the history matching process steered the relative permeability model towards the high end of range for gas mobility. The gas relative permeability curve was set to its high case values. The water mobility plays less of a role in the model but cannot be too small, the Borgsweer water injection pressures need to be matched. The base case relative permeability settings for the water are kept. For the relative permeability of the gas-in-aquifer only the gas Corey exponent was varied, but no change from the base case was needed for an improved match. Figure 7-5 to Figure 7-9 show the relative permeabilities selected in the V6 model and their behaviour.

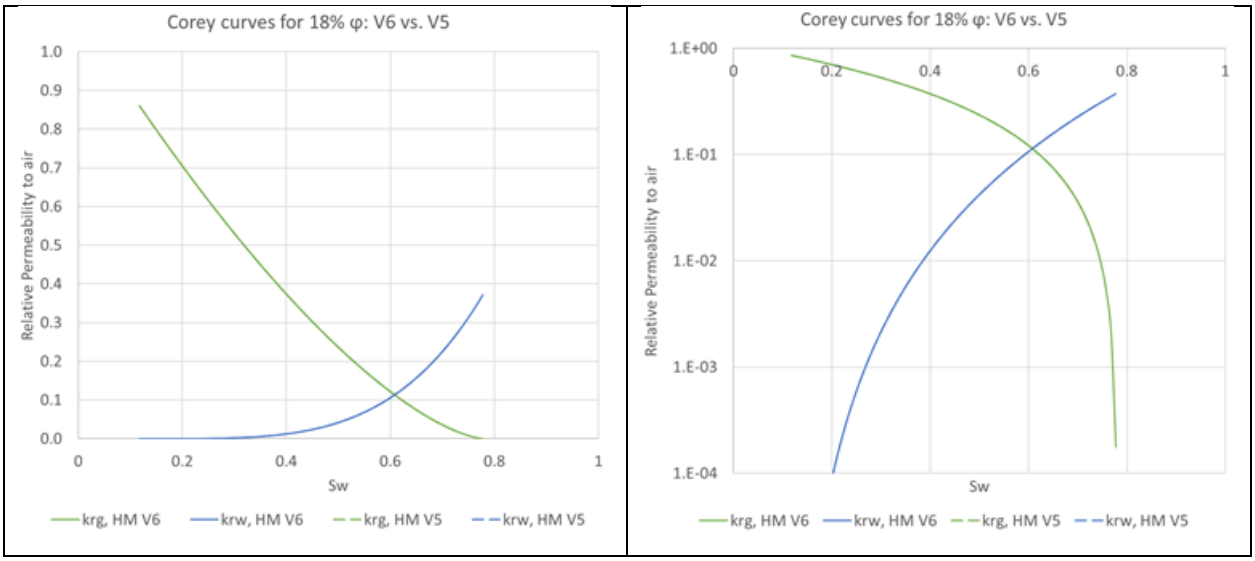

Figure 7-5 V6 and V5 best matched relative permeabilities for 18% porosity, note that both sets of curves overlap.

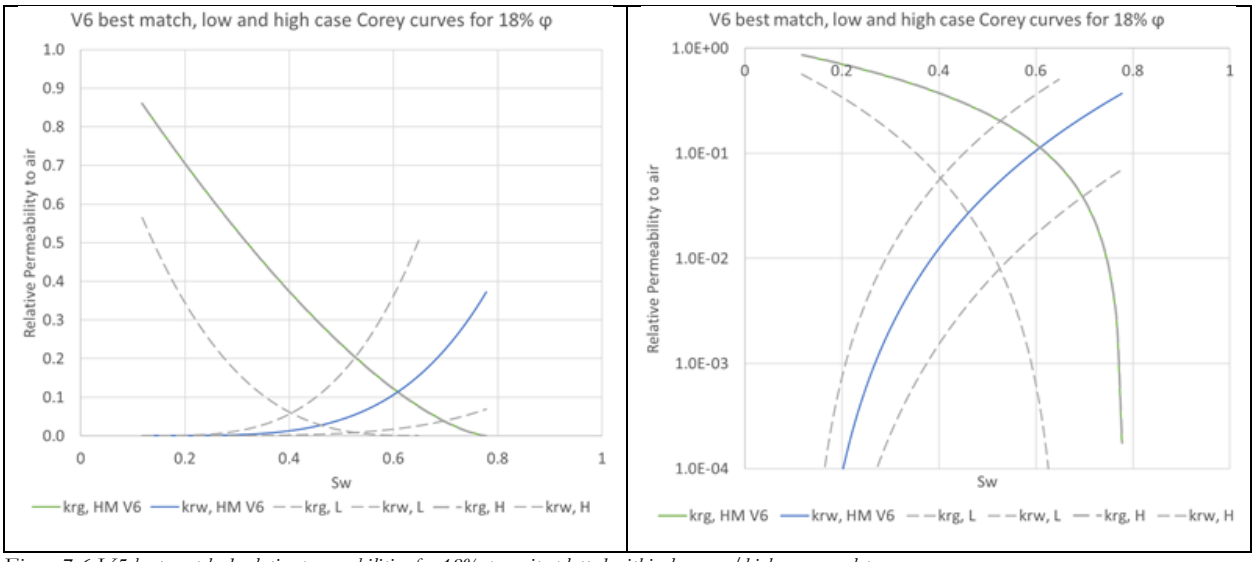

Figure 7-6 V5 best matched relative permeabilities for 18% porosity plotted within low case/high case envelope

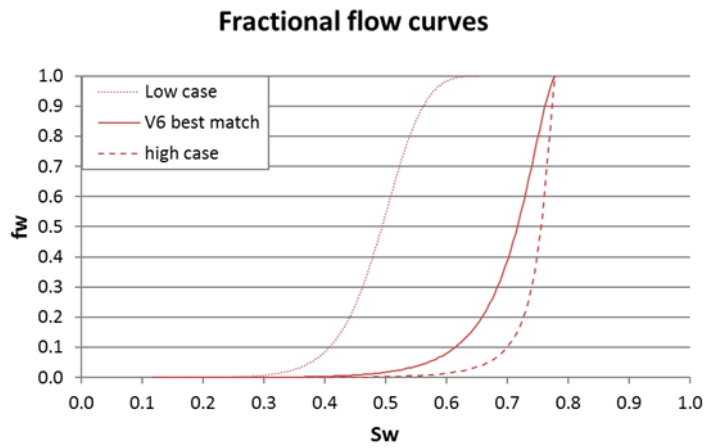

Figure 7-7 Fractional flow curves for V6 best matched relative permeabilities for 18% porosity plotted within low case/ high case envelope.

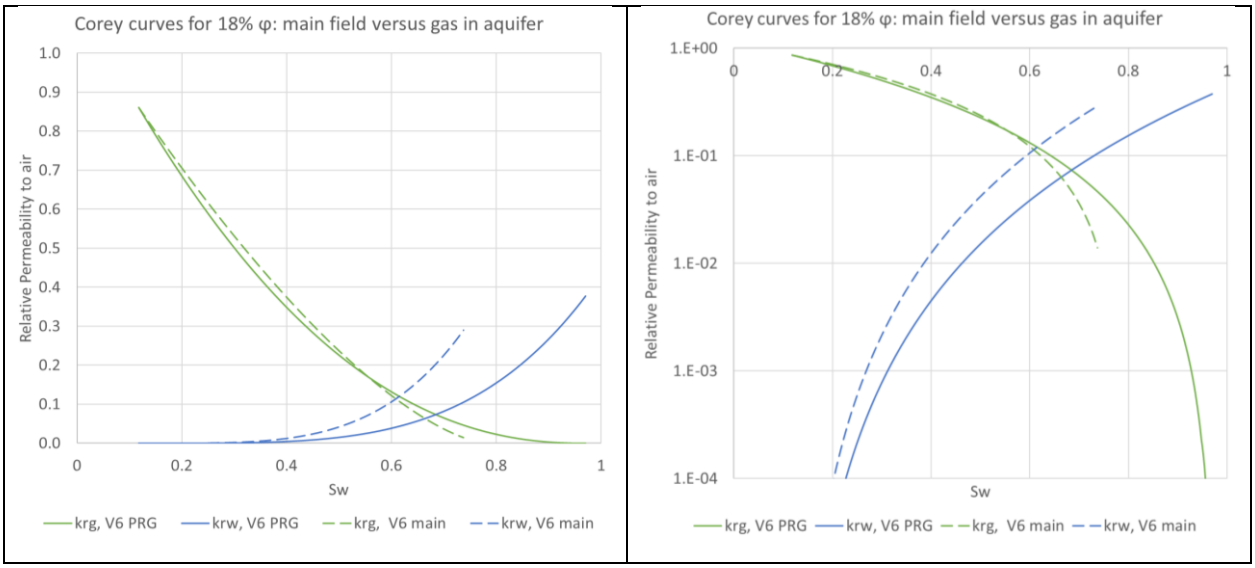

Figure 7-8 Relative permeabilities for 18% porosity for the main gas bearing part of the V6 model and for gas-in-aquifer.

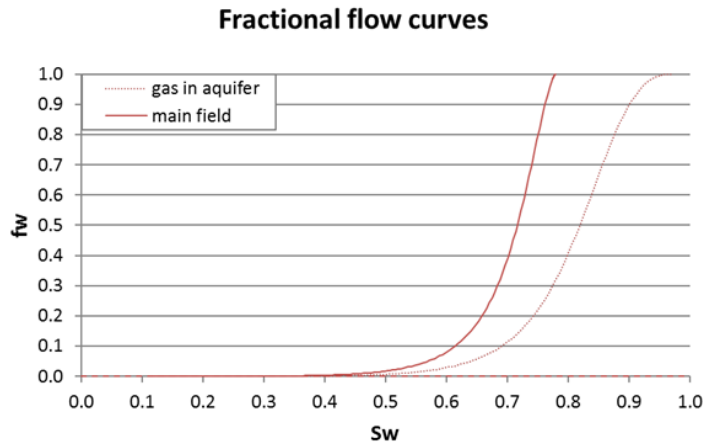

Figure 7-9 Fractional flow curves for 18% porosity for the main gas bearing part of the V6 model and for gas-in-aquifer.

7.4 Permeability multipliers

The history matching process strongly steered model permeabilities to the higher end of the uncertainty envelope. Figure 7-10 shows the permeability multipliers in the field as well as the average permeability multiplier per region.

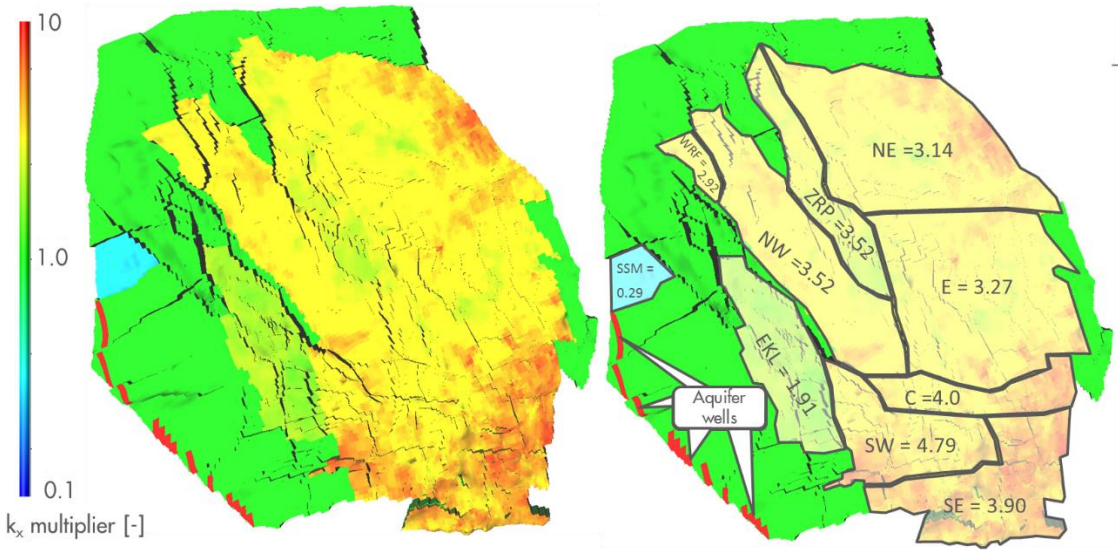

Area	α	Average k_x mult
NE	0.99	3.14
NW	0.99	3.52
ZRP	0.99	3.52
E	0.95	3.27
C	1.00	4.00
SE	0.97	3.90
SW	0.94	4.79
EKL	0.47	1.91
WRF	0.96	2.92
SSM	-1.00	0.29

Figure 7-10 Permeability multiplier map for the top Slochteren layer in the V6 model. Green colors indicate no multiplier, warm colors indicate permeability increase and cold colors indicate permeability decrease. The right map shows the average permeabilty multiplier per region.

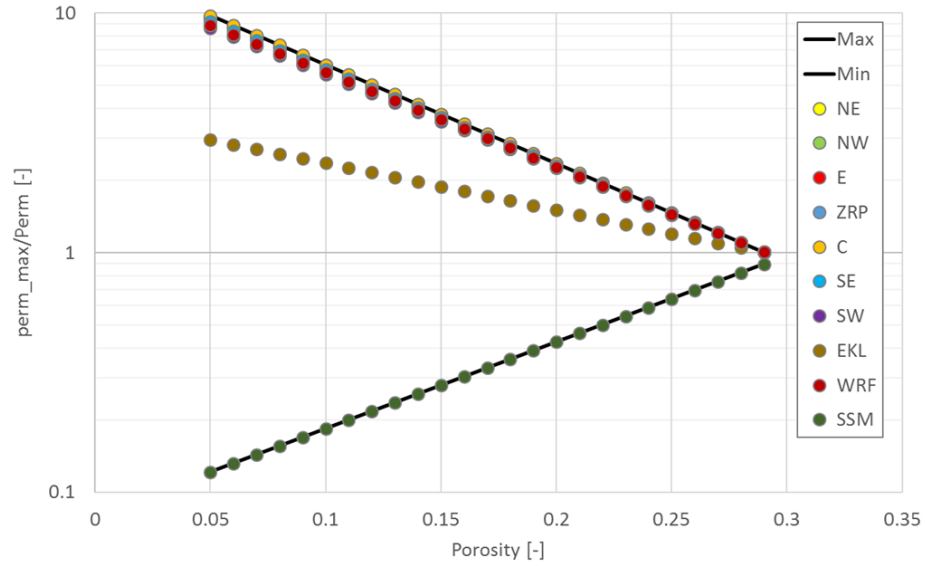

Figure 7-11 Porosity dependent permeability multiplier per region

7.5 Fault seal factors

The history matching exercise was started without any fault seal factor adjustments. Fault seal factors were only applied when data driven:

- in areas where there is direct indication of sealing faults (e.g. KPD cluster),
- when the pressure match requires more separation between areas of the field (e.g. Harkstede area), or
- when the adjoint indicates a need for permeability reduction which is aligned with fault planes (e.g. BIR)

In total 48 fault seal factors were assigned, out of over 600 faults in the dynamic grid. Figure 7-12 provides an overview of the faults which have fault seal factors assigned in the final V6 model, chapter 8 provides a more detailed overview per region. It is recommended to review whether the deterministic choices made can be captured in a more holistic framework..

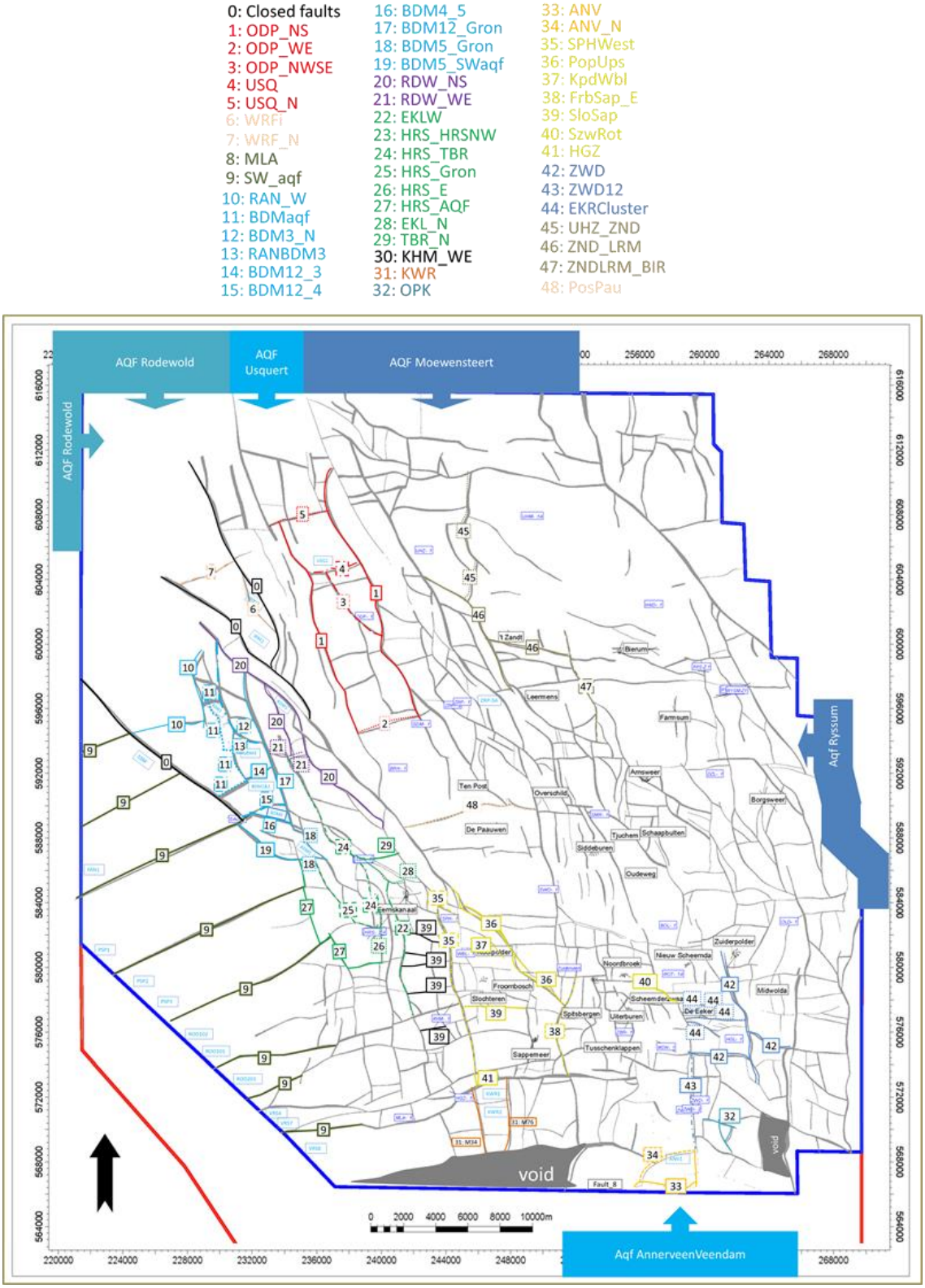

Figure 7-12 Faults with seal factors applied in the V6 model.

7.6 Gas Initially In Place

In this V6 model update the total Groningen GIIP comprises of 3 components:

- Rotliegend gas reservoir.
- Gas-in-aquifer
- Carboniferous gas

Table 7-1 provides the associated breakdown of GIIP volumes for the upscaled static model (without alterations) and for the final history-matched model.

Table 7-1: Gas Initially In Place (N.Bcm) of the upscaled static model versus the best match.

Model	Rotliegend			Carboniferous	Total
	gas reservoir	gas-in-aquifer	total		
Upscaled model	2853.05	103.58	2956.63	20.72	2977.36
V6 history match	2859.50	103.36	2962.86	42.41	3005.27

Similar to V5, a large GBV multiplier was required (2.845) to match the Harkstede region. This is significantly higher than the GBV multipliers applied in the rest of the field. The volume in the Harkstede region is however minor compared to the rest of the field (0.8% of the dynamic GIIP) and the large multiplier can be explained by the relatively large uncertainty in the area, see the V5 report [2] for more detail.

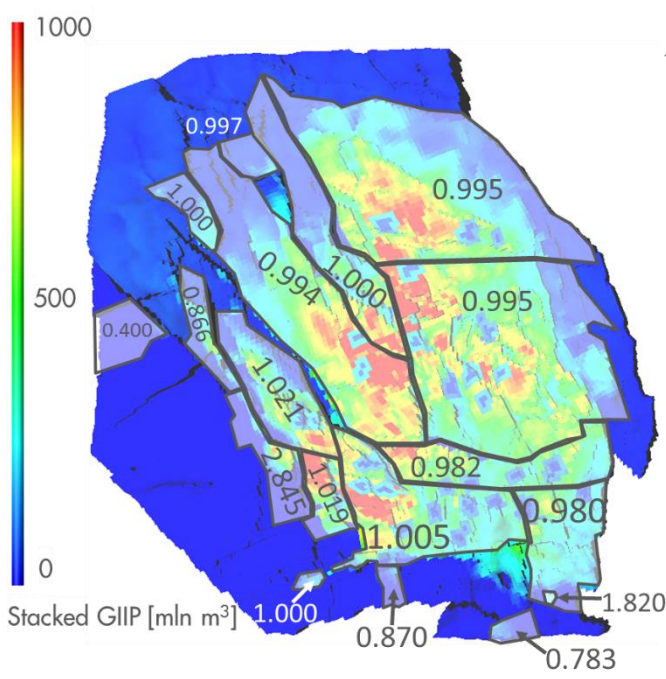

Area	GBV mult [-]	GIIP, excl. Carb [BCM]	GIIP Carb [BCM]	GIIP gas in aquifer [BCM]
NE	0.995	582.2	0.0	24.8
NW	0.994	491.7	0.1	17.9
ZRP	1.000	112.3	0.0	14.6
E	0.995	854.1	2.4	11.5
C	0.982	193.8	6.7	0.0
SW	1.005	341.5	22.3	0.0
SE	0.980	119.4	8.8	0.0
EKL	1.021	122.6	0.8	2.4
KHM	1.019	58.8	0.0	0.0
HRS	2.845	26.5	0.0	0.0
USQ	0.997	4.7	0.0	3.1
OPK	1.820	0.9	0.0	0.0
BDM	0.866	18.9	0.0	5.9
KWR	0.870	1.0	0.0	0.0
FWD	0.400	0.6	0.0	0.0
WRF	1.000	16.0	0.0	4.6
ANV	0.783	1.6	0.0	0.0
MLA	1.000	1.1	0.0	0.0

Figure 7-13 Regional grid block volume (GBV) multipliers shown on a map of the GIIP stacked over the vertical direction. The table on the right provides an overview of the GBV multiplier, the GIIP in the Rotliegend, the GIIP in the Carboniferous and the GIIP in the aquifer. Note that the numbers from Table 7-1 are different than the sum of the table on the right due to the difference in outline for the calculation of the Groningen field GIIP and GBV multipliers.

7.7 Reservoir pressure match

The total reservoir pressure match comprises three datasets. In descending order of importance:

1) SPG data

   The SPG match has the highest weight as this describes the pressure behaviour over the entire field life.

2) CITHP-to-CIBHP data

   CITHP data provides a high data density of pressure behaviour in time, but is only available from 2011 onwards.

3) RFT data

   RFT data provides information on the vertical behaviour of pressure but regarding the full field pressure match provides only 1 data-point.

The following match quality was obtained:

- SPG pressure match: 1.82 bar
- CITHP to CIBHP pressure match: 1.47 bar
- RFT pressure match: 12.71 bar

7.8 Water encroachment match

The fieldwide match of simulated water encroachment to interpreted GWC rise from PNL logs is 2.81 meter.

Additional information on GWC rise from the 2017 PNX logs questions the validity of the interpretations of the flat GWC interpretations from PNL logs, see paragraphs below. The V6 history match has therefore focussed on the match of rising GWCs rather than constraining water rise.

Historically, water encroachment in the field is compared to the interpreted changes in gas water contact (GWC) from PNL logs. The 2017 UHZ-1, ZRP-3A and UHM-1A PNX logs were done to assess the presence of gas-in-aquifer, but also provide a new dataset to assess gas water contact rise. A comparison can be made between the initial open-hole (OH) log interpretation and the 2017 PNX interpretation.

It has been observed that the PNL interpretation of a flat GWC for the UHM-1A well (Figure 7-15 and [24]) is contradicting with a interpreted 30+ meter GWC rise when comparing the 2017 PNX log to the 1965 open hole log, see Figure 7-14.

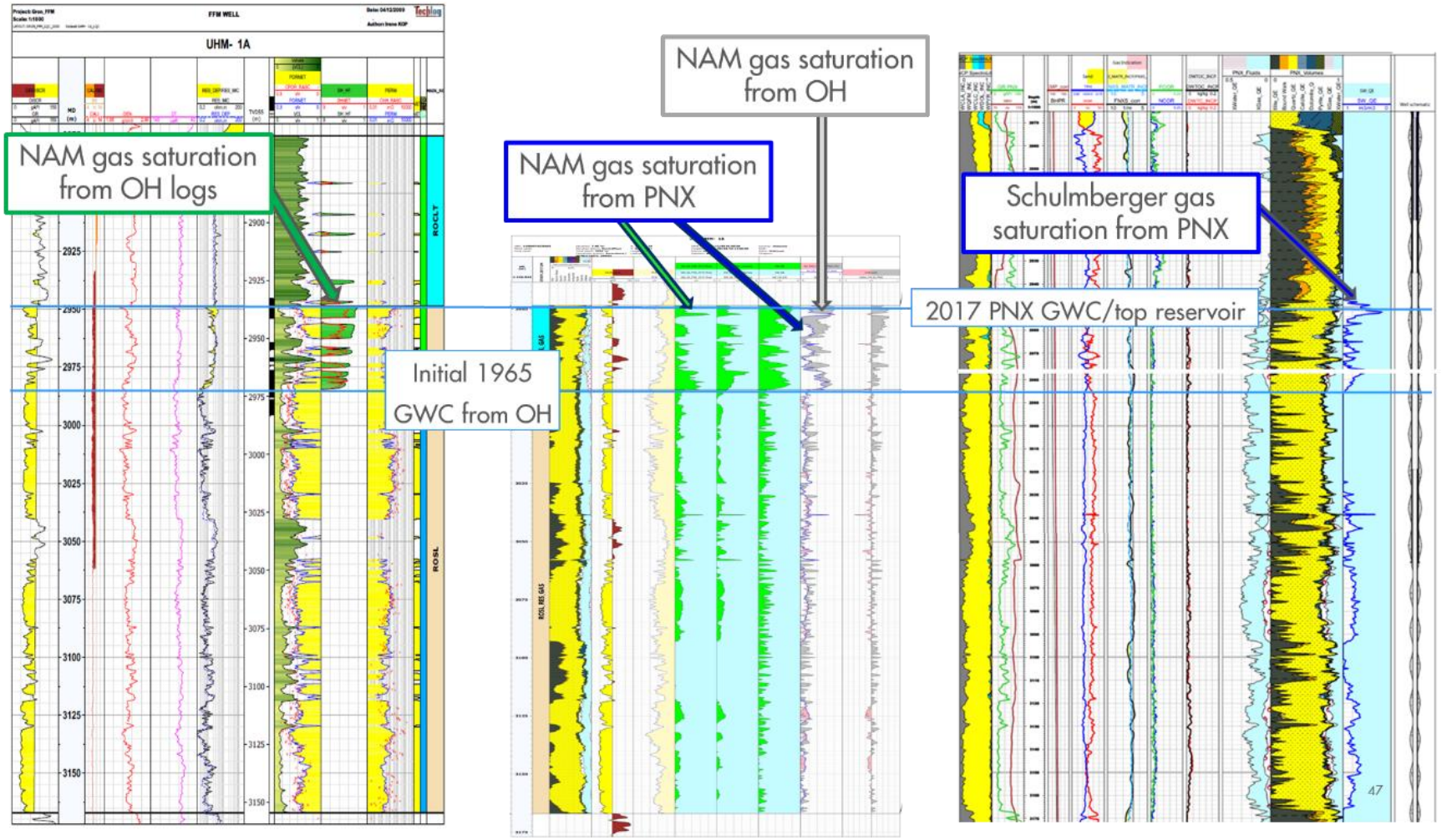

Figure 7-14 Comparison of GWC interpreted from UHZ-1 OH logging suite and from UHZ-1 PNX logging suite by NAM and Schlumberger. The NAM and Schlumberger interpretations of the PNX log show a clear flushed zone of 30+ meters above the initial GWC.

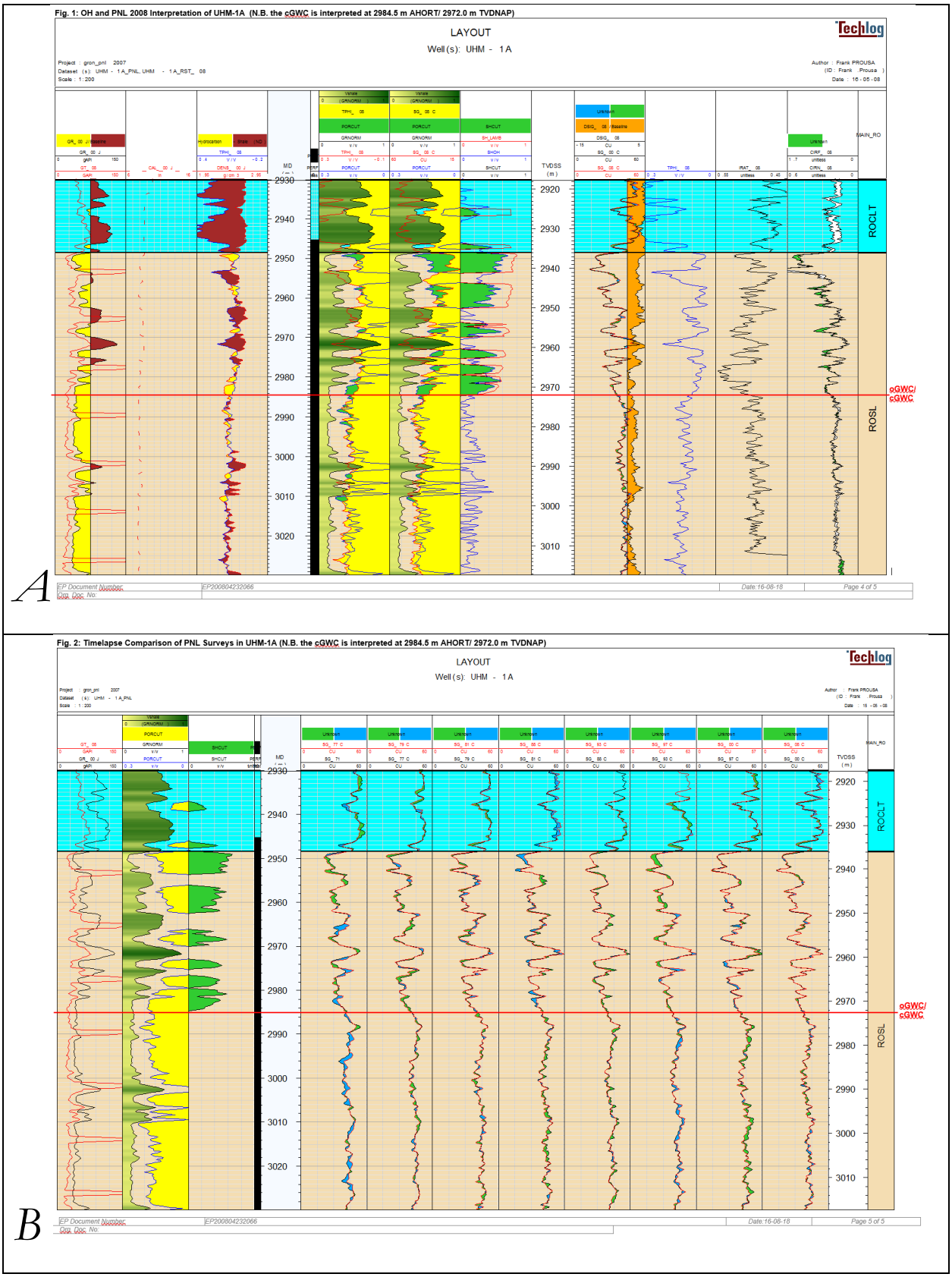

Figure 7-15 2008 PNL GWC monitoring of UHM-1A [24]. Figure A shows the 2008 PNL interpretation compared to the 1965 OH log interpretation. Figure B shows a time laps comparison of PNL surveys in UHM-1A.

7.9 Subsidence match

7.9.1 Methodology

As explained in chapter 5 of the GFR2015 report, Reference [10], a subsidence proxy was implemented in MoReS to steer the pressure match away from well control. The proxy applies a homogeneous version of the Geertsma and Van Opstal equation, Reference [25]. Note that this approach does yield the correct trend, but underestimates the total compaction. For NAM's official long term subsidence calculations, the Geomechanics team uses a rigid basement model [26] and time dependent compressibility. That model calculates higher reservoir compaction to match the surface subsidence than the simplified MoReS proxy. Therefore, the MoReS history matching is restricted to reproducing the depth trend, and not the absolute strain measurements from the DSS cable at Zeerijp-3A, Figure 7-16.

Given that pressures within the Rotliegend gas reservoir are generally well known, the subsidence matching in previous models had only a single unknown: the rock compressibility. However, in the V6 model the Carboniferous is included. This introduces two additional unknows: Carboniferous pressure and Carboniferous compressibility.

The following approach is used to set the rock compressibility in the model:

1) Pressures in the Rotliegend gas reservoir are matched.
2) The Rotliegend compressibility is set to match subsidence above the Groningen gas reservoir.
3) The Carboniferous horizontal and vertical permeability and the transmissibility of the Saalian unconformity are varied to match the trend in compaction decline in the Carboniferous as observed in the DSS cable (see chapter 7.2 for more detail).
4) Iterate between step 2) and 3) until the modelled strain matches the trend as observed from the DSS cable and subsidence above the Groningen gas reservoir is matched, see Figure 7-16.
5) Improve the subsidence match away from well control through updated pressure scenarios.

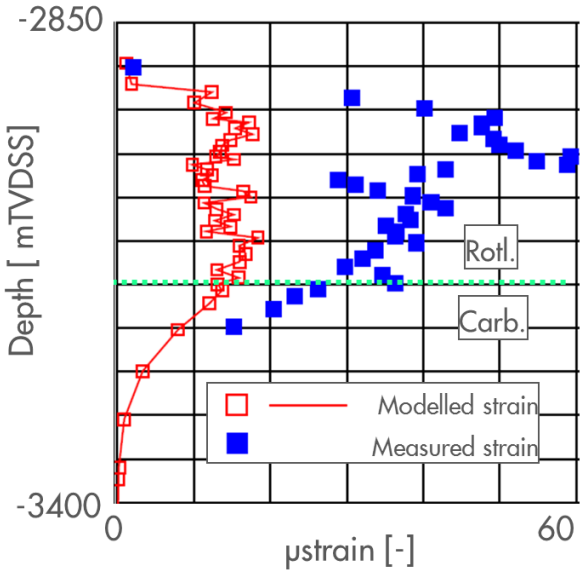

Figure 7-16 Modelled strain matched to the trend in strain versus depth from the Zeerijp-3A DSS cable. Note that the 2015 RFT shows that the vertical pressure match in ZRP-3A is good, such that any deviation in trends should be related to compressibility.

A new methodology is introduced in step 5) where a check is done if there exists a subsidence mismatch within the expected minimum and maximum bands of the compressibility as shown in Figure 7-18. This allows for clearer guidance on where the pressure match needs to be adjusted to achieve acceptable subsidence matches in high fidelity geomechanical models which invert compressibility from subsidence. Figure 7-17 shows the example where the plots B) and D) clearly show the improvement in the subsidence match at Bedum. From the subsidence mismatch which uses only the base case compressibility in plots A) and D), the improvement is not as clear.

Subsidence mismatch = measured absolute subsidence – modelled absolute subsidence from best matched compressibility	Subsidence mismatch = measured absolute subsidence –modelled absolute subsidence from minimum/maximum compressibility range
Bedum aquifer faults open	
A) 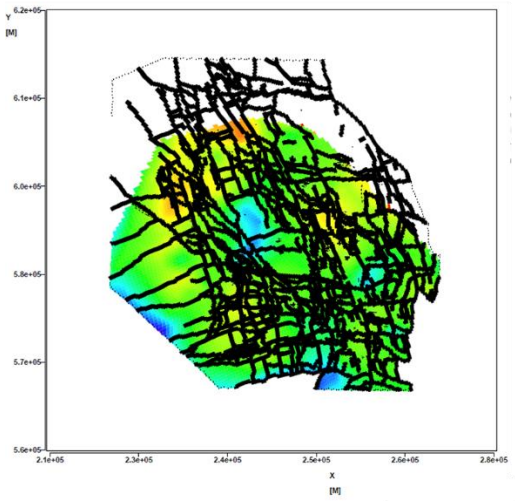	**B)** 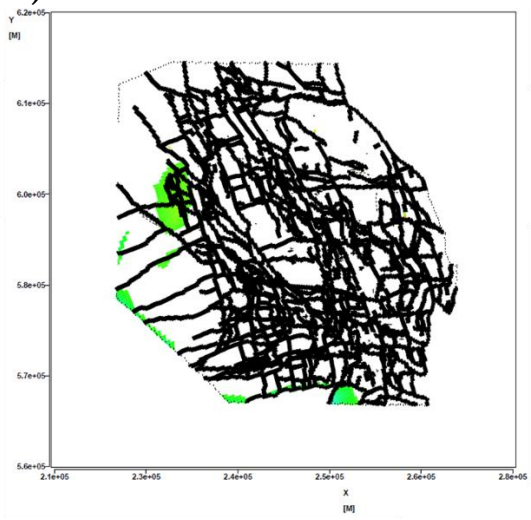
Bedum aquifer faults closed	
C) 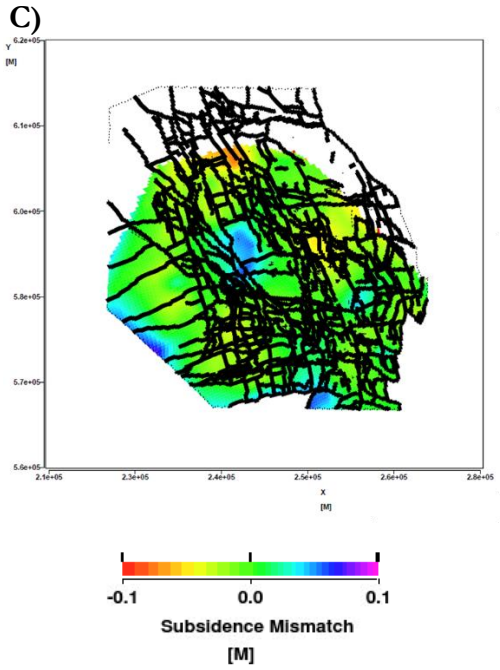	**D)** 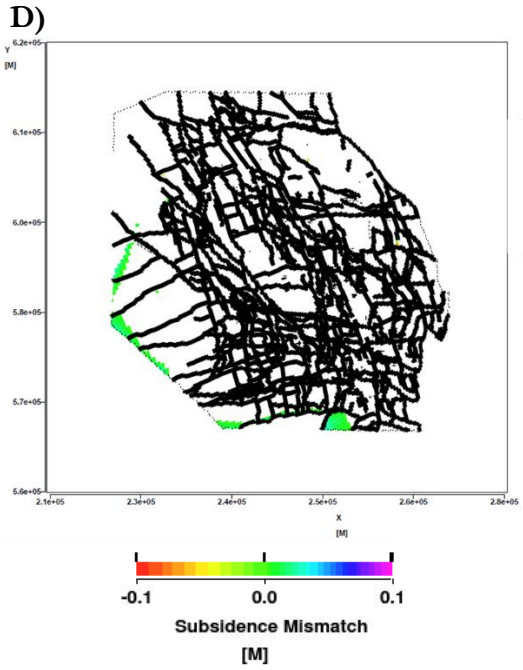

Figure 7-17 Impact of closing the Bedum aquifer fault (fault 11 in Figure 7-12) on the subsidence mismatch around the Bedum field. The right figure clearly shows the improvement where there exists a subsidence match within the bounds of the minimum/maximum compressibility.

7.9.2 Rock compressibility

The range in rock compressibility used for Carboniferous is described in chapter 4.4.5. A single value[10] was used for the Carboniferous uniaxial compressibility:

$$c_m = 1.5 \cdot 10^{-5}\ \text{bar}^{-1}$$

For the Rotliegend part of the reservoir a porosity dependent compressibility is used, based on core data.

Figure 7-18 shows the matched compressibility for the Rotliegend for the V6 and the V5 models. The match is shown together with the minimum and maximum acceptable range[11] in the porosity-compressibility relation measured on Rotliegend core data.

Note that the V6 and V5 porosity-compressibility trends fitted to subsidence data are on the low side of the range. NAM's official long term subsidence calculations delivered by the geomechanical team makes use of different subsidence calculations using a rigid base [26] and time dependent compressibility. The simple subsidence proxy used in MoReS does not incorporate these effects and as a result requires less compaction in the model for the same subsidence.

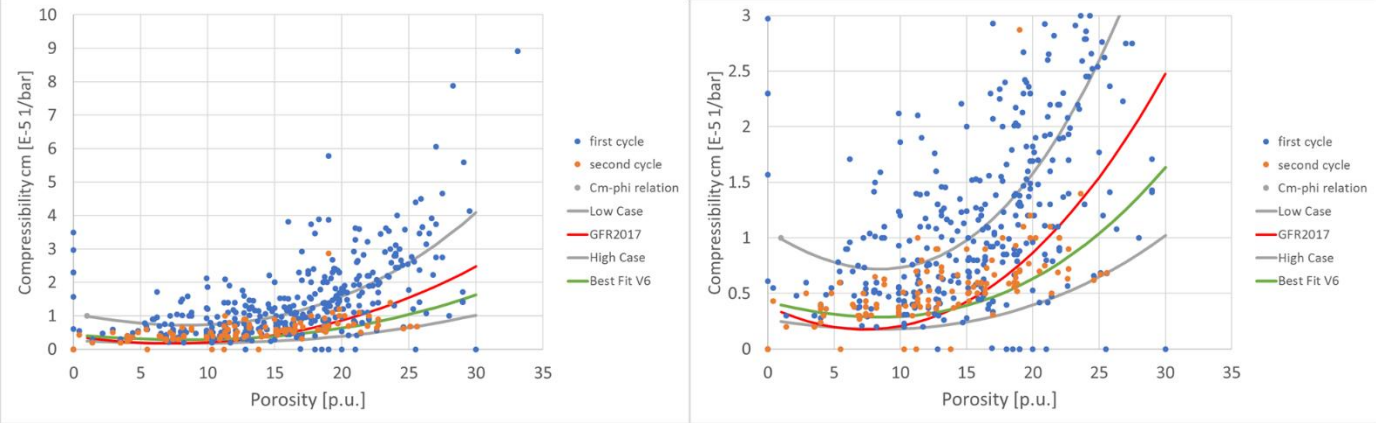

Figure 7-18 Uniaxial compressibility versus porosity as measured from core data. Curves for the minimum and maximum porosity-compressibility relation (grey curves) and the final V6 and V5 porosity-compressibility relation (green and red curves) are plotted over the data.

7.9.3 Match quality

The overall match to subsidence for the V6 model is 2.10 centimetre, as calculated by the subsidence proxy. Note that the MoReS subsidence match is purely used to guide the pressure match away from well control. The official NAM subsidence match and long-term forecasts are generated by high fidelity subsidence models by the NAM geomechanical team for which the MoReS pressure output serves as input. Figure 7-19 and Figure 7-20 show the subsidence match in the field and the distribution of compaction in the Rotliegend and the Slochteren.

[10] In line with the uniform property modelling of the Carboniferous.
[11] Determined by the geomechanics team

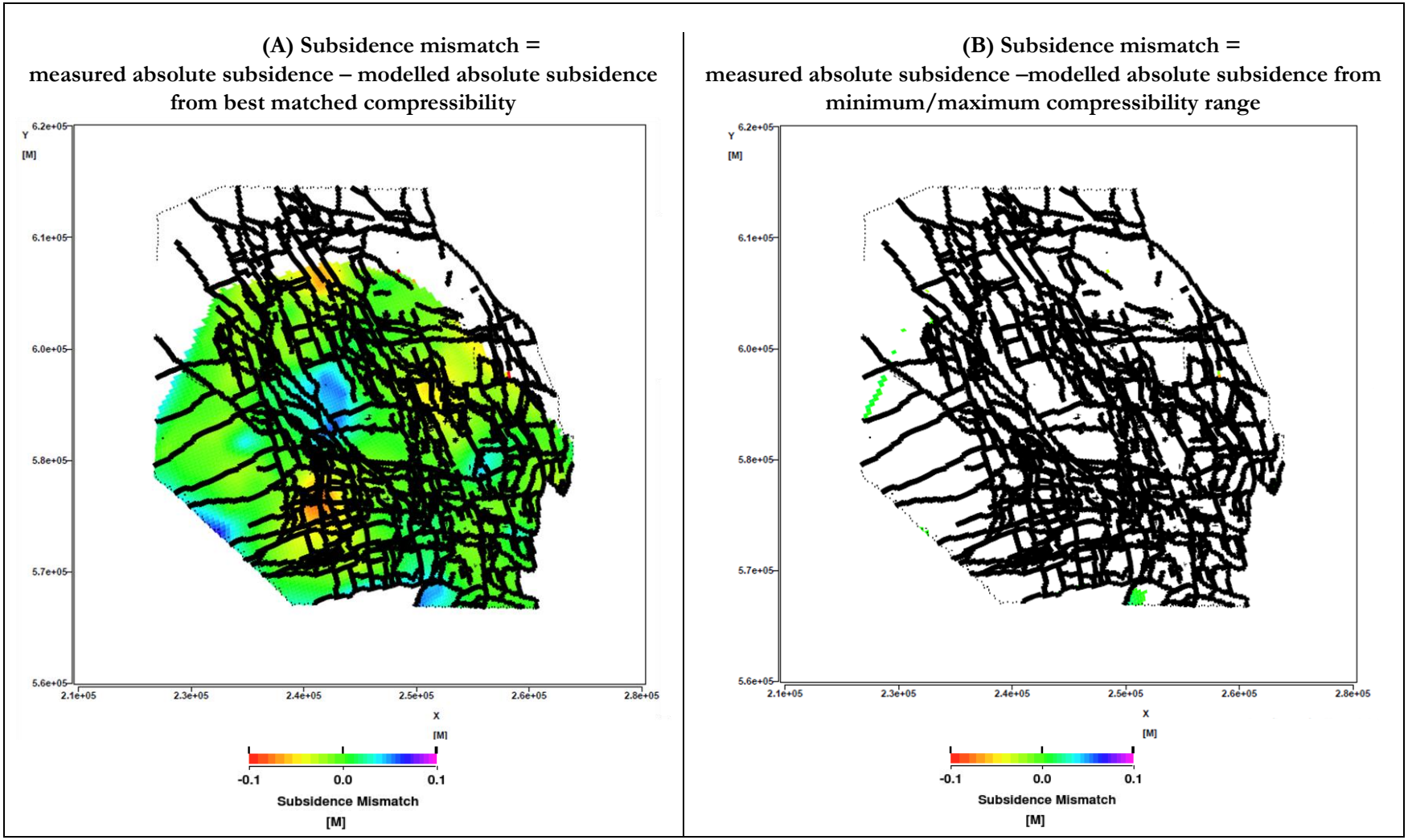

Figure 7-19 Subsidence match achieved by the V6 model. The left figure compares the subsidence from the best matched compressibility to the measured subsidence. The right figure shows the mismatch to measured subsidence remaining when using the minimum or maximum compressibility values from Figure 7-18. The figures show the subsidence mismatch as the measurement minus the model output; warm colors indicate too much subsidence, cold colors indicate too little subsidence and a good match is green.

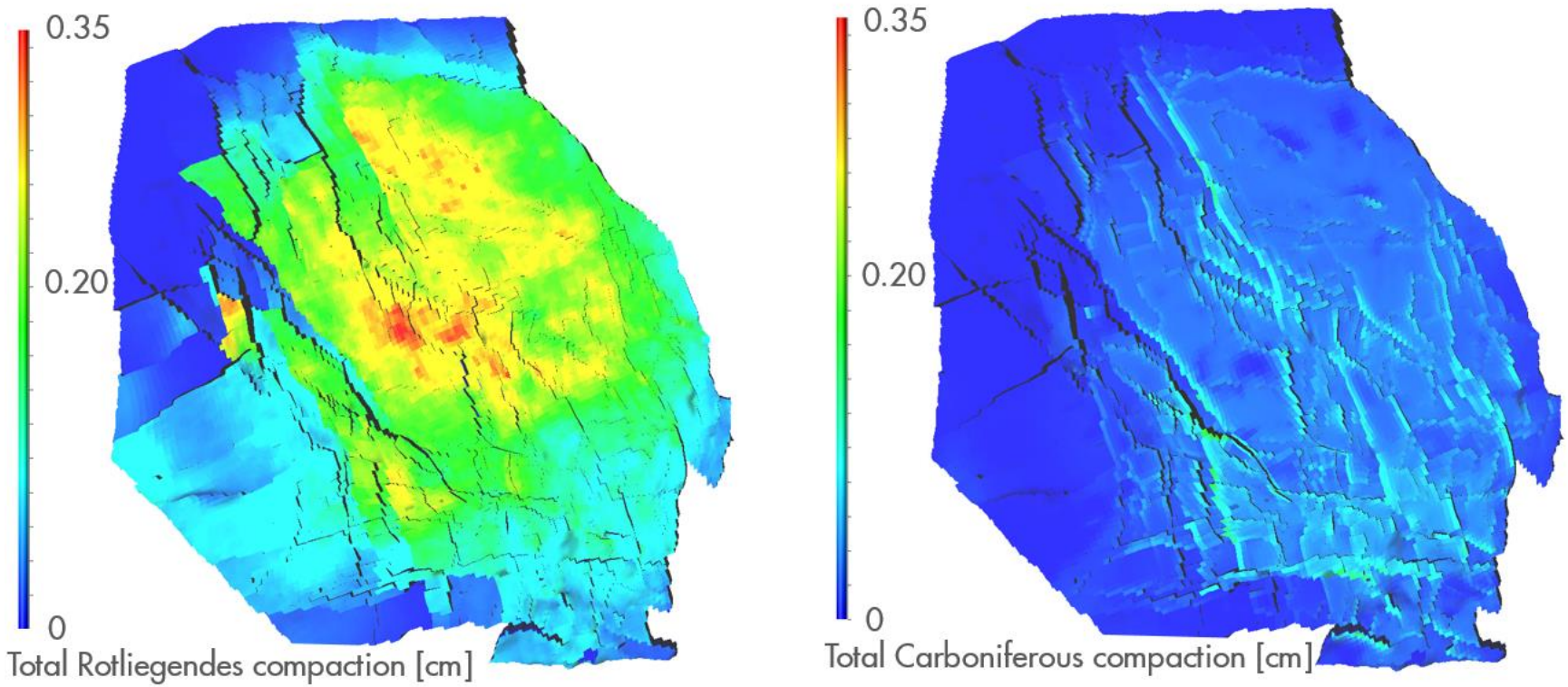

Figure 7-20 Total compaction in the field from the Rotliegend and from the Carboniferous. Note that the Carboniferous is mainly compacting through depletion over faults.

7.10 Gravity match

The overall match to gravity is 4.91 μGal. The gravity match is only used as a final review of the model quality.

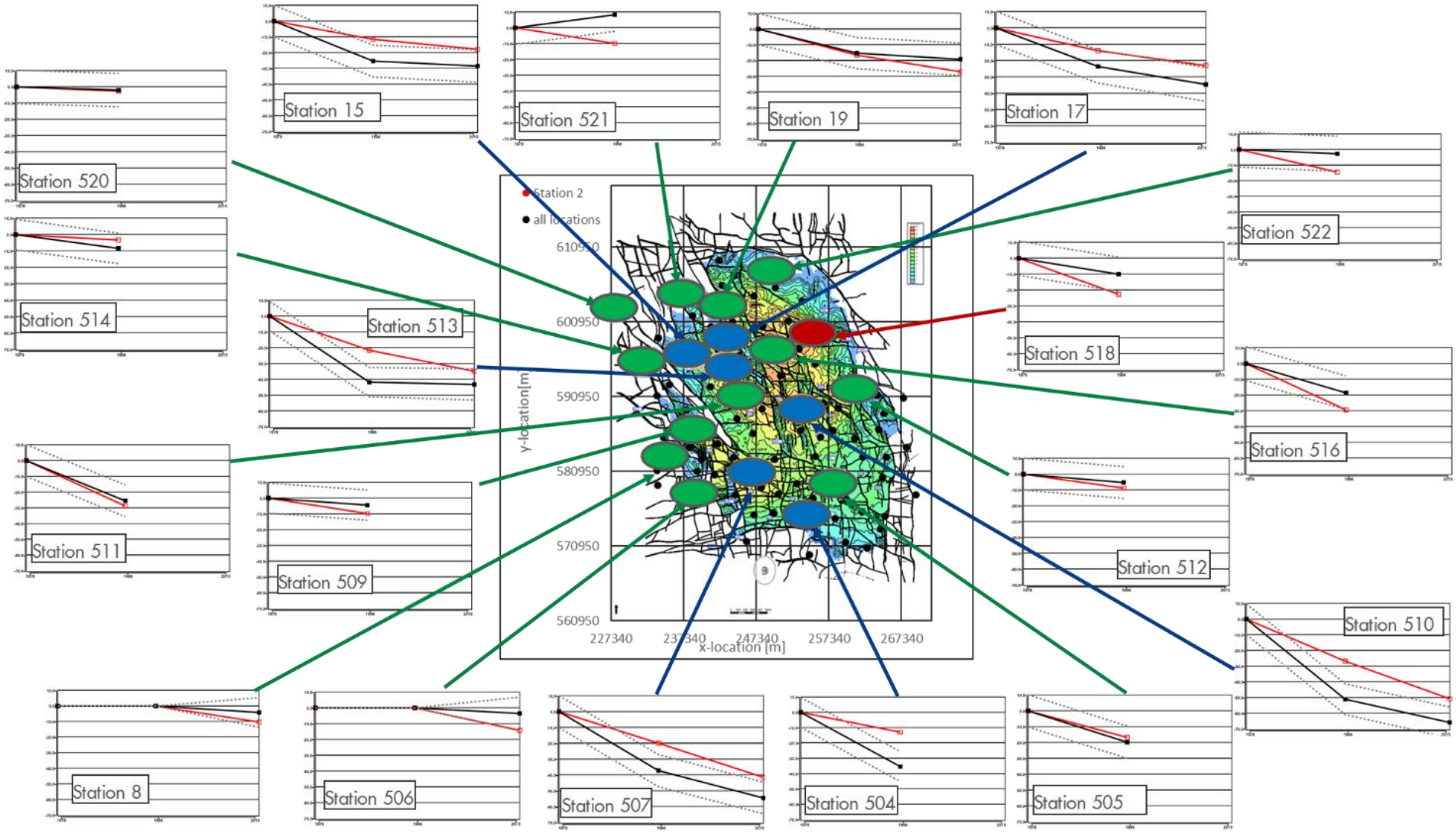

Figure 7-21 Gravity match at each station in the field. The black line is the measured data with the uncertainty in dotted grey lines. The simulated data is represented by the red curve. On the field outline good matches are shown as green ellipses, not enough decline in gravity as blue ellipses and too much decline in gravity as red ellipses.

8 History match – Regional

This section provides detailed information on the history match by area:

- Northwest area
- Northeast area
- East area
- Central area
- South area
- South-West Periphery

8.1 Northwest area

Figure 8-1 gives the total pressure depletion at 1/1/2018 for the northwest area (including the peripheral fields Warffum and Usquert). All (observation) wells and production clusters are indicated as circles. Faults that needed seal factor[12] adjustments are highlighted (and numbered). Note that faults with large offset, such as the one west of UHZ, provide major pressure baffling without applying an additional seal factor.

[12] Mores will calculated fault transmissibility based on the juxtaposed gridblocks. An additional transmissibility reduction across the fault can be defined by means of a seal factor.

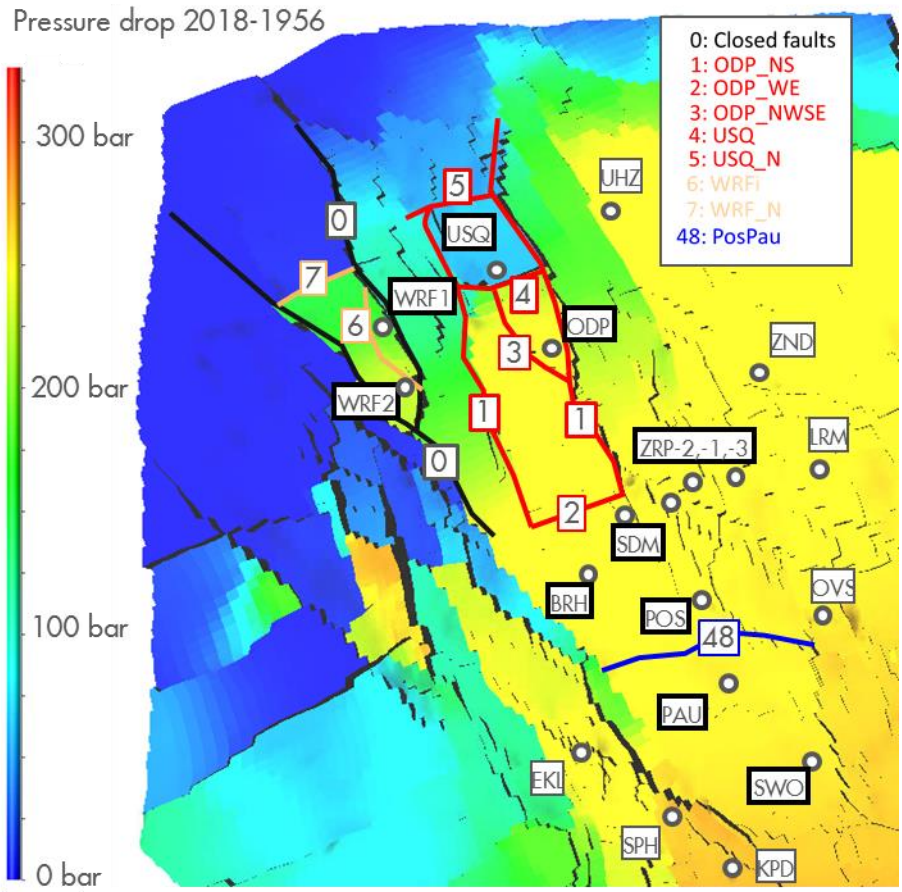

Figure 8-1: Total pressure depletion at 1/1/2018 for the North-West of the field

8.1.1 Main Northwest area and Usquert

Pressures

The introduction of gas-in-aquifer provides more pressure support in this area. Therefore, all SPG's for SDM, BRH, POS and PAU require a reduction in GBV and a high permeability to establish sufficient pressure drainage during field life. ODP and USQ in contrast need to be sealed off with faults 1-4 as depicted in Figure 8-1 to provide sufficient pressure lag. USQ needs limited pressure support from the north, therefore a small seal factor is also set to fault 5. A modest seal factor for the fault between POS and PAU provides the right amount of lag to increase the pressure match of the wells more to the north.

Water rise

The applied settings to establish the pressure match also resulted in a good match on water rise for ODP and PAU, and in an acceptable match at POS. The interpreted flat GWC from PNLs in BRH and in particular SDM could not be matched, but as indicated in section 7.8 there is an uncertainty associated with an absence of GWC movement from interpreted time-lapse PNL's.

The Rodewolt and Usquert aquifers do not need any deviation from their base case sizes.

8.1.2 Zeerijp

Pressures

The permeability increase as applied to the NW main area, also resulted in a good pressure match in the Zeerijp area.

Water rise

An acceptable match on the rise in water and vertical pressure profile from the RFT at ZRP-1 was achieved without further adjustment.

DSS cable

The match on the DSS cable at Zeerijp-3A is a qualitative one as discussed in chapters 7.2 and 7.9. The trend in the simulated strain profile in the Rotliegend appears to be decreasing upwards in comparison to the observed increasing upwards trend. The logging measurements of the Zeerijp-3A well were not yet included in the generation of the static model and therefore the porosity in the upper Slochteren is underestimated in the MoReS model. For any new model updates it is therefore recommended to include the Zeerijp-3A well logging measurements.

8.1.3 Warffum

Pressures

The faults bounding WRF are set sealing to match the initial pressures observed from the WRF2B RFT. The pressures in WRF can then be matched by increasing the permeability with the same order as the rest of the NW area and applying a small seal factor to the internal fault in the field.

Water rise

The water rise in WRF is well matched.

8.2 Northeast area

The pressure depletion over the entire history match period is given in Figure 8-2 for the northeast area. All wells are highlighted, as well as the faults that needed adjustments in fault seal factor. Note that faults with large offset, such as the one west of UHZ, provide baffles without the need for any seal adjustment.

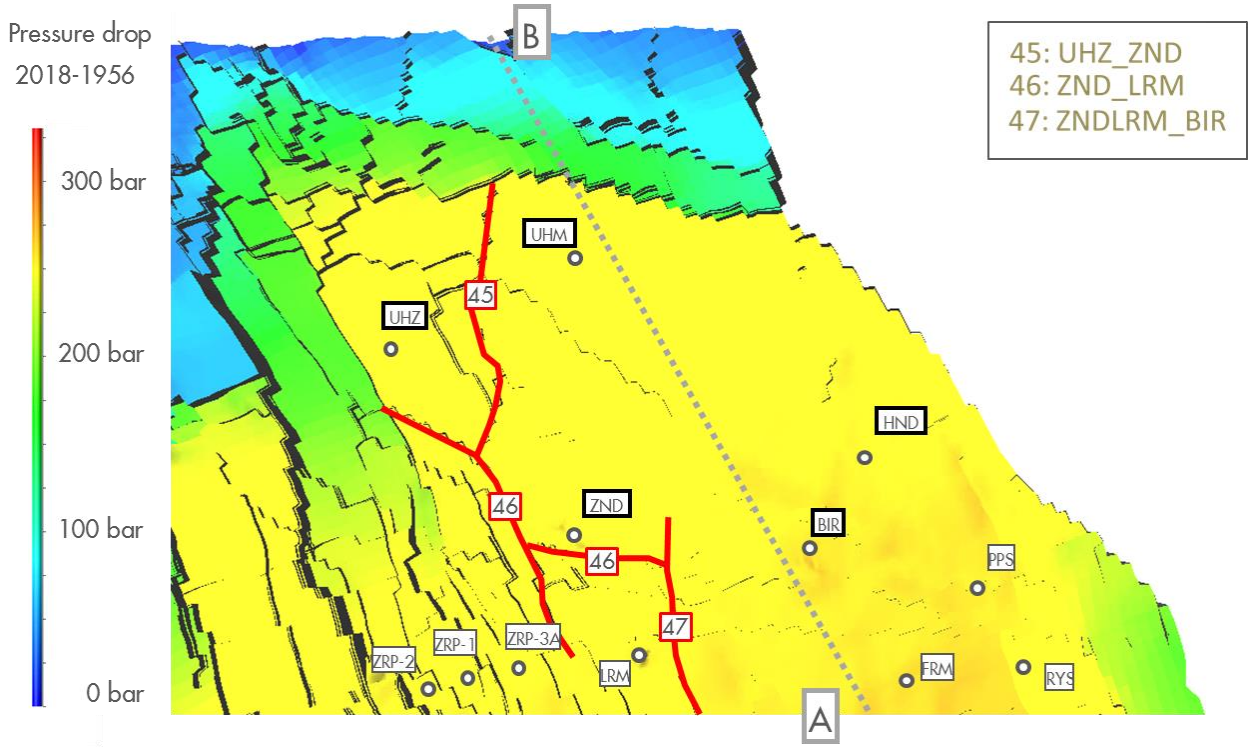

Figure 8-2 Pressure drop over the entire history matched period in the north east of the field.

Pressures

The introduction of gas-in-aquifer requires the overall energy in the area to be reduced in order to match the observed pressures. The porosity-dependent permeability multiplier introduced in section 6.2 then provides the connectivity adjustment needed to match the pressures in the northern observation wells (UHZ-1, UHM-1A and HND-1) as well as the production clusters (ZND and BIR). Fault 45 and 46 are introduced to baffle depletion in UHZ from ZND and depletion in ZND from the south (LRM/AMR).

Figure 8-3 shows that a slight pressure lag in the water leg is obtained for the northeast area, but is smaller than those observed in the UHZ, BIR, PPS, RYS and FRM RFTs. The pressure lag is strongly dependent on the extent of the sealing Ameland shale and the saturation of the gas-in-aquifer, both blocking further depletion. The applied seal-factor to the Ameland shale is limited to the extent where it is thicker than 7.5m[13], see Figure 8-4. The areal extent of the sealing Ameland could be enlarged to obtain a better match in the northeast and east RFTs, but in that case the Zeerijp-3A pressure lag in the water leg will not match anymore. Due to the importance of ZRP-3A in the determination of the Carboniferous settings, the match here is preferred. Increasing the gas-in-aquifer can also improve the pressure lag in the RFTs, but this is not supported by the overall pressure match in the region.

[13] A thinner Ameland shale is less likely to be laterally continuous (and hence vertically sealing).

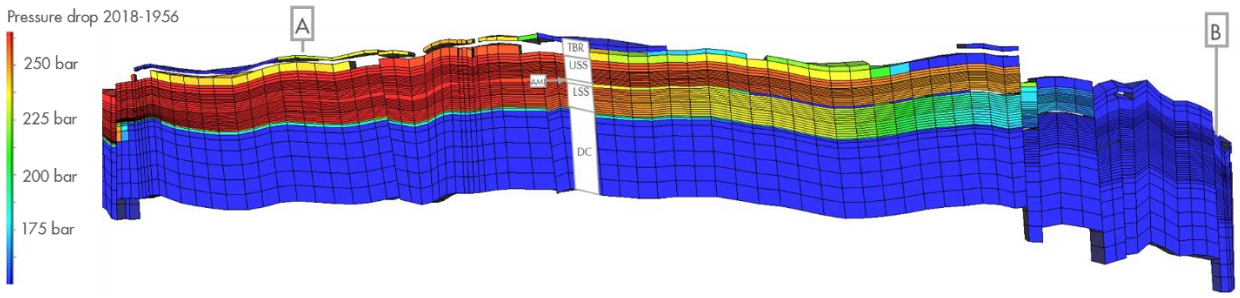

Figure 8-3 Pressure drop over field life for YZ cross-section at x=94 as indicated in Figure 8-2. The 5 main reservoir units are indicated. Note that the vertical axis is enlarged by 650% to highlight vertical differences.

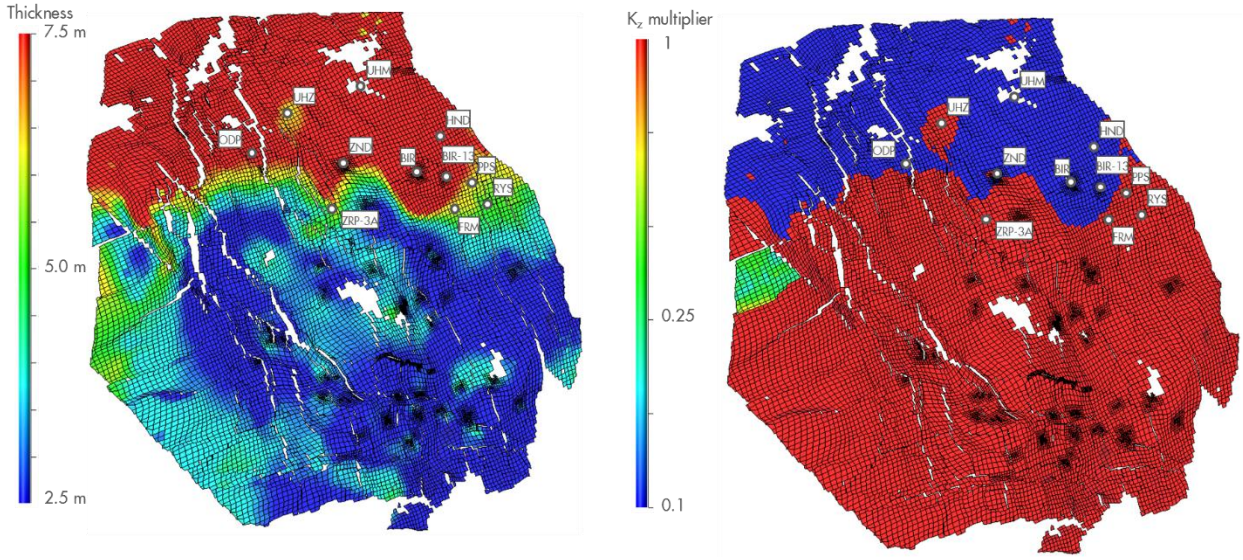

Figure 8-4 Thickness map of the Ameland shale and the vertical permeability multiplier. A vertical permeability multiplier is set for THK > 7.5 m. The locations of the northeast region wells and Zeerijp-3A are highlighted.

Water rise

The observation wells UHM and HND have modelled water rise, but this is not in line with the interpreted PNLs, 7.8 explained already that PNL interpretations with a flat GWC are considered unreliable until further study. Furthermore, the PNL match at ZND is comparing an inconsistent set of data. The first 3 interpretations are from the OH and PNL assessment in ZND-2A, whereas the last data point is from the RFT in ZND-9A. The flat GWC from the model is in line with the first 3 interpreted GWCs. This leaves only the PNLs from BIR to be considered reliable. Water rise has always been hard to match in these BIR wells but is achieved in the V6 model.

8.3 East area

An areal visualisation of the pressure depletion over the entire history match period is given in Figure 8-2 for the east area. Note that faults with large offset, such as the one east of OLD, provide baffles without the need for any seal adjustment.

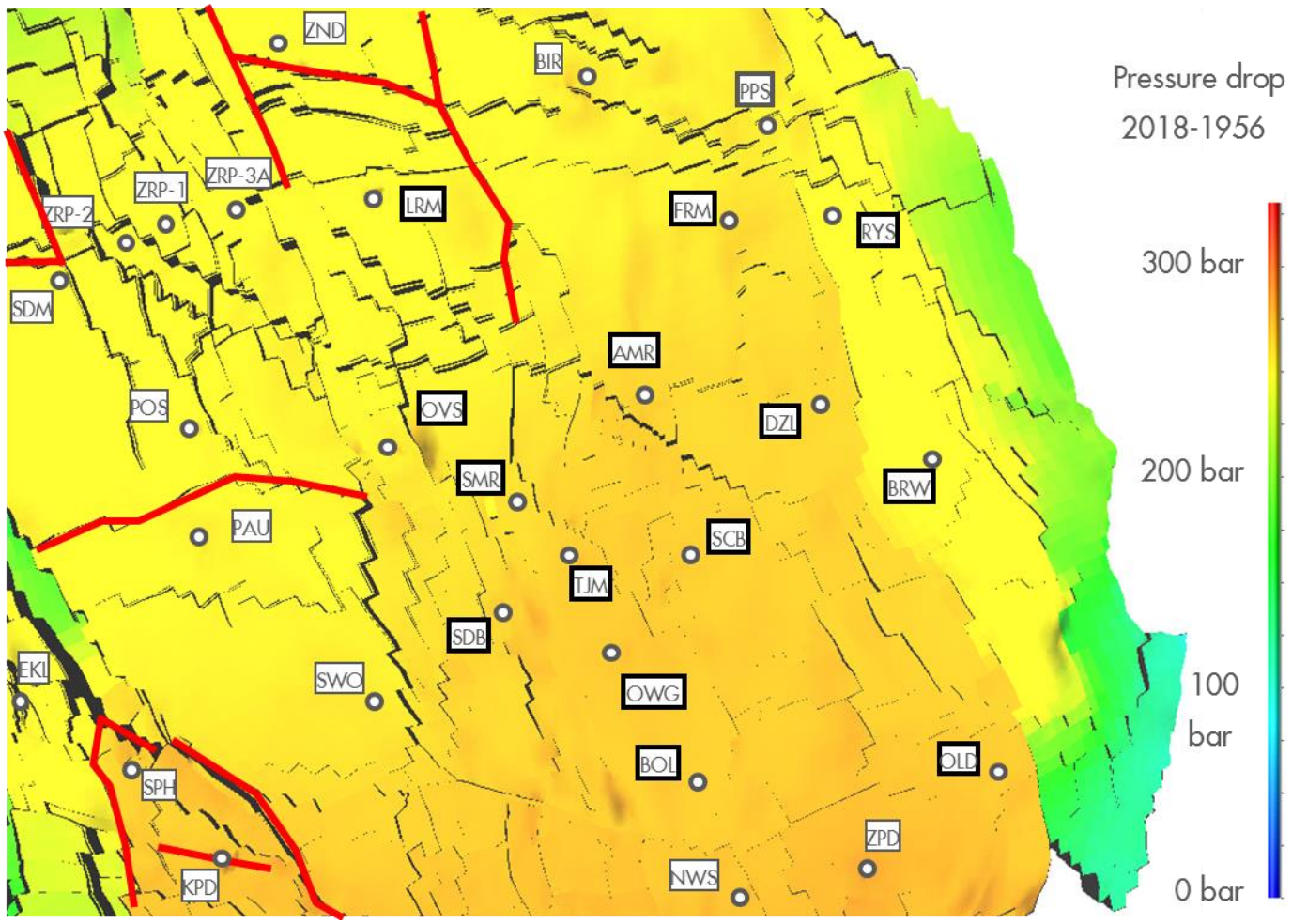

Figure 8-5 Pressure drop over the entire history matched period in east of the field. All wells are highlighted, as well as the faults that needed adjustments in fault seal factor

Pressures

The eastern area is well connected to other areas in the field and needs no further application of seal factors, see Figure 8-5. After reducing the area's volumes and increasing permeability a good pressure match is obtained. The BRW injection wells are a special case. Up to 2006 the pressure behaviour is well matched, but the model shows that in the period thereafter pressures had to be extremely high to inject the given volumes. It is likely that the reservoir has been fracked in this period, which has not been incorporated in the model. The latest pressure measured in 2018 shows that the modelled pressures are too low for BRW2A.

The pressure lag observed in the water leg of the RFTs in RYS, PPS and FRM is already explained in the previous chapter.

Water rise

The small water rise observed in the OVS and SDB PNLs is matched in the model. The water rise more eastwards in FRM is provided as well by the model, albeit some years late. DZL sees too much water rise in the model, but can be explained by the lack of vertical baffling in the model caused by some shales potentially present around the well, see Figure 8-6. It is recommended for further model refinements to investigate the presence of these shales and their inclusion in the model.

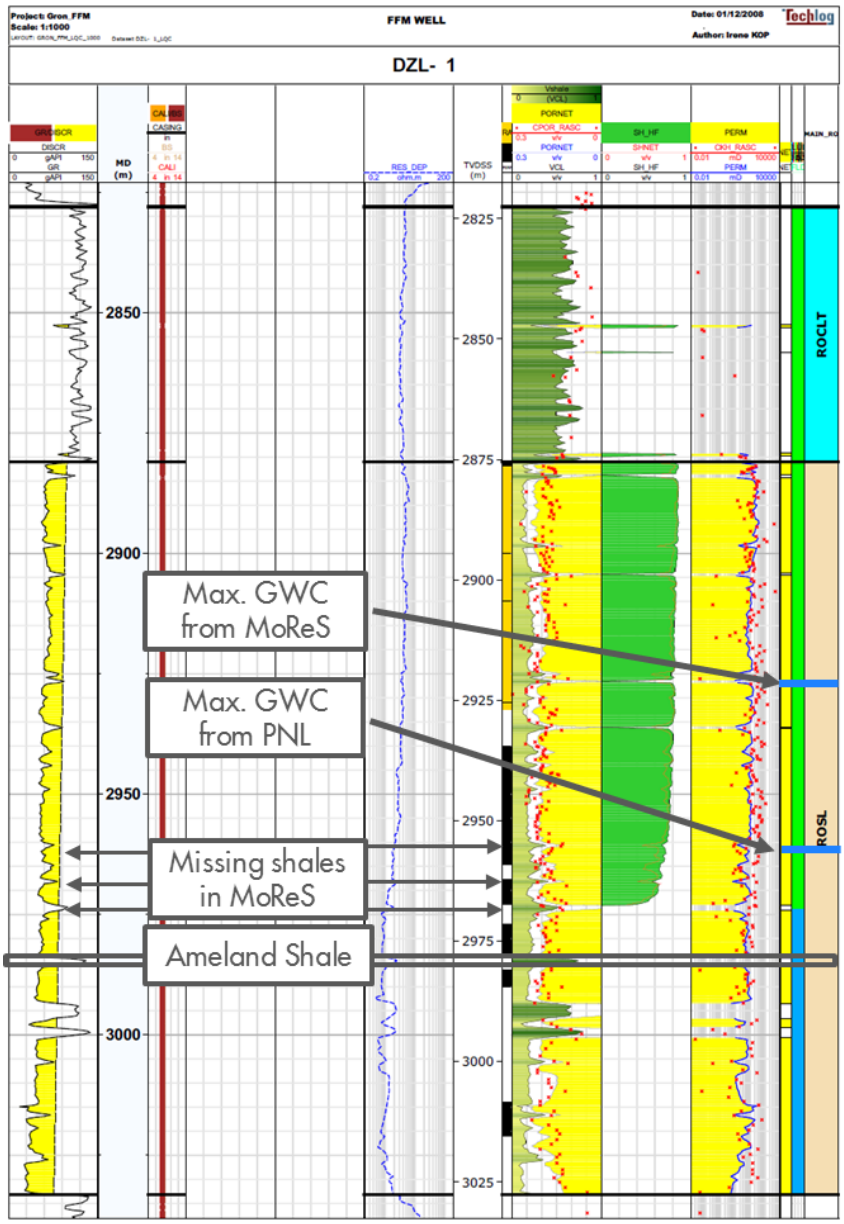

Figure 8-6 Log panel for DZL. Note the initial GWC is indicated by the end of the green gas saturation in the 5th last column. The column left of the gas saturation shows a greenish coloured V_{shale} ,darker green means more shale content. The suspected shale layers are indicated as well as the last measured GWC from PNL and the corresponding modelled GWC.

8.4 Central area

The pressure depletion over the entire history match period is given in Figure 8-2 for the Central area. Note that faults with large offset, such as the one east of OLD-1, provide baffles without the need for any seal adjustment.

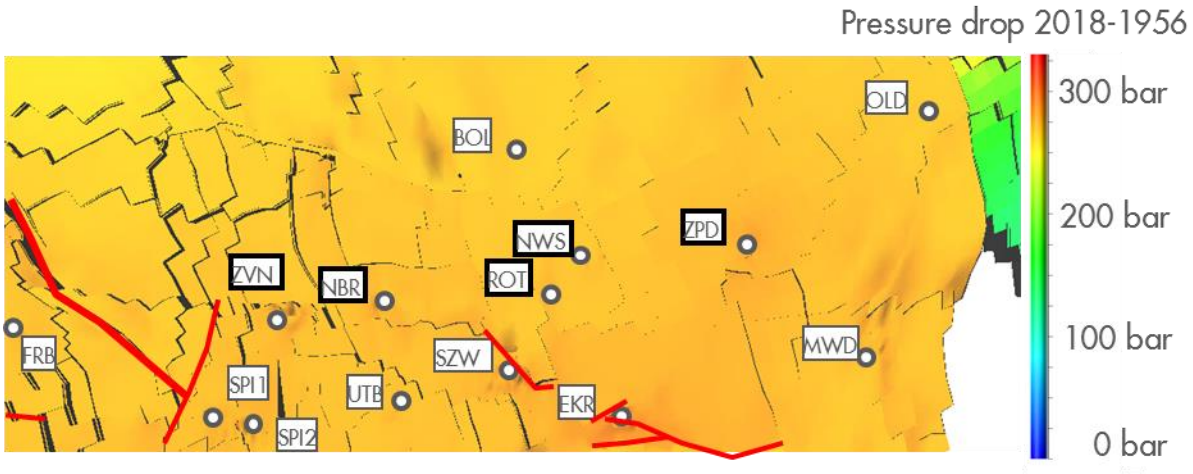

Figure 8-7 Pressure drop over the entire history matched period in the centre of the field. The wells in this area are highlighted, the closest wells and faults in the east, southeast and southwest region are shown as well for reference.

Pressures

In the Central area and further south in the field, there is no aquifer in the Rotliegend present anymore. Therefore the gas-in-aquifer plays much less of role, but the gas bearing Carboniferous starts to provide additional pressure support.

The Central area needs the strongest permeability multiplication to obtain pressure support from the rest of the field in early field life. GFR2017 shows that high permeable streaks can explain the need for high permeability multipliers in the dynamic model [3]. Volumes in the area are scaled down to match late life pressures.

The RFTs in ZPD and ZVN provide only 2 and 1 data point respectively. The ZVN one is outside the model boundary, but seems to be in line with the modelled pressures in the gas reservoir when extrapolated. The 2 data points for ZPD show a decreasing pressure with depth, but the bottom pressure point is matched by the model. This can be noted as interesting as the pressures from ZPD SPGs around the same period (1971) appear te be too low.

Water rise

There is no expected rise in water in the central area given that there is no bottom water (Gas Water Contact within the Carboniferous), therefore GWC monitoring has not been done.

8.5 South area

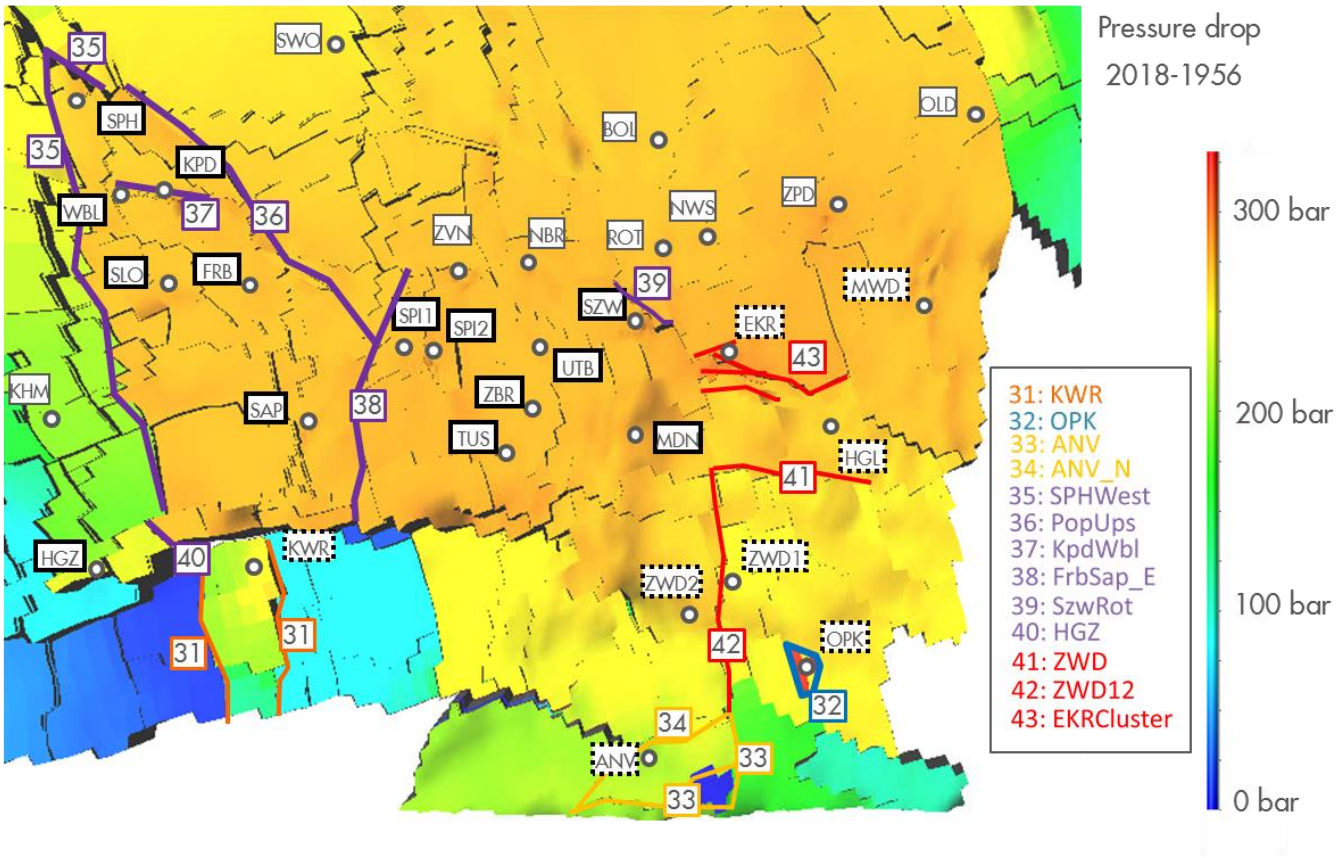

Figure 8-8 Pressure drop over the entire history matched period in the southwest and southeast of the field. The wells (southwest bold black outline, southeast dotted bold black outline) and faults in this area are highlighted, the closest wells in the east, central and southwest periphery regions are shown as well for reference. Note that faults with large offset, such as the one east of OLD, provide baffles without the need for any seal adjustment.

8.5.1 Southeast

Pressures

In previous models the southeast permeability multiplier was limited to the southeast gas reservoir and east of the fault between ZWD1 and ZWD2. Pressures in ANV need an increase in connectivity to the main field however. Also the KWR field needs comparable permeability multipliers as the southeast area to achieve a pressure match. The permeability multiplication region was extended for the southeast area up to the southern model edge and to the western KWR fault (fault 31 in Figure 8-8).

To match the pressures in the region again a strong increase in permeability is needed, as well as a reduction in volumes. Note that the southeast volume multiplier is not applied to OPK, ANV and KWR. Despite the overall permeability increase, faults are needed to arrest some of the depletion to the southern wells, as well as some baffling is needed to match the pressure lag observed between ZWD-1 and ZWD-2, see faults 41 and 42 in Figure 8-8.

Special focus was given to the EKR cluster, which has always been troublesome to match. The now available CITHP data shows up to 3 bar pressure differences between cluster wells at different sides of faults, proving

the sealing capacity of the faults at EKR[14]. Besides the main fault separating the blocks with EKR-205 and EKR-209 other faults around the cluster are set sealing as well to decrease the pressure support to the EKR cluster and improve the CITHP match, see Figure 8-9 and fault 43 in Figure 8-8.

Furthermore EKR-204 was initially modelled as being located south of a minor fault block near the EKR cluster. This results in a different pressure behaviour than the nearby wells EKR-5,-6,-11 & 205, whereas the CITHP shows the wells should behave alike. The EKR-204 well was therefore moved north into the same fault block as EKR-5,-6,-11 & 205, see Figure 8-9.

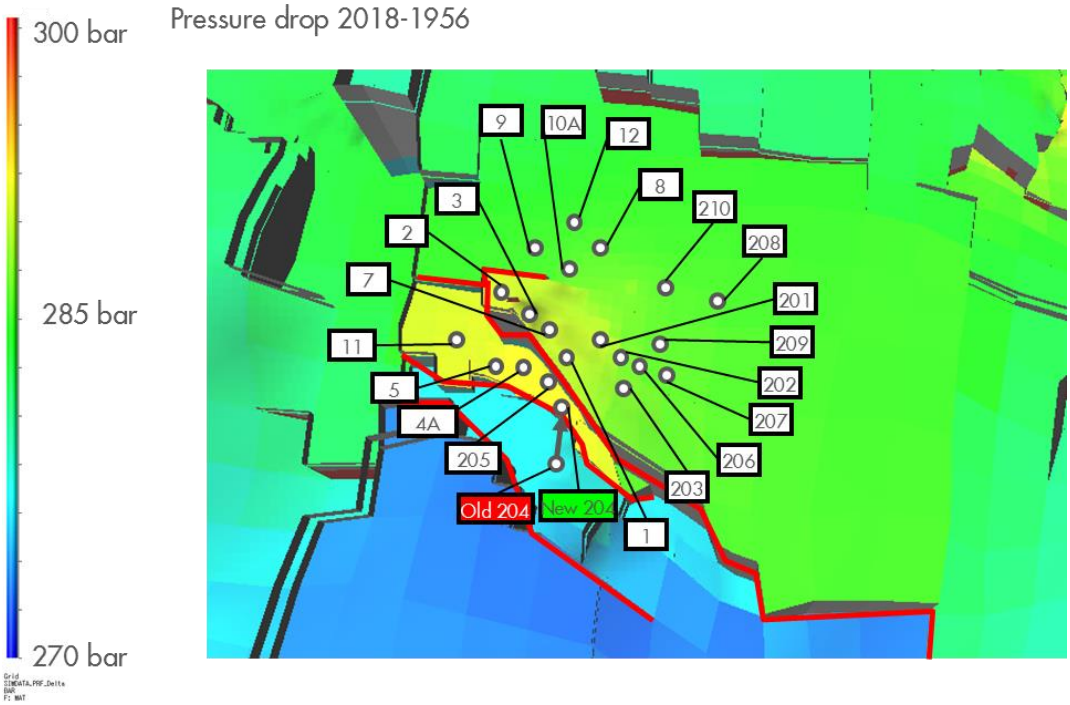

Figure 8-9 Pressure drop zoomed in around EKR cluster wells to illustrate the different pressure regions. The movement of the EKR-204 well is highlighted as well.

A re-assessment was made of the only HGL SPG measurement. The data point was obtained from a long term memory gauge. Previously, a gas column had been assumed to convert from gauge depth to datum pressure. However, a water column was reported at the time of the actual measurement. Therefore, the registered pressure was changed from 95.8 bar to 104.8 bar.

Water rise

The only part of the southeast area subject to water rise is ZWD which has been difficult to match in previous models. The extended permeability multiplication region provides enough connectivity to match the measured water rise in V6, without the need for an active Annerveen-Veendam aquifer.

8.5.1.1 Oude Pekela

The OPK in-place volume was adjusted in line with the GIIP as reported from p/Z analysis: 0.89 N.Bcm [10]. The permeability was multiplied according to the southeast permeability multiplier. Large structural uncertainty exists in the area due to imaging problems from an overlying salt dome [10]. This justifies the relatively large volumetric multiplier needed in OPK. The main factor governing the OPK's pressure

[14] Confirmed 3 bar pressure difference from the EKR-205 and EKR-209 SPGs from 14 August 2017.

behaviour is however the faults separating it from the Groningen field to which a sealing factor has been applied, see fault 32 in Figure 8-8.

8.5.1.2 Annerveen-Veendam

As for the OPK field, ANV is very much affected by the overlying salt dome in the area. Therefore, the large volumetric multiplier needed to scale down volumes and match the observed depletion in the well is justified. Permeability has been reduced by the extended southeast permeability multiplier. The connection of the ANV to the main Groningen field is governed by setting faults 33 and 34 in Figure 8-8. Finally, to match the pressures at ANV, the AnnerveenVeendam aquifer size is diminished. This does not affect the water rise observed in ZWD.

8.5.1.3 Kiel-Windeweer

The Groningen model is too course to match the actual behaviour of the KWR field: the internal separation of the field by a fault as well as the pressure depletion of the low permeable field are not captured [10]. To be able to match the KWR pressure behaviour the permeability is multiplied by the southeast permeability multiplier and the volumes are scaled down. Two pressure points from the 1997 RFT indicate that there is depletion in the Carboniferous in KWR before production from the field has started. This is however not in line with the other SPG measurements and therefore a seal factor is applied to the faults bounding the field to prevent pressure depletion before production starts.

8.5.2 Southwest

Pressures

The southwest of the field is the only area of the main field (excluding the southwest periphery) which needs an increase in volumes to match pressures. Permeability needs a strong increase, although there are some faults needed.

GFR2017 showed that faults are needed to compartmentalize the KPD/FRB/SLO/SAP area from the SPI/TUS/UTB area as indicated by the observed 3-5 bar pressure difference [2], see faults 36 and 38 in in Figure 8-8. GFR2017 also indicated the need for a sealing factor to the KPD cluster fault to match the northern as well as the southern KPD cluster wells [2], see fault 37.

The HGZ well has initially too high pressure, a seal factor to fault 41 as depicted in Figure 8-8 is needed to block depletion from the southwest area. To prevent too much depletion in EKL from the southwest a seal factor is needed at the SPH fault, this is indicated by fault 35 in Figure 8-8. Late life pressures observed in the CITHP data at SZW are slightly too high, a sealingness of the fault north of the cluster helps to bring pressures further down, see fault 40 in Figure 8-8.

Water rise

There is no expected rise in water in the southwest area, therefore GWC monitoring has not been done.

8.6 South-West Periphery

The South-West Periphery is the most complicated area within the Groningen field due the extensive faulting in combination with low-quality seismic signal as a result of the overlying salt. Fault seal factors were applied to create different dynamic compartments that match the pressures observed in the wells.

The EKL production cluster dominates depletion in South-West Periphery. Together with the EKL-13 extended reach well, it depletes the Lauwerzee aquifers southwest of the field. The Lauwerszee aquifer is also depleted by the land fields FAN, PSP, ROD and VRS.

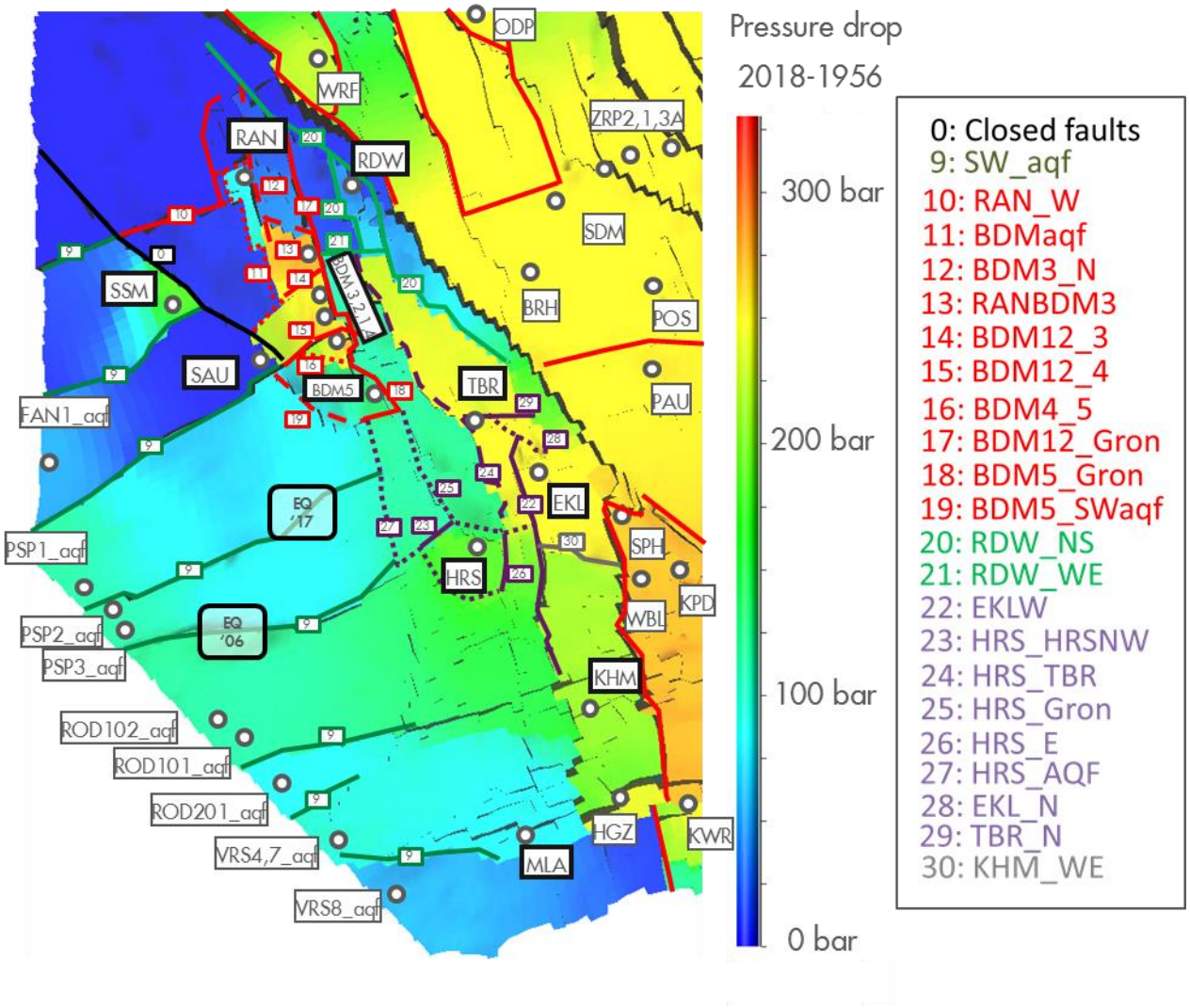

Figure 8-10 Pressure drop over the entire history matched period in the southwest periphery of the field. The wells in this area are highlighted, the closest wells and faults in the southwest and northwest regions are shown as well for reference. Note that faults with large offset, such as the one southwest of BRH, provide baffles without the need for any seal adjustment. The approximate locations for the 2006 Eelderwolde and 2017 Paddepoel earthquakes are indicated as well.

8.6.1.1 Ten Boer layer thickness

The static model has not properly incorporated the Ten Boer layers in this area in the field. The Ten Boer reservoir unit consists of 3 layers in the model, where the deepest unit in the Ten Boer (layer 3 in the dynamic

model) is a thick layer with relatively good properties and the shallower layers become thinner with worse properties. The shallower Ten Boer units, layer 1 and 2 are in most areas discarded as non-reservoir layers based on their weak properties. In the V6 static model the thickness of the Ten Boer layers is not incorporated correctly, where the TBR-3 layer is very thin and the TBR-1 layer is very thick. As a result, much of the Ten Boer is cut-off in the dynamic model as the thick TBR-1 layers are non-net reservoir and only a small TBR-3 layer remains. In most areas of the field this does not result in much issues as the gas column in the Slochteren dominates all dynamic effects. Towards the edges of the gas reservoir however, the Ten Boer can play a large role. When most of the gas column is located in the Ten Boer, the model is missing this connectivity. This effect plays a large role in the connectivity between BDM-4 and BDM-5 and the connection of the Harkstede block to the block to its northwest. It has been decided to continue with the mismodelled Ten Boer in the V6 model as the issue was discovered only at the end of the modelling work and only plays a role locally with the mismatch in BDM-5.

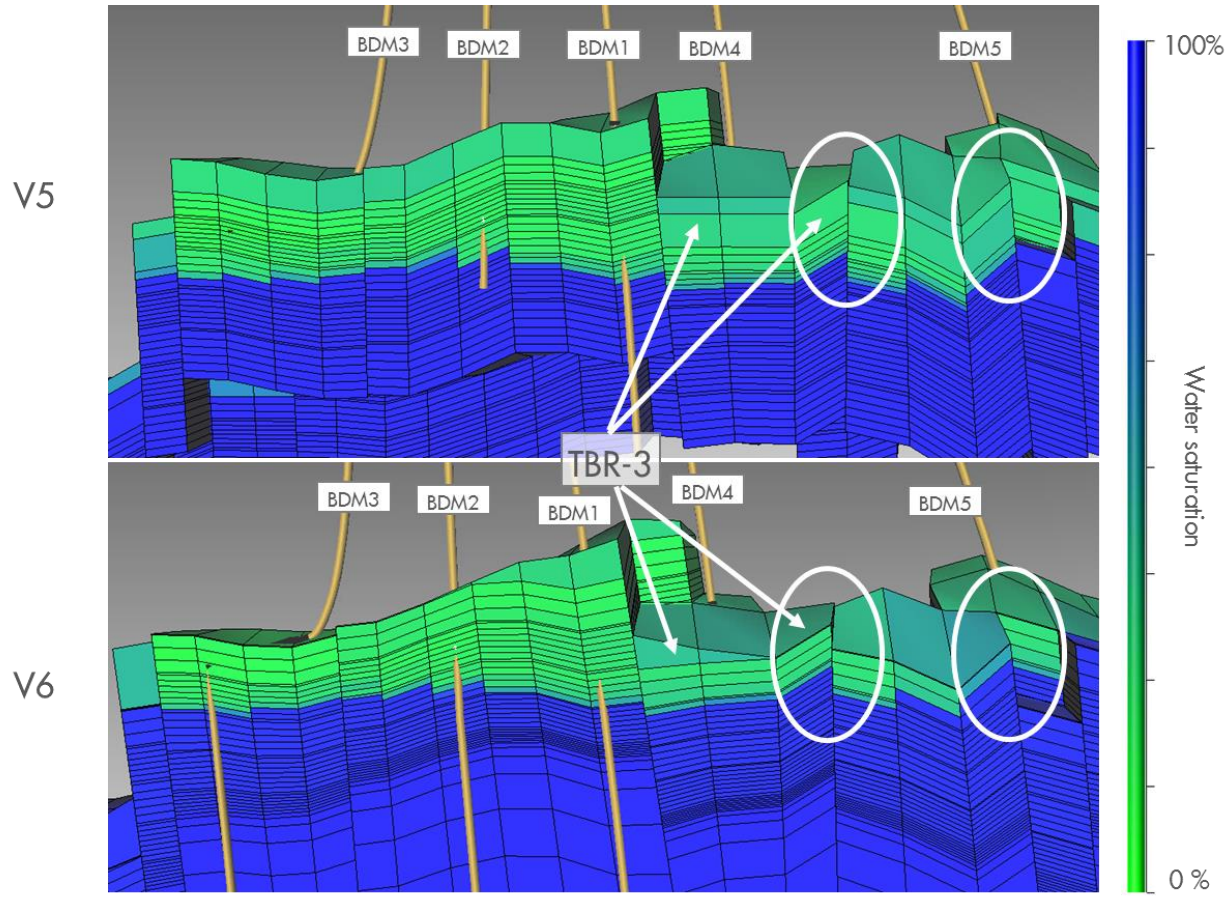

Figure 8-11 Comparison of gas column in x-layer 30 between V5 and V6. The decreased gas-gas connection in V6 between BDM-4 and BDM-5 due to the mismodelling of the TBR-3 layer is highlighted.

8.6.1.2 Kolham, Eemskanaal, Ten Boer and Rodewolt

The EKL cluster needs a GBV and permeability multiplication to obtain enough pressure support. Furthermore the fault between SPH and EKL needs a small seal factor to reduce the connectivity to the main field, see fault 35 in Figure 8-8.

The Rotliegend sandstones in the KHM blocks are offset by two large faults bounding it west and east, leaving a depletion path towards the north the EKL cluster. An increase in GBV in the KHM blocks and a fault seal factor as indicated by fault 30 in Figure 8-10 are needed to match its depletion via EKL. The vertical pressure profile as observed from the 1989 RFT in KHM-1 is well matched.

The TBR observation wells need a seal factor for faults 22,28 and 29 to prevent too much depletion from the EKL cluster. Enough depletion still has to occur via the TBR location to match the HRS/EKL13 pressures. The interpreted flat GWC from PNLs in TBR could not be matched, but as chapter 7.8 already indicated there is a need for a reassessment of flat interpreted GWCs from PNLs.

The Rodewolt observation well was drilled in 1998 and provides a pressure measurement from its RFT. Seal factors were applied to faults 20 and 21 to block depletion of RDW and match the pressure at the time of the RFT.

8.6.1.3 Harkstede

The volumes in the HRS block from the static model are 6.0 N.Bcm and need a large GBV multiplier to match the connected 17 N.Bcm gas as expected from p/Z- analysis of the EKL-13 well [27][15]. A match has been obtained by having the connected 17 N.Bcm all present in the HRS block, resulting in a GBV multiplier of 2.845. Appendix 5 in [2] provides the justification for the large GBV multiplier used based on the uncertainty in reservoir top, fault location and the FWL of neighbouring blocks. An attempt has been made to match the dynamic behaviour is the HRS block by connecting the block to the gas volumes in the HRS north and east blocks additionally to a GBV multiplier in the Harkstede block only. On top of this, extra connectivity was created between the HRS block and the block to its northwest via permeability multipliers to compensate for the strongly reduced thickness in the TBR-3 layer. This attempt did not result in an improved match however.

Besides the directly connected gas volumes in the Harkstede block, pressures are governed by a combination of pressure support from the gas bearing blocks to its north and depletion from the EKL cluster via the trough connecting HRS from its east and via TBR. Seal factors are applied to faults 23,24,25 and 26 to obtain a reasonable pressure match. This match could only be obtained by separating the blocks directly north of HRS from the EKL main cluster, thereby providing a slow pressure support to the HRS block. Depletion of the HRS block from the EKL cluster is then dominated by fault 26.

The modelled water rise in HRS is well matched. In EKL13 change in GWC is well matched, although the modelled GWC is 25m higher than the interpreted GWC from the PNL.

8.6.1.4 Lauwerszee aquifer

The minimum pressure depletion of 90 bar at the times of the 2006 Eelderwolde and 2017 Paddepoel earthquakes has been matched by depletion via HRS by keeping fault 27 open and by depletion from the land fields(Faan and mainly Roden and Pasop). The water extraction mimicking actual gas production from these fields has been scaled down sufficiently to keep the simulated pressures of the aquifer wells roughly above the measured pressures in their gas reservoir, but no attempt was made to match these pressures. Only the observed pressure lag between the different land fields has been roughly matched by applying a fault seal factor to faults 9.

[15] The volumes from the static model are some 2.5 BCM lower in the V6 model than the V5 model due to the mismodelling of the Ten Boer as described in 8.6.1.1.

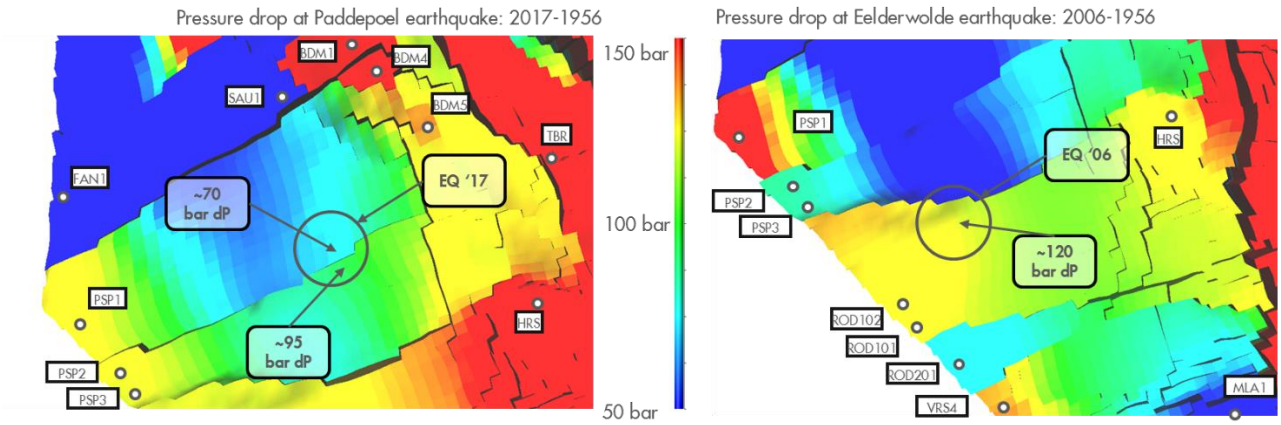

Figure 8-12 Pressure drop at the time of the Eelderwolde earthquake (left) and at the time of the Eelderwolde earthquake (right).

The Midlaren well is a small oil reservoir with a gas cap which has not been modelled explicitly, see chapter 6.12 in [28]. Therefore the pressures in the model are roughly matched to the observed pressure drop. The faults separating the Roden wells internally and the Vries-4 and -7 wells were not fully extended eastwards to maintain enough depletion in the Midlaren well[16].

The most southwestern area of the model is also likely to be subject to depletion from the Vries field alike the Roden, Pasop and Faan fields more towards the north. It was decided to include the Vries field to obtain potential effects of depletion of the Vries field in the model, although there are no hard constraints to the modelled pressures as the actual Vries field is not captured in the model. The pressures in the model are only constrained by keeping the pressures in the aquifer wells roughly above the observed pressures in the actual Vries field. Vries-8 is separated from VRS-4 and -7 in the model, but in reality the wells are quite well connected, see chapter 5.2. Therefore part of the production from VRS-4 and -7 is assigned to VRS-8 to obtain some of the expected pressure drop in the area.

In the northern Lauwerszee area, the Sauwerd observation well observed virgin pressure in the 1995 RFT. Depletion from Feerwerd and the Eemskanaal region is blocked enough by the seal factor applied to faults 9. Depletion from Bedum is blocked by the fault north of Sauwerd, which was set fully sealing.

The Feerwerd field is a tight reservoir which is hydraulically fractured. The coarseness of the model resulted in the wrong placement of SSM-2A in the model, therefore the well was manually shifted. The modelled permeabilities are too high compared to the interpretation from a 2002 well tests (0.35-0.74 mD) and therefore a permeability reduction is applied [29]. The well found virgin pressures in 2000, therefore depletion from Bedum is blocked by the fault north of Feerwerd, which was set fully sealing (this is the same fault as the sealing fault north of Sauwerd). A GBV multiplier has been applied to reduce the volume of Feerwerd, see chapter 6.12.12 in [10].

8.6.1.5 Bedum region

The Bedum field has been initialised in previous models using the aquifer gradient which was used in the land field: 1.15 bar/10m. For the V6 model it was chosen to keep the aquifer gradient in line with the Groningen

[16] Note that this is also supported by the small pressure drop observed in VRS-4 pre-production SPGs.

aquifer gradient of 1.17 bar/10m and therefore not fully seal off the Bedum field from the Groningen field. Figure 8-13 shows that the RFT data of Bedum-2 supports both aquifer gradients.

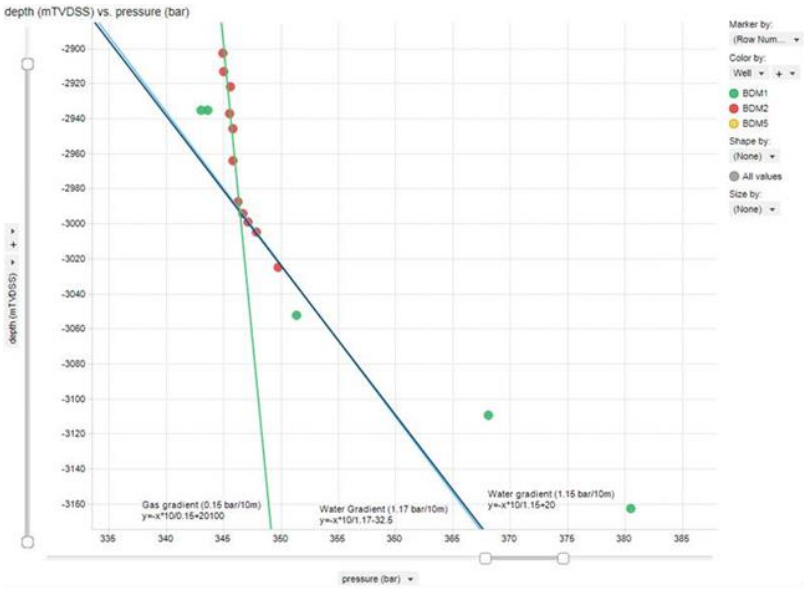

Figure 8-13 Bedum RFTs compared to hydrostatic pressures using a gradient of 1.15 bar/10m (dark blue line) and 1.17 bar/10m (light blue line).

The updated aquifer gradient implies that the Bedum field was not found at initial pressure as was assumed in previous models, but shows a 5-8 bar depletion based on the RFTs in 1977 in BDM-1 in 1984 in BDM-2. The model captures part of the depletion in 1984 in BDM-2 by not fully sealing the faults connecting Bedum to Groningen.

The gas volumes in Bedum result in too much pressure support in the model, therefore a GBV multiplier is used to decrease the Bedum energy. Note that the resulting 12.9 N.Bcm are still within the static uncertainty range from the Bedum 2016 RCCN.

The SPG measurements in Bedum and the RFT measurement in RAN show that Bedum is very compartmentalized. This behaviour is matched by setting faults 12-19. There remains a lack of connectivity to BDM-5 as a result of the mismodelling of the Ten Boer layer thickness, see chapter 8.6.1.1.

Subsidence towards the northwest of Bedum requires depletion to be arrested by applying seal factors to faults 11,10 and 12.

The model observes a rise in GWC in the Bedum wells, although the interpreted rise in GWC from PNLs in BDM-1 and BDM-2 is earlier than modelled.

9 Recommendations for future work

9.1 Gas-in-aquifer

9.1.1 Alternative gas-in-aquifer hypothesis

The V6 model was built upon the hypothesis that the gas-in-aquifer is present as a remnant of a bottom charge from below the field. At the time of constructing the model this was considered to be the best fit to the available data.

Since then, further petrophysical understanding was developed and a Basin Modelling study was initiated to improve the understanding of gas-in-aquifer. Subsequent insights suggest that an original gas-water contact (a paleocontact) was established at greater depth than the present-day contact, and that the gas-in-aquifer was trapped in response to the rising contact.

It is therefore recommended to initialise a new model update with gas-in-aquifer based on the paleocontact hypothesis:

- The ZRP-3A PNX found a gas-down-to of 3148 mTVDSS for gas-in-aquifer. Basin modelling work suggests a potential paleocontact at 3158 mTVDSS (structural spillpoint).
- Gas saturations are in line with the residual saturations for the Rotliegend. Slightly lower saturation could possibly be explained by diffusion of the gas over geological timescales.
- The relative permeability model for the gas-in-aquifer is the same as in the gas reservoir.

9.1.2 Additional gas-in-aquifer data acquisition

PNX log in southwest of the field

To establish the lateral extent of gas-in-aquifer towards the southwest of the field an additional PNX acquisition is recommended in this area.

PNX logging over the expected paleo-contact

The PNX logs only established a gas-down-to within the aquifer; no paleo-contact depth was established. Basin modelling work suggests a spill point at 3158 m TVDSS. It is recommended to run a PNX log on a well with sufficient aquifer penetration to cover this depth.

Dedicated well test

A dedicated well test over an interval within the aquifer would provide an unambiguous confirmation of gas presence, and provide data to calibrate relative permeabilities curves for the gas-in-aquifer.

In June 1995, a production test was done on the aquifer leg of MGT-1, some 20km West of the Groningen field. Associated gas was produced, with a decreasing GLR over time. Unfortunately, from the welltest report, Reference [30], it is clear that:

- MGT-1 tested an "HPHT" type reservoir. This may affect the relative permeability behavior (e.g. make it non-transferable to Groningen which is a hydrostatic field)
- There are no detailed recordings available of production rate versus time (for gas and water).

As such, this test is unsuitable to calibrate relative permeability curves.

9.2 Static model

9.2.1 Update Petrel model for correct intra-Ten Boer layer thickness

Section 8.6 describes that extrapolation artefacts have locally affected the the intra-Ten Boer thickness distribution (unrealistic thickness variations between the 3 Ten Boer layers). This error has locally suppressed connectivity between adjacent fault blocks with a small gas column, hampering the history matching in the Southwest Periphery.

It is recommended to correct the Ten Boer layer thickness model in a further model update.

9.2.2 Thickness of Ameland shale near BIR-4

The V6 model has a local anomaly in the modelled thickness of the Ameland shale near the BIR-4 well, Figure 9-1. If a new static model is made, the thickness should be updated line with the local trend.

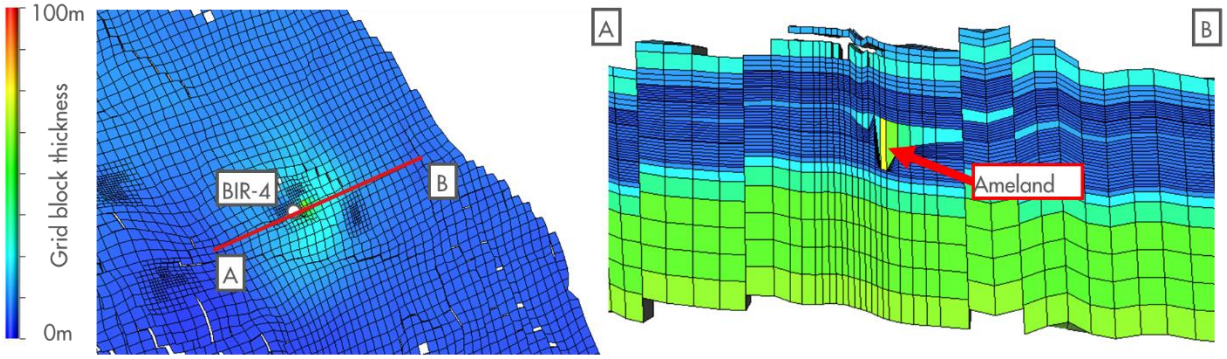

Figure 9-1 *Left: plan view of the reservoir simulation grid near the Bierum cluster, showing gridblock thickness for the layer that represents the Ameland shale (z=20). Right: Thickness of the grid blocks over the cross-section indicated on the left map.*

9.2.3 Extension of the model towards the southwest

The V6 model has investigated the impact of the depletion of the land fields southwest to the Groningen field on the pressure depletion in the Lauwerszee aquifers. A first step was made by introducing the effects of depletion using pseudo-wells in the aquifer. To more accurately describe the dynamic behaviour resulting from the depletion of these fields on the Groningen model it would be beneficial to extent the Groningen static model to include the Vries, Roden, Pasop and Faan fields.

9.3 Reassessment of GWC rise interpretations from PNL logs.

Chapter 7.8 describes the difference between flat GWC obtained from PNL interpretations and the rise in GWC as obtained from PNX data. In the V6 model, the GWCs which have been interpreted as flat are considered of too low confidence to constrain the model to. A reassessment of the GWC rise from PNLs in the field is therefore recommended.

9.4 Update values for Corey gas exponent

The V6 model uses the same relative permeability model as in the V5 dynamic model. New work in the SCAL experiments on the ZRP-3A well, Reference [31], provide an update of the ranges for the Corey gas exponent: $n_g \in [1.8, 3.3]$ instead of [1.5, 3.0]

It is recommended to use the updated range for new model updates.

9.5 Match of ZRP-3A strain data within Rotliegend

The strain measurements as obtained from the ZRP-3A DSS cable show some variability within the Rotliegend. It is recommended to investigate whether this trend can be better reproduced in the model.

9.6 Local V6 model improvements

9.6.1 Bedum-5 SPG mismatch

The pressures modelled in the BDM-5 well are too high compared to the SPG measurements. Chapter 8.6.1.1 already indicates that the mismatch could be a result of the mismodelling of the Ten Boer layer thickness. The mismatch should be further investigated.

9.6.2 Borgsweer history match improvement

The Borgsweer history match shows that during 2006-2010 the model has issues to inject the water in the reservoir (very high pressures). After this period, the latest 2018 SPG measurement shows higher pressures than the pressures modelled. It is recommended to further investigate the impact of the 2006-2010 injection period on the reservoir in Borgsweer and its potential effect on the history match.

9.6.3 Eemskanaal-13 PNL match

The model shows too much water rise in the EKL-13 PNL. It is recommended to further investigate this mismatch.

9.6.4 Assessment of the baffling capacity of shale interbeds

The V6 model overestimates water rise in the DZL-1 well. If reassessment of PNL data confirms the interpreted GWC rise, it may be good to examine in more detail how the well is captured in the static/dynamic model. As marked in Figure 9-2, the well penetrates several potentially baffling shale layers. Their ability to obstruct water ingress may have been underestimated in the dynamic model.

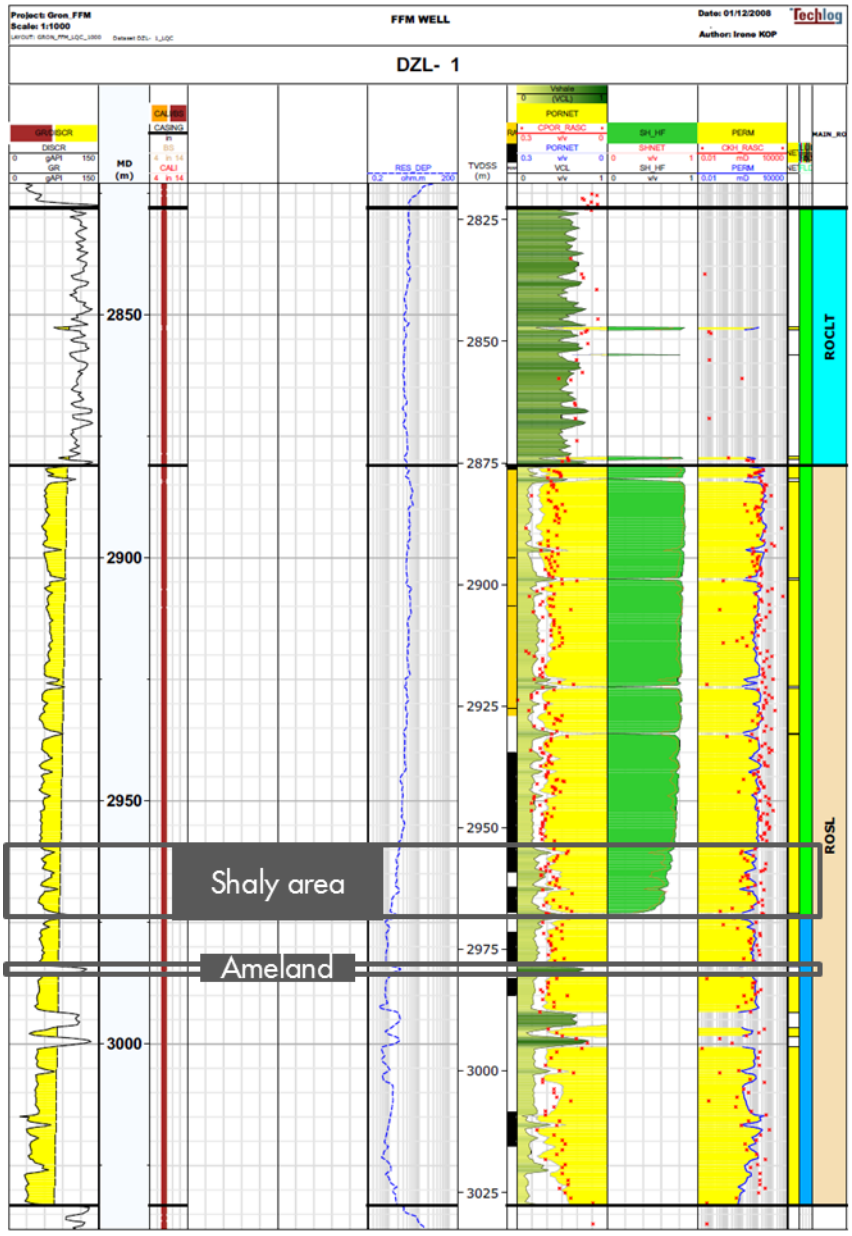

Figure 9-2 DZL-1 log panel with the Ameland shale and the suspected baffling area marked.

10 References

[1] Q. De Zeeuw and L. Geurtsen, Groningen Dynamic Model Update 2017 – V5, Assen: NAM, September 2017.

[2] Q. de Zeeuw, L. Geurtsen, "Groningen Dynamic Model Update 2017 - V5," NAM, Assen, 2018.

[3] H. Van Oeveren, P. Valvatne and L. Geurtsen, "Groningen Dynamic Model Updates 2017," NAM, Assen, September 2017.

[4] A. Boscolo Gallo, "CTD stack evaluation for residual gas detection over the Groningen field aquifer," NAM, Assen, July 2018.

[5] G. Ishmukhametova, "Investigation of gas presence in the aquifer of the Groningen field," NAM, Assen, 13/9/2017.

[6] G. Ishmukhametova, Investigation of gas presence in the aquifer of the Groningen field - Addendum, 28/9/2018.

[7] "Groningen Field Review 2012 - Static Modeling and Hydrocarbon Volume Determination," NAM, Assen, 13/3/2012.

[8] "Groningen Field Review 2003 - Static Modeling and Ultimate Recovery Determination," NAM, Assen, December 2003.

[9] G. Ishmukhametova, "Investigation of gas presence in the aquifer of the Groningen field," NAM, Assen, 2017.

[10] U. Burkitov, H. van Oeveren and P. Valvatne, "Groningen Field Review 2015 Subsurface Dynamic Modelling Report," NAM, Assen, 2016.

[11] H. Bosscher, Groningen Basin Model, 2018.

[12] H. van der Veen, B. Connely, F. Prousa et al., "Groningen Carboniferous Appraisal Project - Feasibility Report," NAM, Assen, 2009.

[13] E. Fokkema, "Groningen Carboniferous development petrophysics 2004-2007," NAM, Assen, 2007.

[14] B. van Assema, "Seismic interpretation and depth conversion of Top Carboniferous in the Groningen field, northeast Netherlands," NAM, Assen, 2017.

[15] J. Seubring, "Petrophysical evaluation of the Groningen field Carboniferous," NAM, Assen, 1994.

[16] L. Vos, "Groningen Field RFT and FIT Data & Information on Limburg Connectivity," NAM, Assen, 2003.

[17] L. Vos, " Groningen Field RFT and FIT Data & Information on Limburg Connectivity," NAM, Assen, 2003.

[18] M. Glegola, H. van Oeveren, L. Geurtsen and P. Valvatne, Groningen 1978-2015 time-lapse gravity surveys results interpretation and scenario testing, Assen: NAM, August 2017.

[19] P. Kole, "Estimation of ranges for Cm in the Carboniferous," NAM, Assen, 2018.

[20] Shell Production Handbook, "Volume 3 and Chapter 9," Shell, Rijswijk, 1991.

[21] I. message, "Volumentric GIIP Carboniferous Groningen Field," NAM, Assen, 1989.

[22] P. Kole, "Strain data obtained by Zeerijp-3A DSS for implementing in Groningen RE model," NAM, Assen, 2018.

[23] R. Van Eijs, "Correlation between hydrocarbon reservoir properties and induced seismicity in the Netherlands," Elsevier, 2006.

[24] F.Prousa, "2008 PNL GWC Monitoring of UHM-1A," NAM, Assen, 2008.

[25] J. Geertsma, "A basic theroy of subsidence due to reservoir compaction: the homogeneous case," Shell, Rijswijk, 1973.

[26] G. v. Opstal, "The effect of base-rock rigidity on subsidence due to compaction," Shell, Rijswijk, 1972.

[27] H. v. Oeveren, "Production Forecast Pop-up blocks Kooijpolder and Froombosch," NAM, Assen, 2015.

[28] U. Burkitov, H. van Oeveren, P. Valvatne , "Groningen Field Review 2015 Subsurface Dynamic Modelling Report," NAM, Assen, 2016.

[29] E. van Kersbergen, "SSM_2a well test interpretation," NAM, Assen, 2015.

[30] W. Andersen, "Evaluation of MGT-1 welltest - part 1: ROSLL and lower part ROSLU," NAM, 14/9/1995.

[31] Q. d. Zeeuw, "Numerical Analysis of Zeerijp-3 Steady State experiments," NAM, Assen, 2018.

[32] L. Vos, D. Lee and A. van der Graaf, Study of Aquifer Activity around the Groningen Field, 1/2/2003.

[33] G. Berthereau, "Carboniferous Feasibility study," CGG Veritas, Aberdeen, 2007.

[34] Onno van der Wal, "Usage of acoustic logs for static cm calculation," NAM, Assen, 2001.

[35] A. Mockovciakova and B. Pandula, "Study of the relation between the static and dynamic moduli of rocks," metlurgija 42, 2003.

[36] H. Sone and M. Zoback, "Mechanical properties of shale-gas reservoir rocks - part 1: static and dynamic elastic properties and anisotropy," Society of Exploration Geophysicists, 2013.

[37] R. Gill, "Carboniferous prospects Groningen gas field," NAM, Assen, 1977.

[38] W. Van Eijndthoven, "Considerations Origin of N2 in the Greater Groningen Area," NAM, Assen, 2016.

[39] C. Bueker, "Groningen Field Basin Modelling," NAM, Assen, 2002.

[40] H. Van Oeveren, Implementation of time-lapse gravity data in the Groningen dynamic model, Assen, April 2017.

[41] C. Visser, "Petrographic aspects of the Rotliegend of the Groningen field," NAM, Assen, 2016.

[42] F. Seeberger, "Update of methodology of predicting gas- adn aquifer pressures in the Waddenzee development area," NAM - EP201505216677, Assen, 2015.

[43] A. Boscolo Gallo and E. Rumpfhuber, "Probabilistic seismic inversion for the Groningen field, Closing the loop," NAM, Assen, 2017.

Appendix A V6 best match

SPG match RMS = 1.82 bar	GRO_2018_ED_v77_V6_SPTG.pdf
RFT match RMS = 12.72 bar	GRO_2018_ED_v77_V6_RFT.pdf
CITHP2BHP match RMS = 1.48 bar	GRO_2018_ED_v77_V6_CITHP.pdf
PNL match RMS = 2.81 meter	GRO_2018_ED_v77_V6_PNL.pdf
Subsidence match RMS = 2.10 cm	GRO_2018_ED_v77_V6_Subs.pdf
Gravity Match RMS = 4.84 μGal	GRO_2018_ED_v77_V6_Grav.pdf
ZRP strain DSS RMS = 24.23 μstrain	GRO_2018_ED_v77_V6_DSS_Match.pdf

Appendix B Slochteren property modelling from seismic inversion

B.1 Seismic inversion workflow

To follow-up on recommendations made by external reviewers, in the V4 model update the property modelling was upgraded to by using seismic inversion. Although both porosity and thickness were variable parameters in this seismic inversion, only the porosity from the seismic inversion has been used to steer the final static model's porosity. The thickness was kept constant.

A delta-thickness map depicts where the final static model has a different thickness than the thickness from seismic inversion. It was recommended in chapter 5.2.2. of the V5 dynamic model report to investigate the use of this delta-thickness map.

Therefore, cross plots for each reservoir zone were created and analysed to check any correlation between thickness differences and porosity differences between the final static model and the seismic inversion output.

The cross plots were created as follows:

$$x\_axis = diff\_thickness\_relative = \frac{(Inversion\ output\ thickness - Static\ model\ output\ thickness)}{Static\ model\ output\ thickness}$$

$$y\_axis = diff\_porosity\_relative = \frac{(Inversion\ output\ porosity - Static\ model\ output\ porosity)}{Static\ model\ output\ porosity}$$

It can be observed from Figure B-1 that no correlations were found which would justify another seismic inversion iteration where reservoir unit thickness is kept constant.

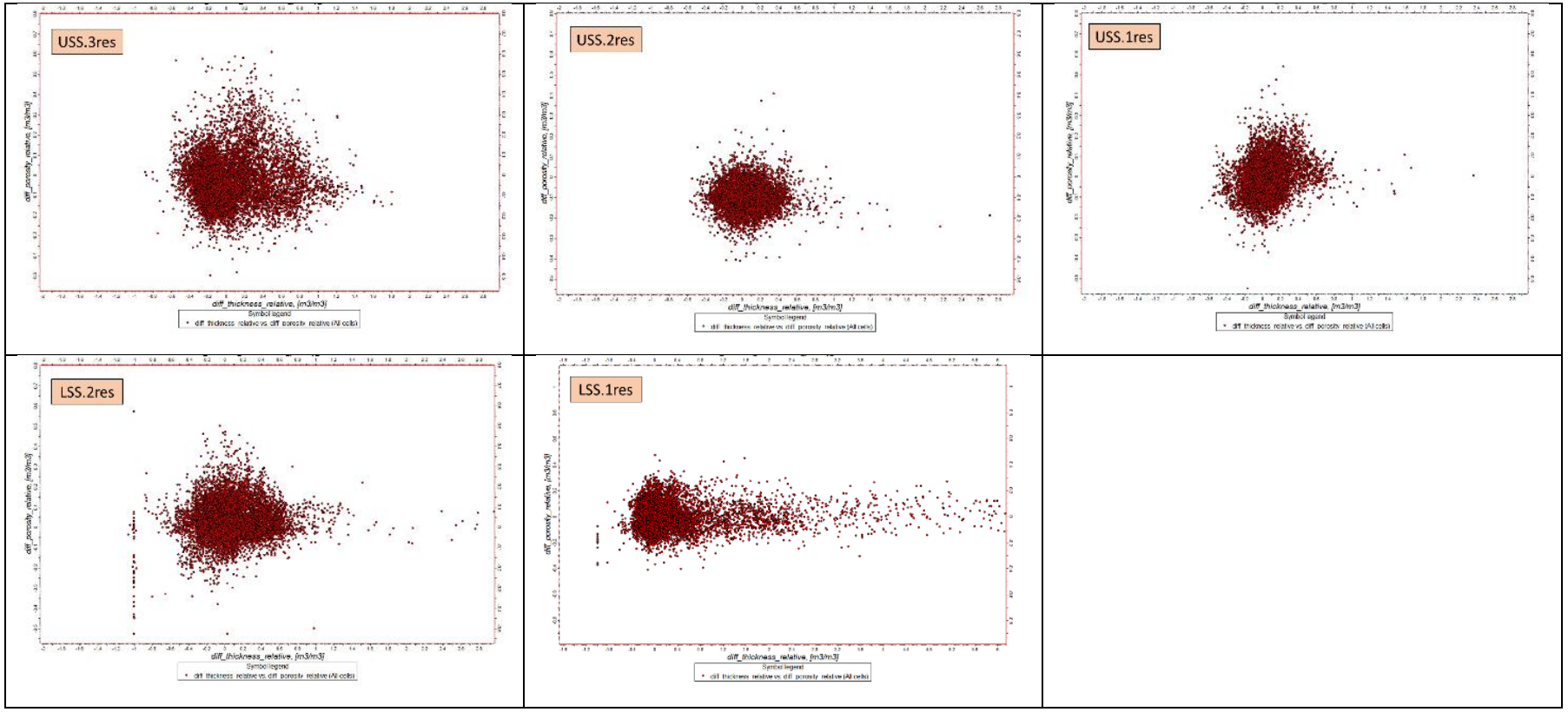

Figure B-1 Cross plots between normalized thickness and porosity differences between the seismic inversion output and the static model output.

B.2 Sensitivity study for depletion and water encroachment

It was recommended in chapter 5.1 in the V5 dynamic model report to execute an additional seismic inversion iteration. The previous seismic inversion had assumed initial reservoir conditions, whereas the seismic data was acquired in 1985. The preceding 30 years of production history had depleted the reservoir by some 150 bar (reduced gas density) and water ingress up to 10-20m was observed at various places in the North of the reservoir. The rise in water level in the northeast of the field was expected to result in higher porosities in the flushed zone as obtained from a seismic inversion. In turn, this was expected to increase modelled permeabilities in the northeast of the field, locally improving the pressure match between the observation wells and the production clusters.

The expectation was that when including gas-in-aquifer, the match of the aquifer encroachment would improve, a new seismic inversion would be executed on an intermediate history match, from which a new property model would be established that would feed in to the final history match.

NAM's Quantitative Interpretation team ran a sensitivity study to further investigate the impact of a flushed gas zone (aquifer encroachment) on the acoustic impedance as compared to the initial conditions. Figure B-2 shows results for the UHZ-1, UHM-1A and HND-1 wells. There are two main observations:

- When comparing a fully water bearing zone (Sw=100%) to the initial conditions in the gas reservoir (Sg~80%) there is a clear different in Acoustic Impedance.
- However, when comparing the initial conditions in the gas reservoir (Sg~80%) to a situation after aquifer encroachment (Sg~20%) the difference is minimal, if apparent at all.

Consequently, there is no impact of updating the seismic inversion for water encroachment. Based on the analysis, no third seismic inversion is done for the V6 model.

Note that the pressure match in the northeast of the field has been improved in this V6 model update by the introduction of the porosity dependent permeability multipliers, section 8.2.

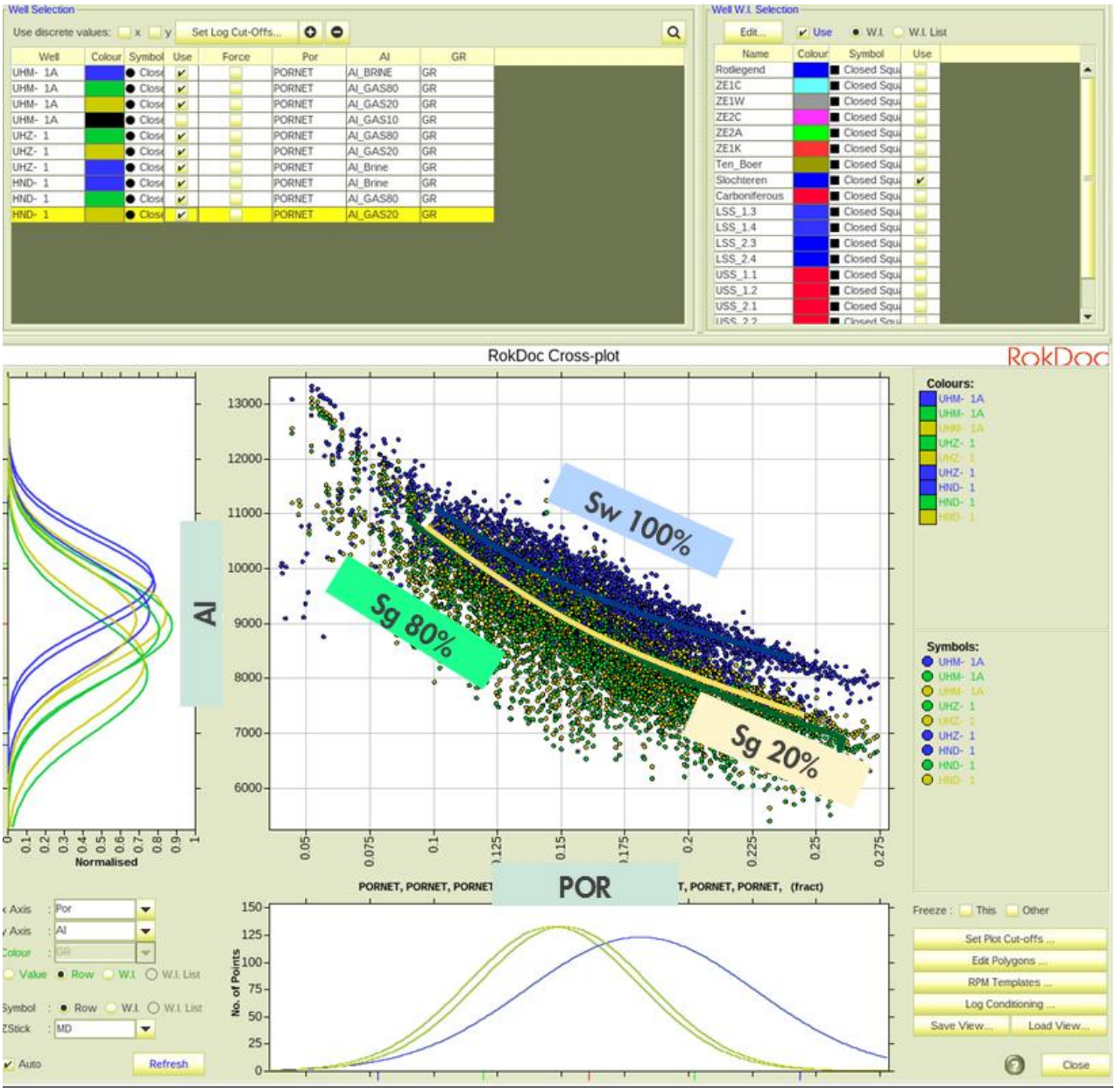

Figure B-2 Acoustic impedance vs. porosity trend for 100% brine, 20% gas and 80% gas saturations.

B.3 Semblance

It was recommended in chapter 5.2.1. in the V5 dynamic model report to investigate the use of the semblance map in the history matching process, as it was expected to provide information on the lateral spread of uncertainty in the static model.

Figure B-3 shows the output of the investigation of semblance versus porosity or permeability during the V6 modelling effort. No relation between semblance and porosity could be found, nor with permeability. Hence no justification was established to incorporate semblance as a parameter to steer porosity or permeability laterally during the history matching process.

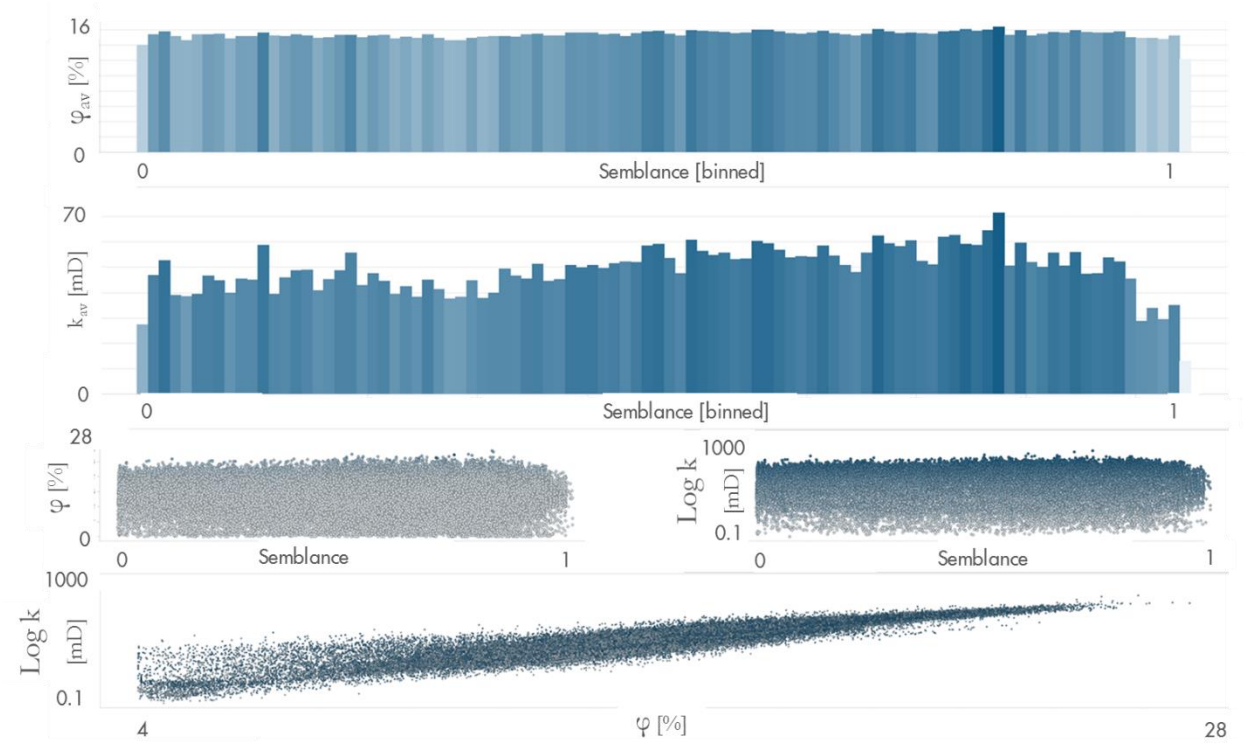

Figure B-3 Porosity and permeability normal and logarithmic relations to semblance including por-perm relation graph on the bottom.

Appendix C Analytical evaluation of gas-in-aquifer

C.1 Objective

This analysis provides a high-level assessment on the impact of gas-in-aquifer on the water rise in the Groningen field. Combinations between different observed pressure drops in the aquifer and different hypothesis on the fill of gas-in-aquifer are tested. For these scenarios the expected water rise in the northeast area of the field is calculated and compared to the water rise measured from PNL's in the region.

C.2 Methodology

C.2.1 Material Balance simplification

The North-Eastern part of the reservoir (as per initialisation region Groningen NE, Reference [10]) was taken to be a stand-alone reservoir element and approximated by simple 1-dimensional material balance tank. Thus it was assumed that aquifer encroachment can be approximated by bottom-water-drive, Figure C-1. The volume of the lateral aquifers (Mowensteert and Rysum) is lumped into the bottom-aquifer.

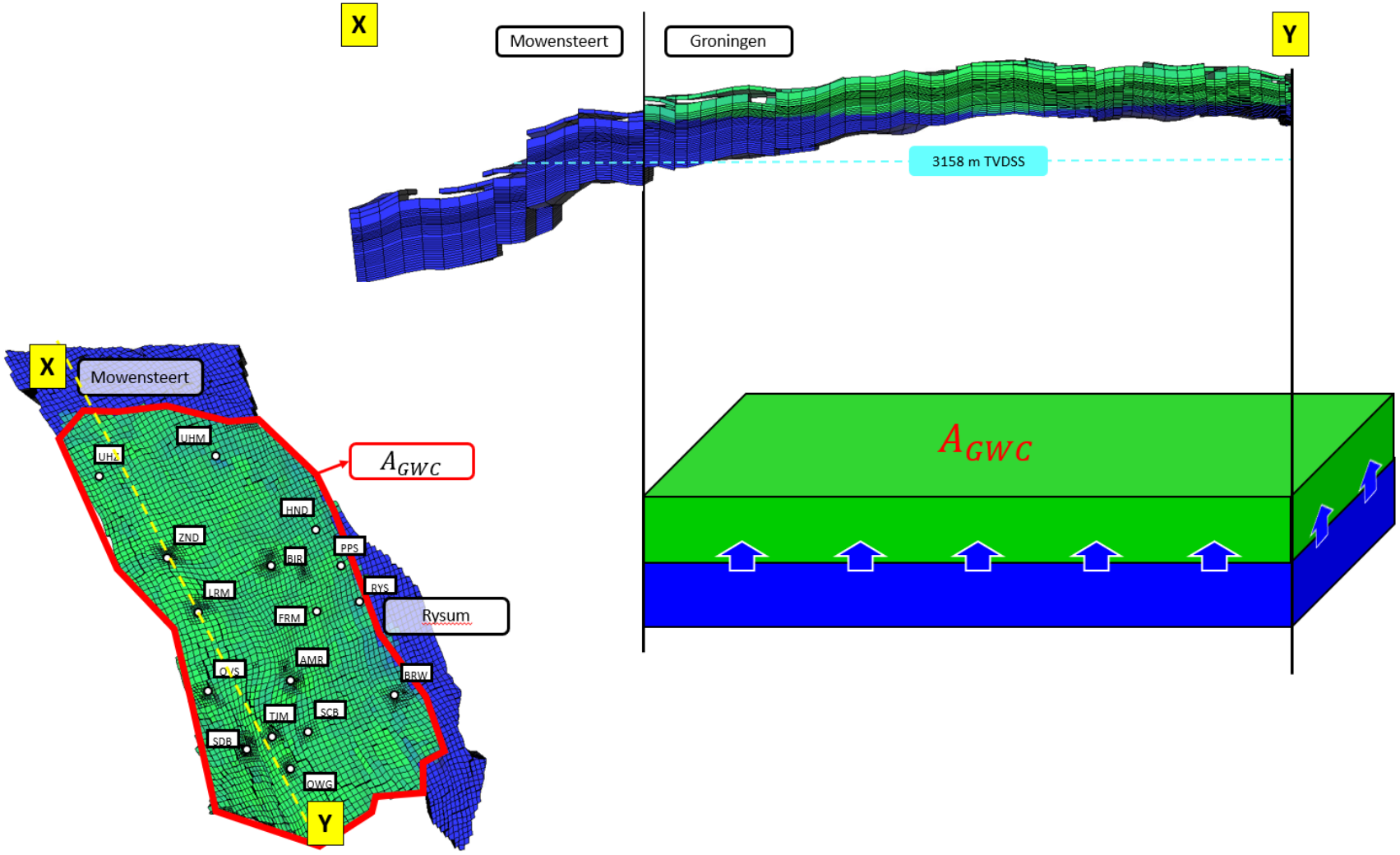

Figure C-1:Simplifying reservoir configuration assumptions

The bottom-water-drive is implemented in the simplified Material Balance approach as an instantaneous Pot Aquifer, thus assuming an instantaneous reaction of the entire aquifer to pressure drop.

It is assumed that gas expansion dominates the aquifer influx: gas-in-aquifer can expand due to pressure depletion, but is assumed to be bound be relative permeability. Then, the net effect will be that only water encroaches above the GWC. Consequently, the basic principle of this analysis is a material balance where fluid expansion within the aquifer equals the volumetric rise in GWC:

$$\text{Water expansion in aquifer} + \text{Gas-in-aquifer expansion} = \text{Water encroachment in reservoir}$$

The aquifer expansion terms are calculated as follows:

$$\text{Water expansion in aquifer} = WIIP \cdot c_w \cdot \Delta P$$
$$= GRV_{AQ} \cdot \varphi_{AQ} \cdot (1 - S_{g,AQ}) \cdot c_w \cdot \Delta P$$

$$\text{Gas-in-aquifer expansion} = \left(\frac{GRV_{AQ} \cdot \varphi_{AQ} \cdot S_{g,AQ}}{B_g(P)} - \frac{GRV_{AQ} \cdot \varphi_{AQ} \cdot S_{g,AQ}}{B_{g,i}(P_i)}\right) \cdot B_g(P)$$

whereby:

c_w	Water compressibility
GRV_{AQ}	Aquifer gross rock volume
φ_{AQ}	Aquifer porosity.
$S_{g,AQ}$	Saturation of the gas-in-aquifer, varies for different scenario's.
$S_{g,i}$	Initial gas saturation in the flushed zone.
S_{gr}	Residual gas saturation in the flushed zone.
$B_g(P_i)$	Gas formation volume factor at initial pressure ($P_i = 348$ bar).
$B_g(P)$	Gas formation volume factor at depleted pressure
$WIIP_{AQ}$	Water initially in place in the aquifer

The associated water encroachment in the gas reservoir is defined as:

$$\text{Water encroachment in gas reservoir} = A_{GWC} \cdot \Delta h_{GWC} \cdot \varphi_{AQ} \cdot (S_{gi} - S_{gr})$$

whereby:

A_{GWC}	Area of the gas reservoir exposed to the aquifer.
Δh_{GWC}	Rise of the GWC.

C.2.2 Input data

Various input parameters were kept fixed in the calculations, as defined in Table C-1. Most values are extracted from the V6 MoReS model.

Parameter	Value	Unit	Source
$GRV_{AQ,RYS}$	13.88	R.Bcm	NAM200304000814.
$GRV_{AQ,MOW}$	31.73	R.Bcm	NAM200304000814.
$GRV_{AQ,GRON}$	38.03	R.Bcm	V6 MoReS model
$GRV_{AQ,total>3158m}$	43.8	R.Bcm	V6 MoReS model
$c_{w,@100\,°C,200\,bar}$	$3.0 * 10^{-10}$	1/Pa	V6 MoReS model
φ_{aqf}	0.14	Fraction	NAM200304000814
$S_{g,i}$	0.8	Fraction	V6 MoReS model
S_{gr}	0.22	Fraction	V6 MoReS model
$B_{g,i}$	$4.2*10^{-3}$	Ratio	V6 MoReS model
B_g	f(Pressure)	Ratio	V6 MoReS model
A_{GWC}	$4.51*10^{8}$	m2	V6 MoReS model

Table C-1: Fixed input parameters

Note that the pressure dependency of the water compressibility is limited (Figure C-2). The water compressibility was taken as a constant value, defined at 100°C and 200 bar.

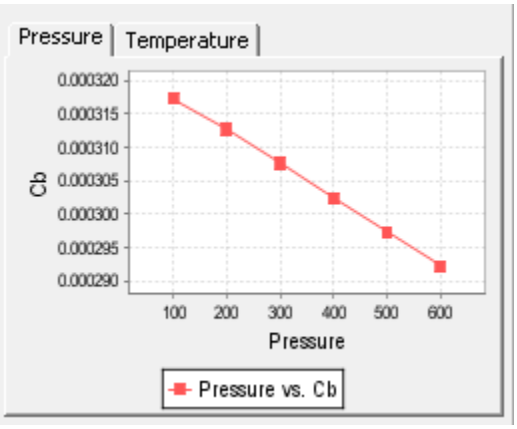

Figure C-2:Water/Brine isothermal compressibility [1/mPa] at 100°C and for 250,000 ppm NaCl. Source: PVT Calculator

The Mowensteert and Rysum aquifers extend beyond the Groningen model outline; the associated aquifer properties (size and porosity) are taken from the 2003 Groningen aquifer study, Reference [32]. An extract from this study is reproduced in Figure C-3

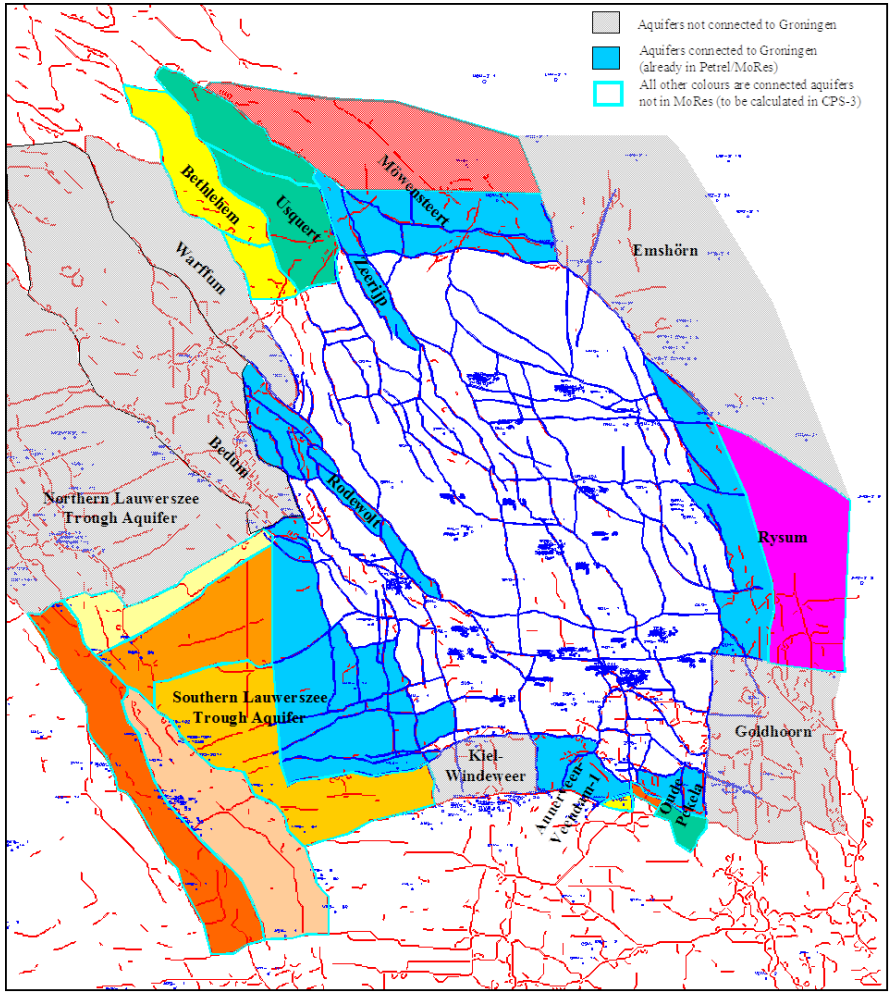

Aquifer Region	Isochore (m)	N/G	Porosity
ANV-1	78	0.91	0.12
NPK_Blk_1	74	0.97	0.14
NPK_Blk_East	75	0.97	0.13
Rysum_outer	**128**	**0.94**	**0.12**
Möwensteert	**259**	**0.64**	**0.15**
Usquert_inner	286	0.82	0.15
Usquert_outer	324	0.73	0.15
Bethlehem_inner	289	0.86	0.17
Bethlehem_outer	337	0.76	0.15
Pasop_north	215	0.97	0.16
Pasop	210	0.99	0.16
Roden_Vries	154	0.99	0.14
Norg	132	0.99	0.15
New_Roden_Norg_South	144	0.97	0.17

Aquifer Region	Area (10^6 m^2)	GRV (10^9 m^3)	NRV (10^9 m^3)	NPV (10^9 m^3)
ANV-1	2.2	0.17	0.15	0.02
NPK_Blk_1	7.5	0.55	0.54	0.08
NPK_Blk_East	1.8	0.14	0.13	0.02
Rysum_outer	**108.0**	**13.88**	**13.11**	**1.54**
Mowensteert	**122.7**	**31.73**	**20.18**	**3.06**
Usquert_inner	47.8	13.68	11.16	1.73
Usquert_outer	36.2	11.73	8.57	1.30
Bethlehem_inner	14.8	4.26	3.67	0.61
Bethlehem_outer	48.4	16.31	12.36	1.86
Pasop_north	38.1	8.19	7.92	1.28
Pasop	74.2	15.59	15.46	2.53
Roden_Vries	115.2	17.74	17.49	2.52
Norg	106.4	14.01	13.86	2.13
New_Roden_Norg_South	94.7	13.59	13.22	2.24

Table 34: Aquifer Volumetrics.

Figure C-3 Left: Overview maps of Groningen aquifers. Right: Table with calculated aquifer volumes. The aquifers connected to the NE of Groningen are highlighted. Reference [32].

C.2.3 Observed water level rise

Figure C-4 shows the observed water rise in the northeast of the field as measured from PNLs in several wells. The more northern wells (20+ meter) indicate a larger water rise than the southern wells (5-20m). This may be related to thickness variations in the bottom-water leg, see Figure C-1.

An average was established for the total reservoir element as indicated by the red line in Figure C-4.

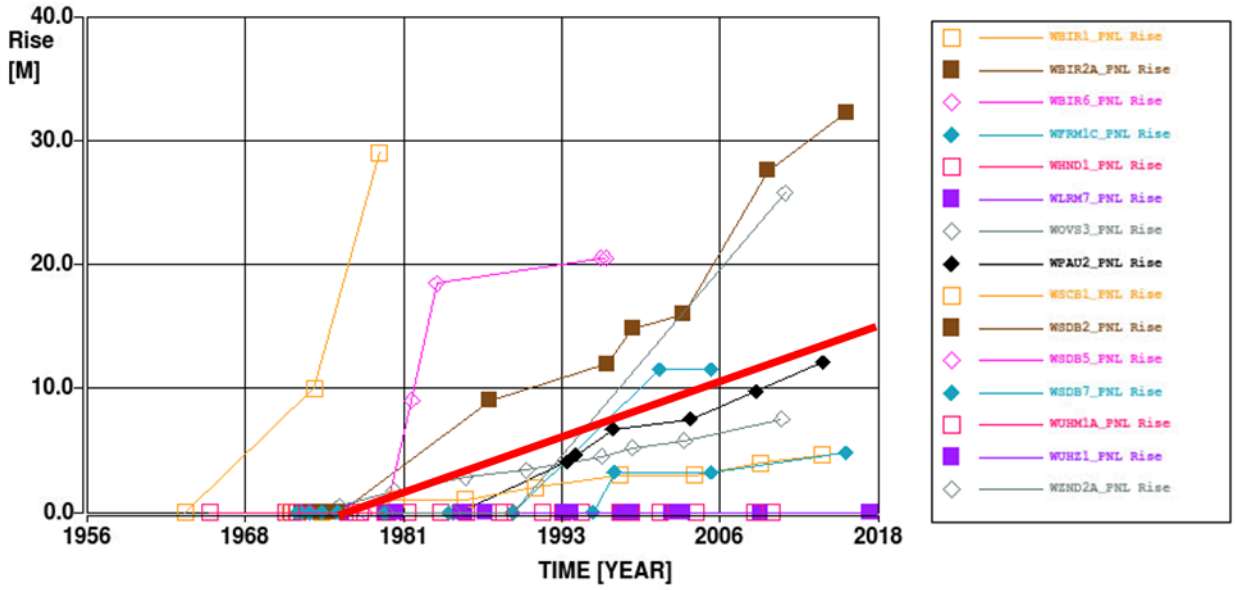

Figure C-4 Water rise measured in the wells in the northeast of the Groningen field. The thick red curve proposes an average water rise throughout the area.

C.2.4 Scenario definition

Aquifer depletion

Pressure differences between the aquifer and the gas reservoir were observed from the various RFT measurements across the field. The RFT data is not conclusive towards a single scenario so multiple scenarios are considered. The time dependency of the different scenario's is eliminated by considering the aquifer depletion as a percentage of the depletion in the gas reservoir. Figure C-5 shows 2 examples which provide different scenarios:

- Scenario 1: The pressure in the aquifer is lagging behind some 42% to the gas reservoir pressure, based on the UHZ-1 RFT. This equals a pressure drop of 0.42*(347-89.6)= 108 bar.
- Scenario 2: The pressure in the aquifer is lagging behind some 5% to the gas reservoir pressure, based on the FRM-1 RFT. This equals a pressure drop of 0.95*(347-89.6)= 245 bar.

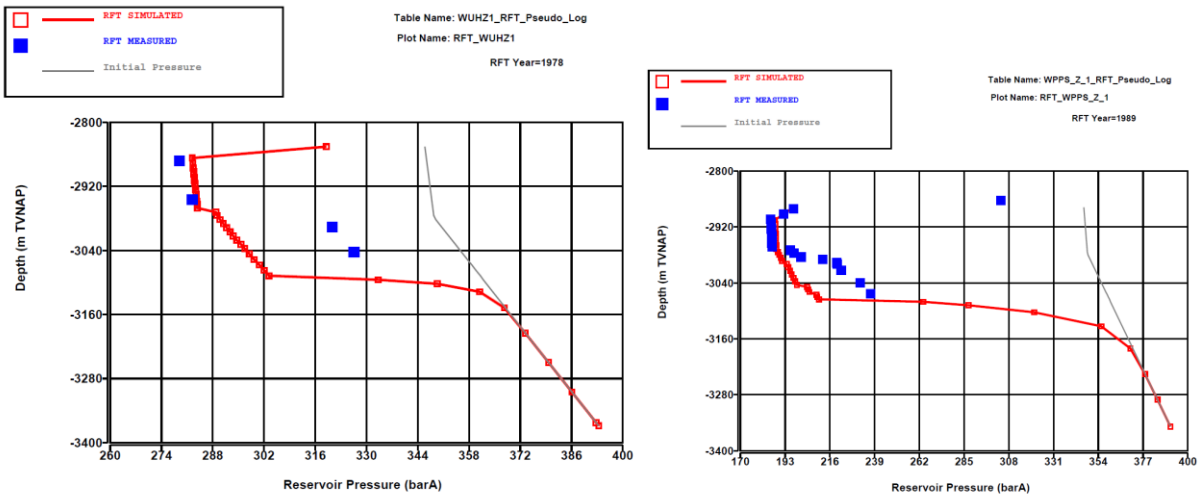

Figure C-5 Left: RFT measurements in UHZ-1 in 1978. Right: RFT measurements in FRM-1 in 1989.

Gas-in-aquifer saturation

The gas-in-aquifer saturation is uncertain. Two different hypotheses were entertained during the history matching process:

- Bottom charge: the gas-in-aquifer results from a bottom charge under the field and saturations are expected to be around the critical gas saturation of ~5%.
- Paleocontact: gas saturations should be in line with the residual gas saturations from the gas reservoir, which is ~ 22%. Note that the depth of the paleocontact is expected at 3158m TVDSS based on basin modelling work which identified this depth as the spill point when the Groningen closure was filled completely.

For reference, a case where there is no-gas-in-aquifer was tested as well. Finally, the obtained best match value for gas-in-aquifer from the V6 full field model was tested as well.

In total 4 scenarios for gas-in-aquifer saturation were tested:

- 0 % S_g : reference case
- 3 % S_g : V6 history matched value, downscaled from the uniform bottom source hypothesis.
- 5 % S_g : Aligned to uniform bottom source hypothesis.
- 22 % S_g : Aligned to paleocontact hypothesis.

C.3 Results

Table C-2 shows the calculated water rise resulting from the different scenarios. The water rise can be compared to the observed water rise in the northeast of the field. The actual observed water rise is some 15 m from the PNL measurements at the BIR and ZND production clusters.

Table C-2 Water rise in the northeast of the Groningen field calculated for different gas-in-aquifer saturation scenarios and different aquifer depletion scenarios. The observed water rise from PNLs in the region is ~15m over the entire field life.

			Aquifer depletion	
			ΔP_{AQ} = 245 bar	**ΔP_{AQ} =108 bar**
Gas-in-aquifer saturation	**Reference case:**	**0%**	2.5 m	1.1 m
	V6 full field model:	**3%**	22.9 m	4.3 m
	Bottom charge hypothesis:	**5%**	34.8 m	6.5 m
	Paleocontact hypothesis:	**22%***	77.1 m	13.7 m

*) above 3158mTVDSS (paleo-contact)

Without gas-in-aquifer, the aquifers cannot provide enough water rise. Both hypothesis on the gas-in-aquifer extent which are entertained during the V6 history match can provide the observed rise in water level.

The pressure lag in the aquifer determines how well a certain scenario matches the observed water rise. This pressure lag is expected to be larger for the paleocontact hypothesis than for the bottom charge hypothesis.

Appendix D RFT pressure lag indications

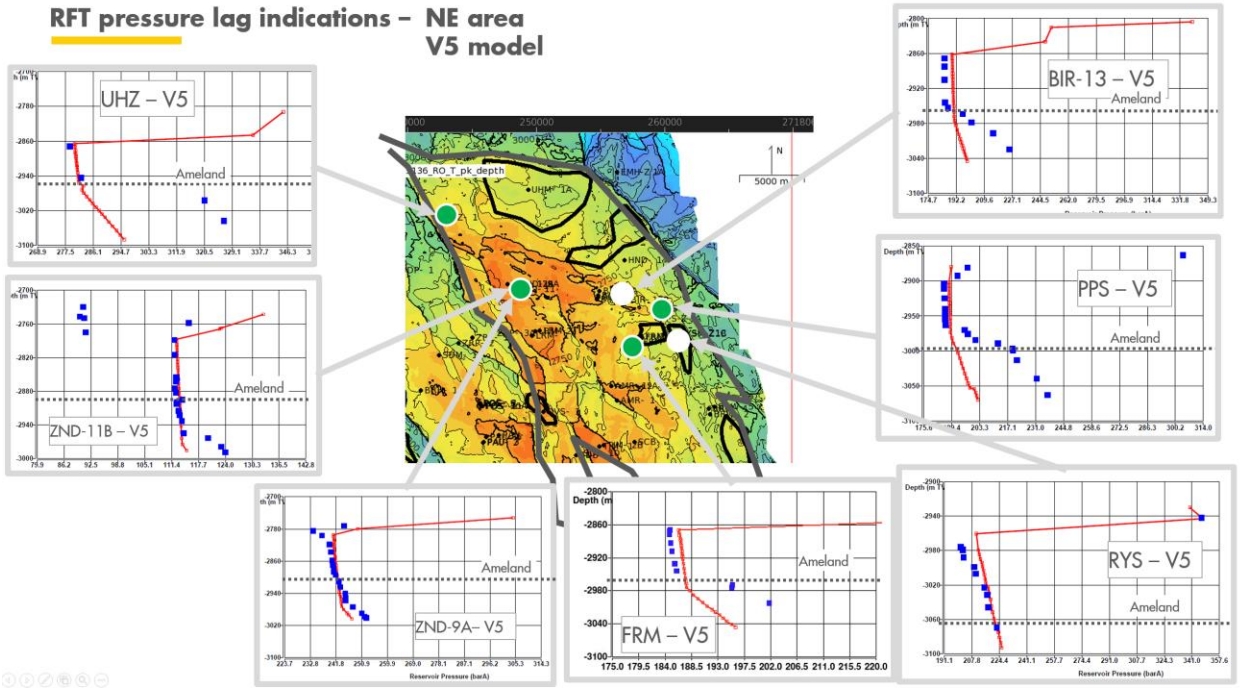

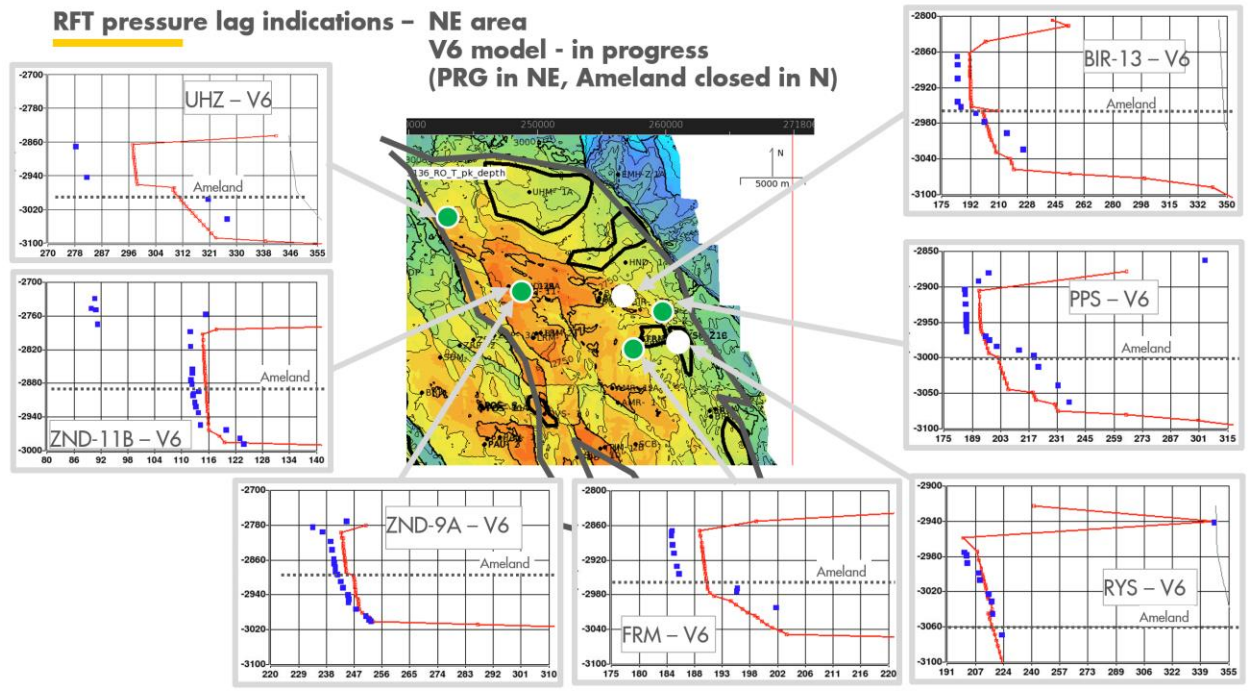

RFT pressure lag indications – NW area V5 model

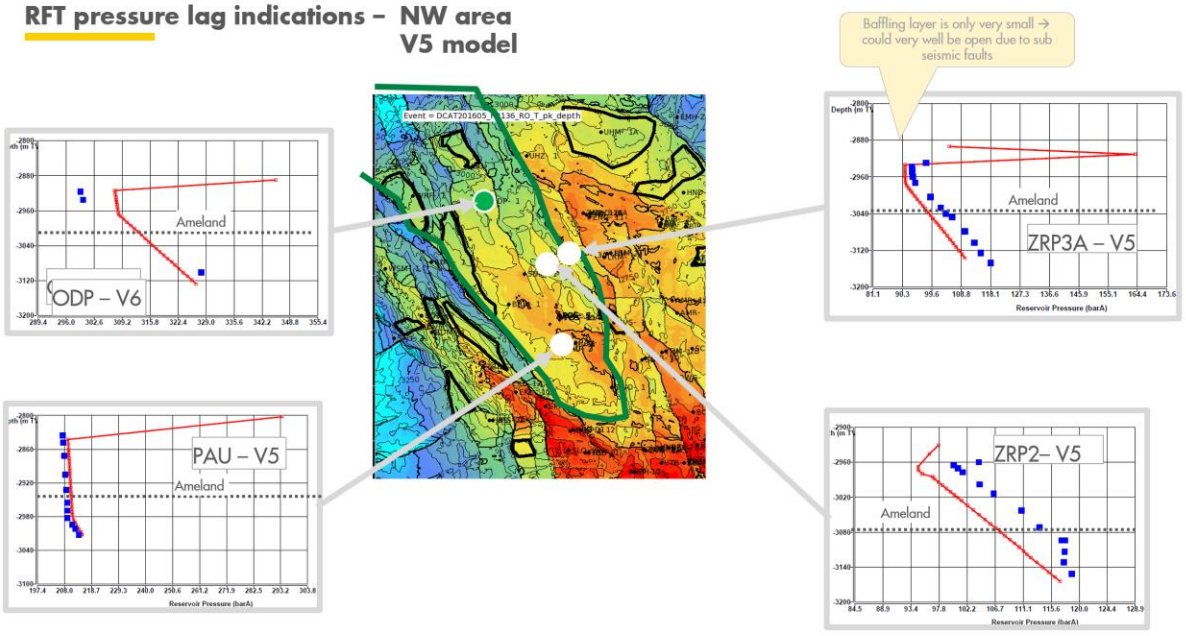

RFT pressure lag indications – NW area V6 model - in progress (PRG in NW, Ameland only in N)

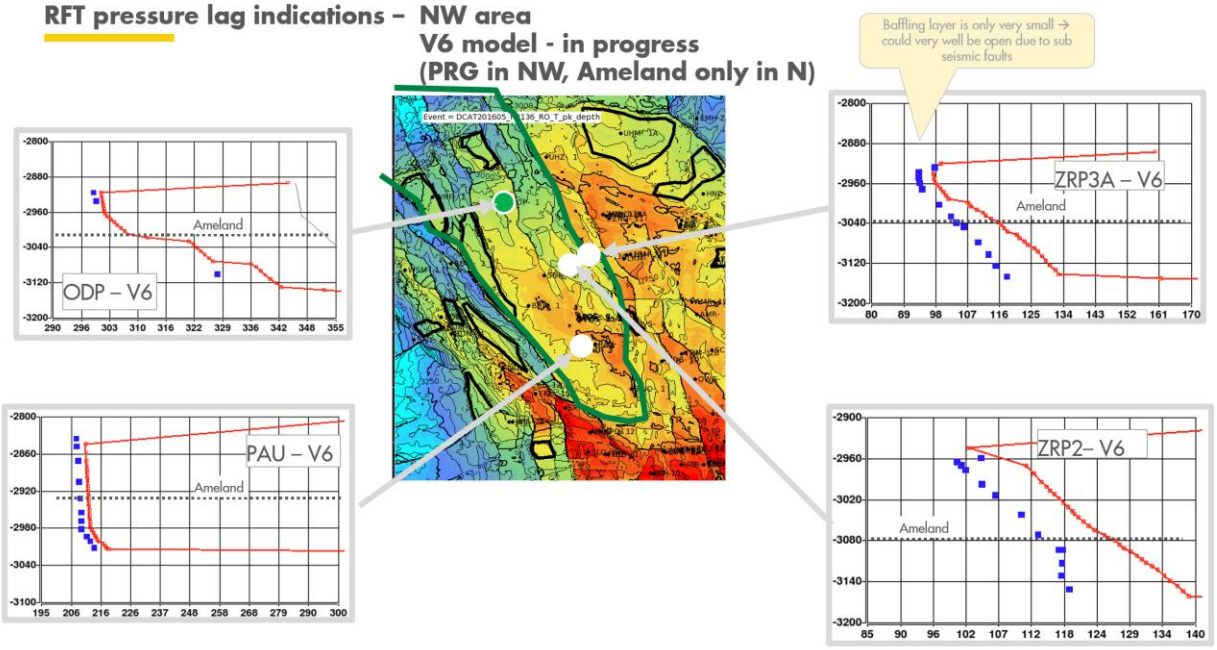

RFT pressure lag indications – SW area V5 model

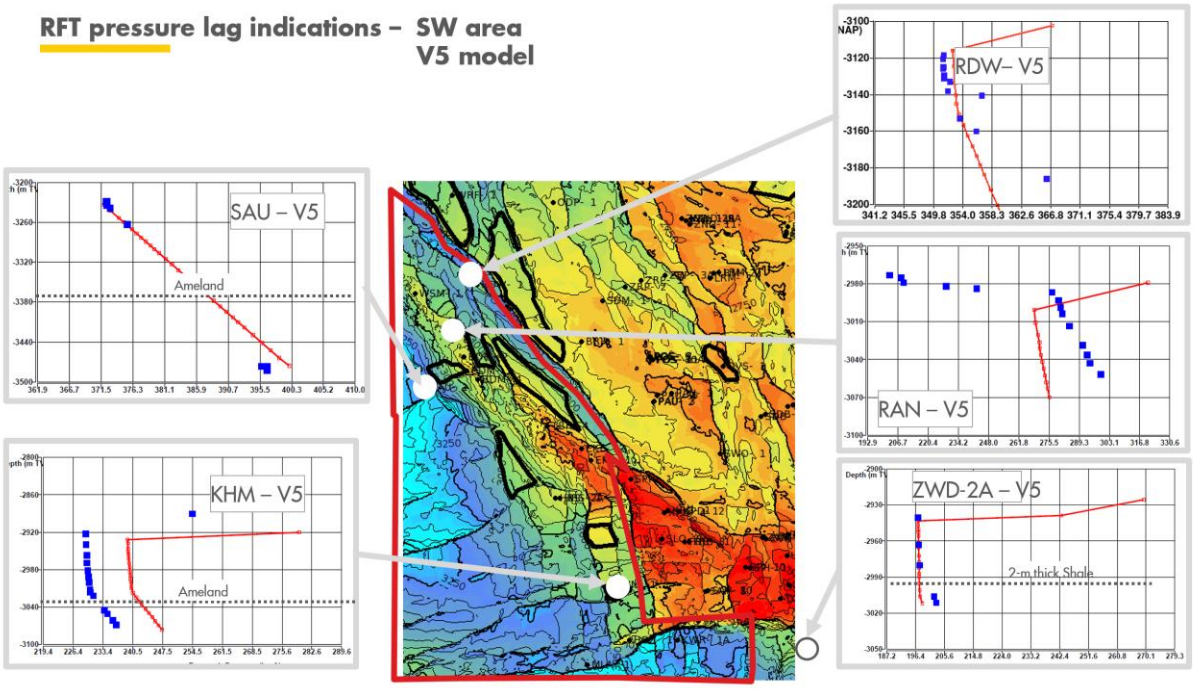

RFT pressure lag indications – SW area V6 in progress model (No PRG in SW)

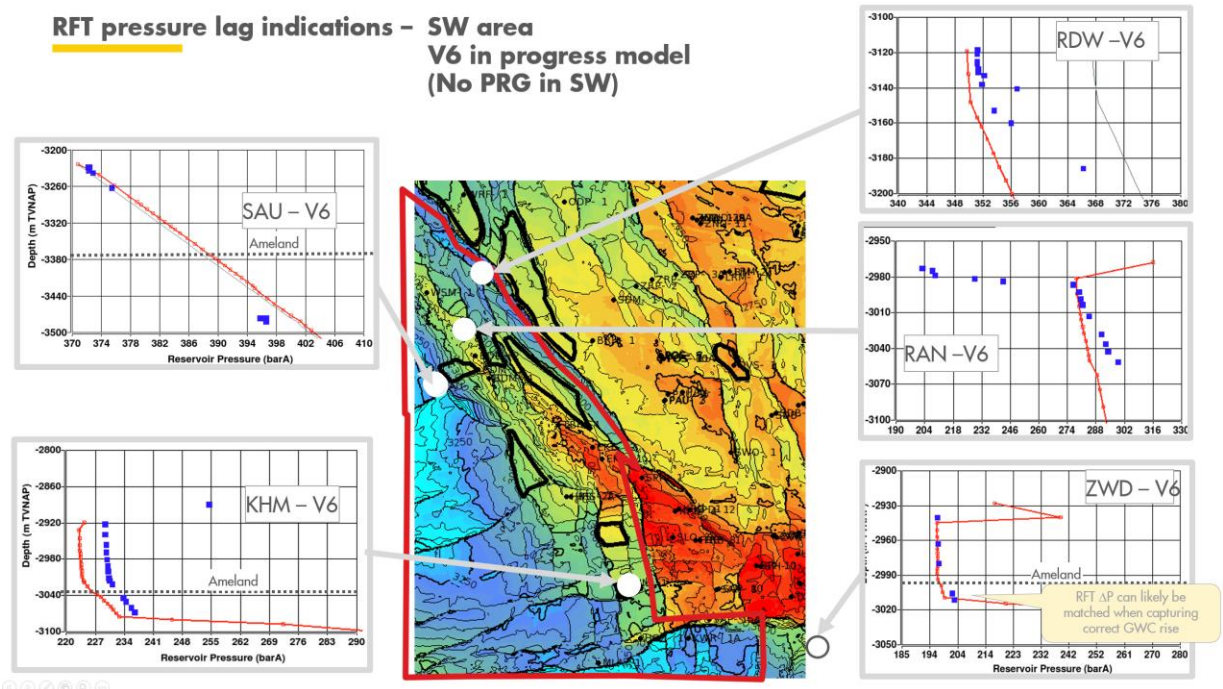

RFT pressure lag indications – SW area
V6 in progress model
(PRG in SW)

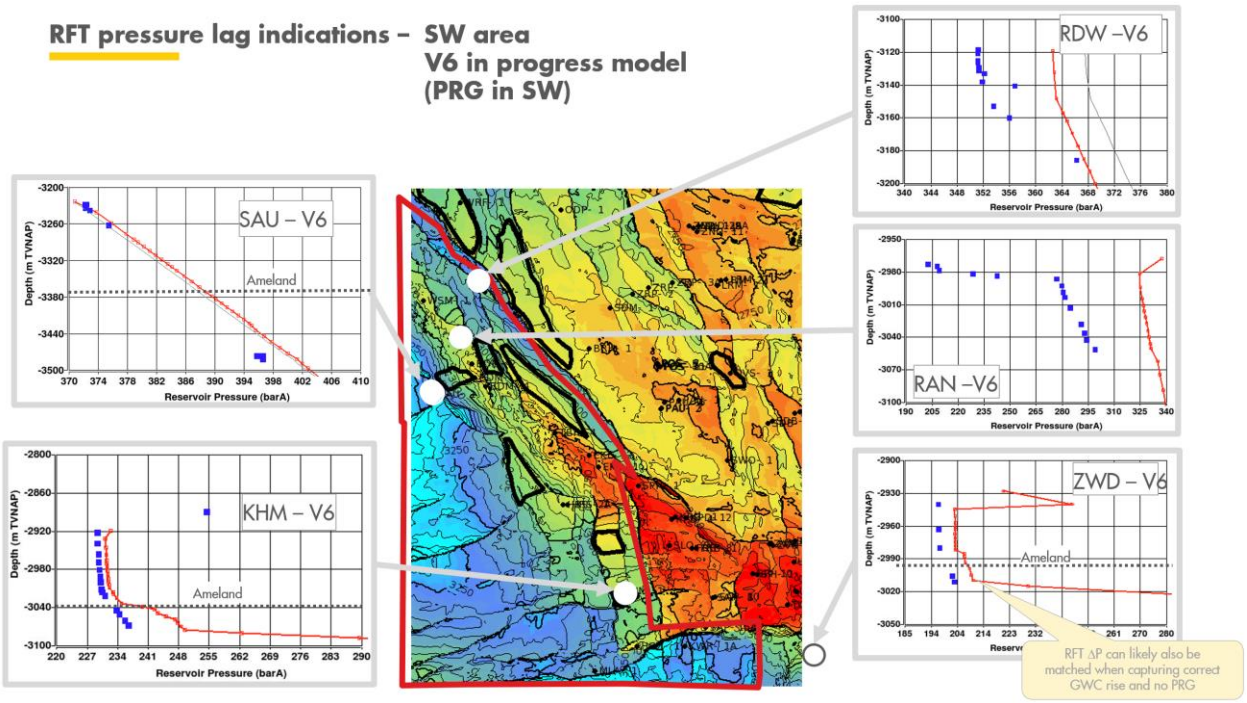

RFT pressure lag indications – NE area
V6 model - in progress
(PRG in NE)

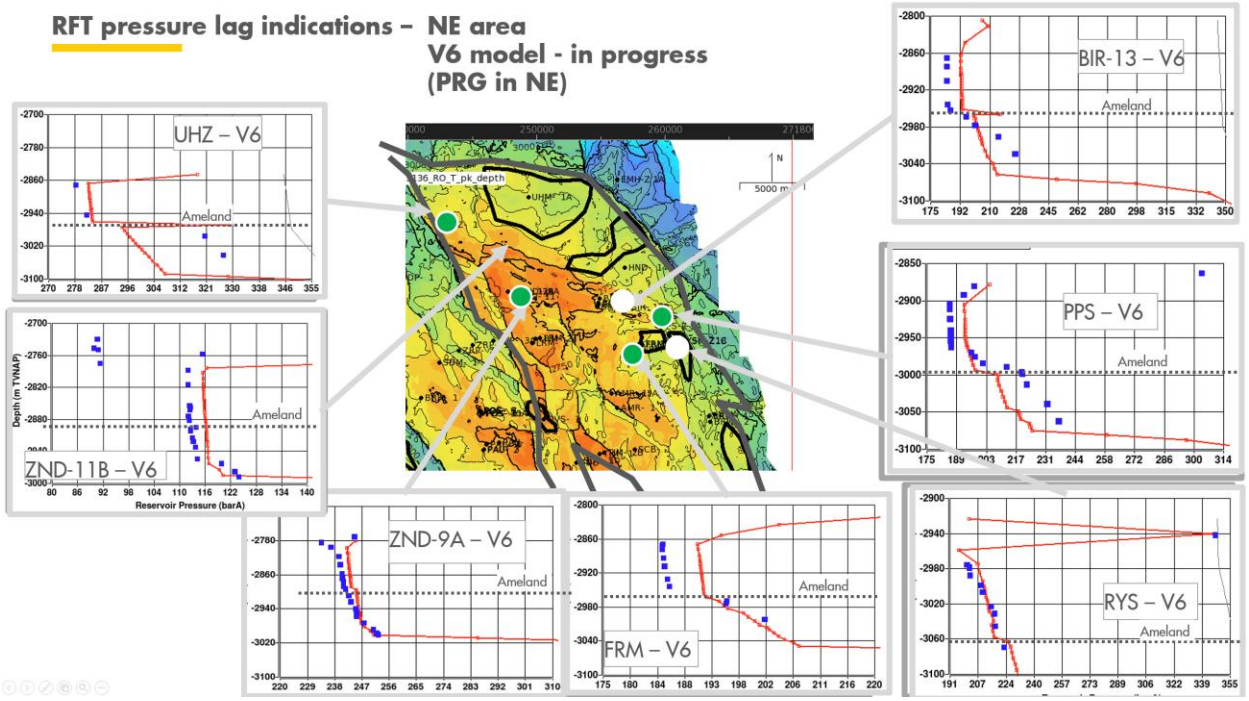

RFT pressure lag indications – NW area V6 - in progress (PRG in NW)

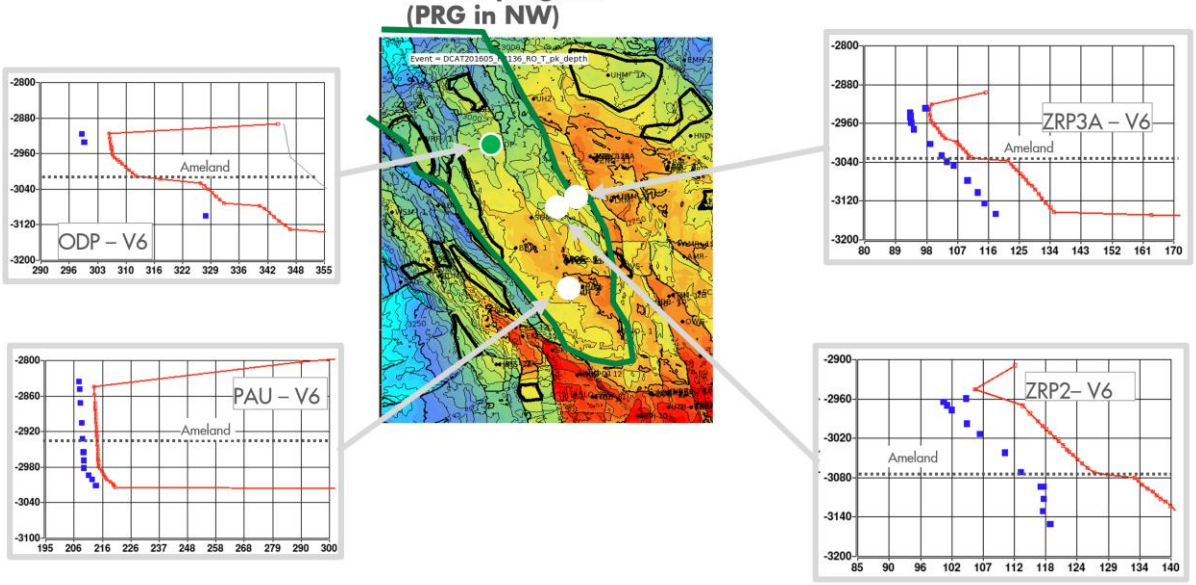

Appendix E PNL water rise

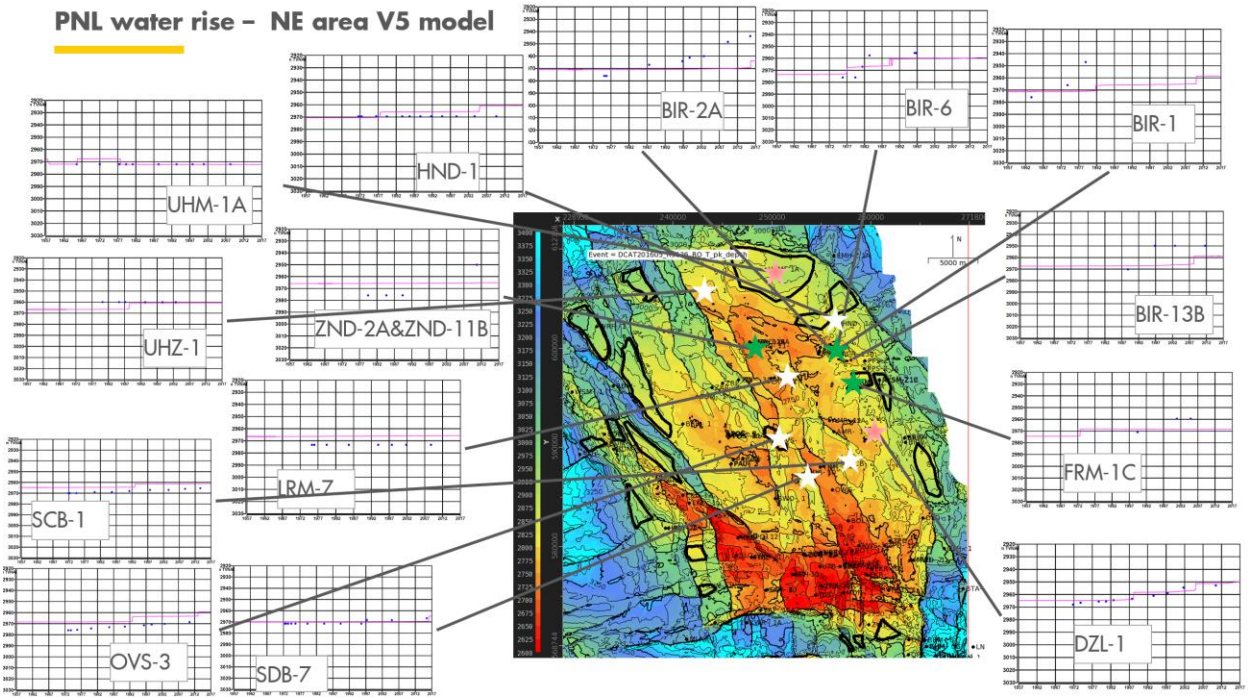

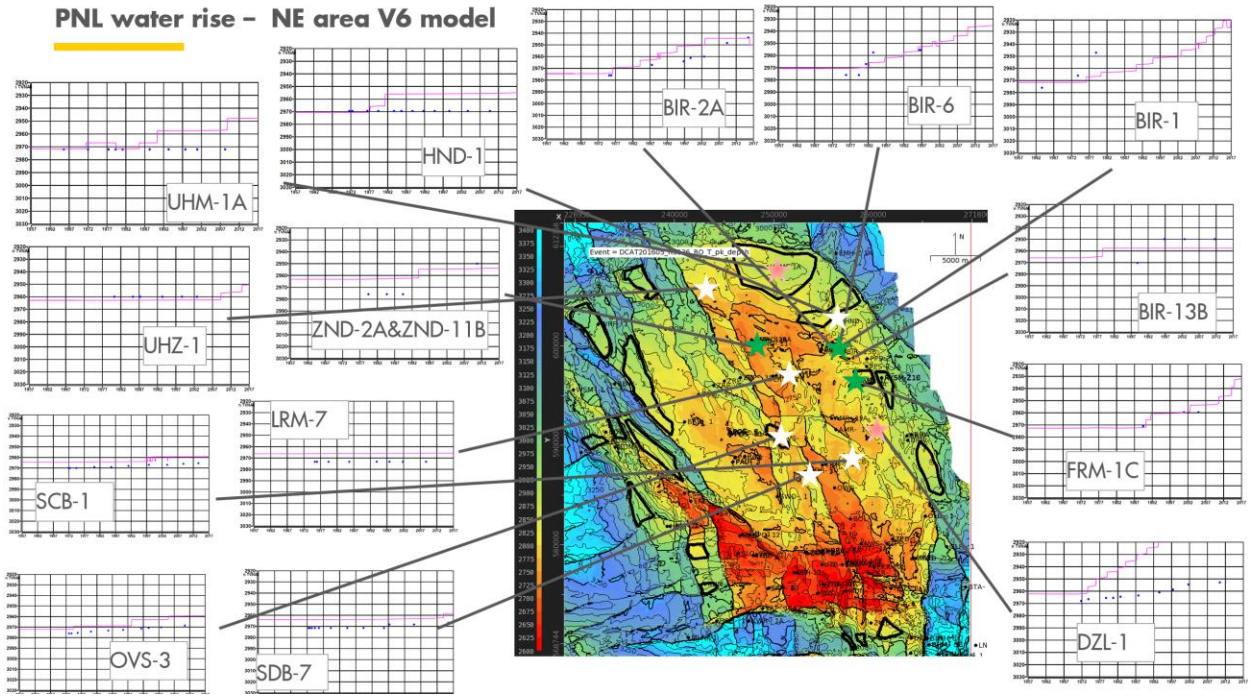

PNL water rise – NW area V6 model

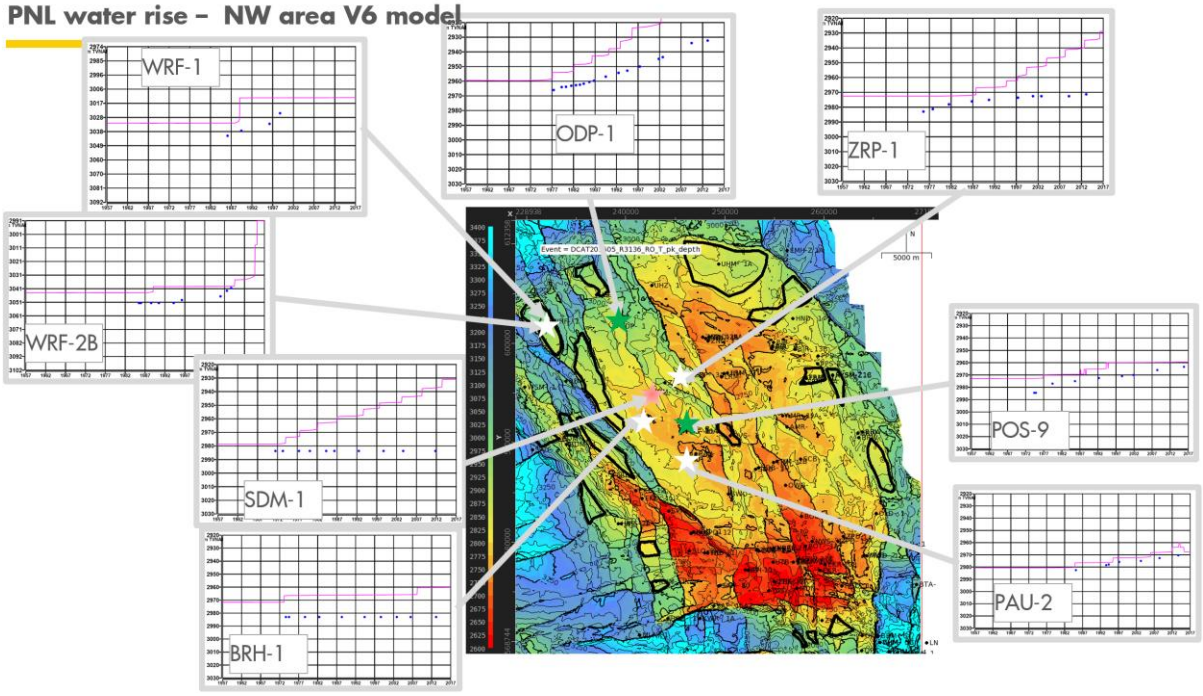

PNL water rise – SW area V5 model

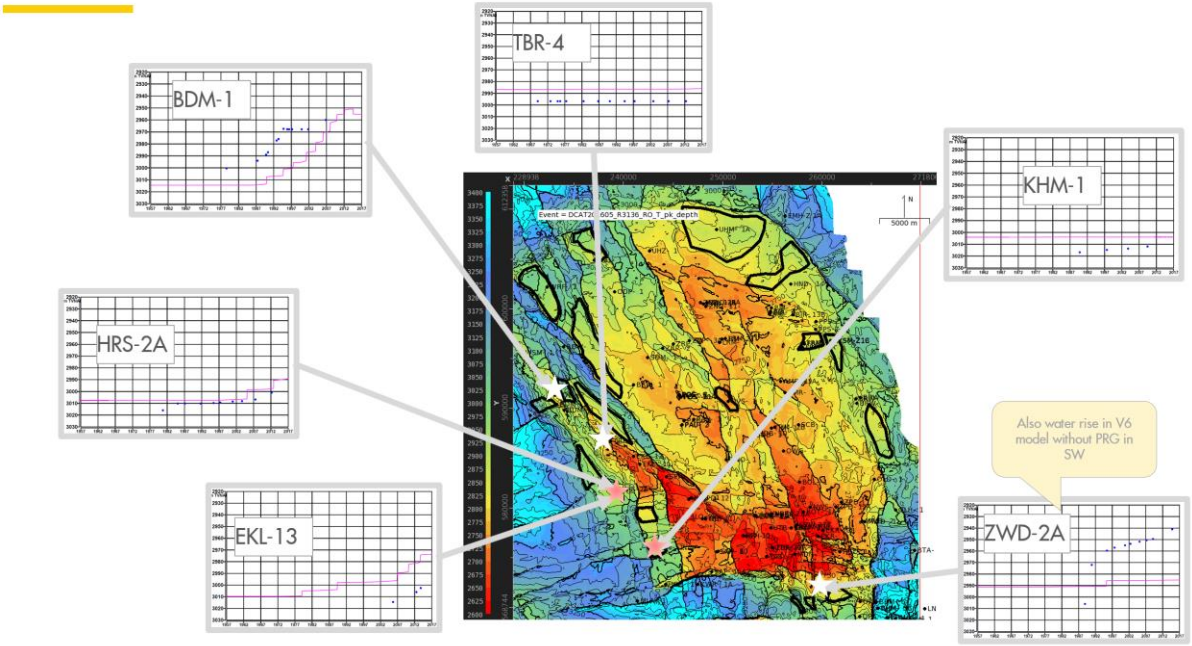

PNL water rise – SW area V6 model

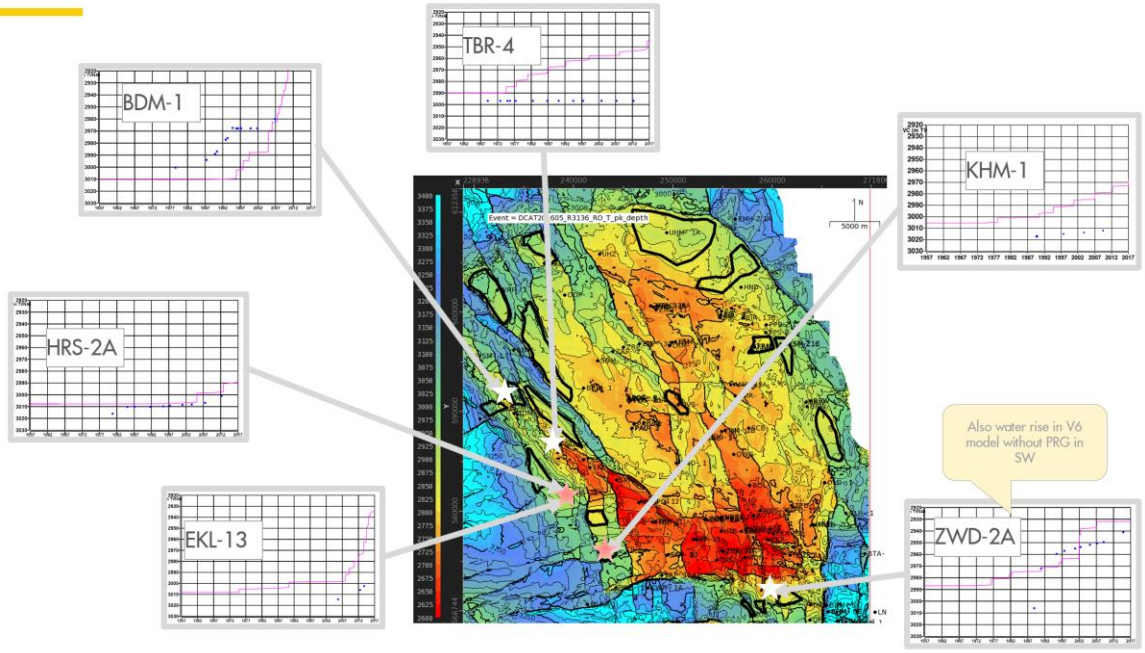

PNL water rise – SW area V6 model – no PRG in SW